

Copyright

by

Miloš Milošević

2003

The Dissertation Committee for Miloš Milošević  
certifies that this is the approved version of the following dissertation:

**Maximizing Data Rate of Discrete Multitone Systems  
using Time Domain Equalization Design**

Committee:

---

Brian L. Evans, Supervisor

---

Ross Baldick

---

Gustavo de Veciana

---

Edward J. Powers

---

Robert van de Geijn

**Maximizing Data Rate of Discrete Multitone Systems  
using Time Domain Equalization Design**

by

**Miloš Milošević, BSEE, MSEE**

**Dissertation**

Presented to the Faculty of the Graduate School of

The University of Texas at Austin

in Partial Fulfillment

of the Requirements

for the Degree of

**Doctor of Philosophy**

**The University of Texas at Austin**

May 2003

I dedicate this work to my family.

# Acknowledgments

During the course of my life I have come to realize that a man does not stand on his own as there always are those who care and who help along and without whose support nothing would be possible. This is especially true in my case.

I want to start by thanking my parents Djordje and Zorica Milošević who selflessly supported me in my endeavors sometimes against their better judgment. I thank them for sacrificing in order to provide me with I deemed necessary, the opportunity to see the world and make my own mistakes. I thank my girlfriend and best friend Meike Hauschildt who persevered by my side through ups and downs although I know that I was not always the easiest person to deal with.

I express my gratitude to Prof. Brian L. Evans for taking a chance on me and guiding me in my doctoral studies. I have learned to appreciate and mimic his clarity of expression and attention to detail. He has my respect and friendship.

I want to thank Dr. Lucio F. C. Pessoa without whose friendship and willingness to engage in discussion, it would have been very difficult for me to finish my doctoral studies and in deed overcome some tumultuous situations in my professional life. I thank Prof. Ross Baldick for the time he put aside early in my research that has helped me clarify my research ideas.

I thank my dissertation committee, Prof. Ross Baldick, Prof. Brian L. Evans, Prof. Gustavo de Veciana, Prof. Robert van de Geijn and Prof. Edward J. Powers for their service and constructive help.

I also thank present and former members of the Embedded Signal Processing Laboratory Gregory E. Allen, Dogu Arifler, Serene Banerjee, Ming Ding, Kyungtae Han, Vishal Monga, Zukang Shen, Ian Wong, Guner Arslan, Niranjan Damera-Venkata, Biao Lu, Wade C. Schwartzkopf and K. Clint Slatton for the camaraderie and helpful research suggestions. I would especially like to thank Ketan J. Mandke and Esther I. Resendiz for the Matlab implementation of a portion of the proposed time domain equalizer design algorithms.

Finally I would like to thank Dr. Lloyd D. Clark and Dr. Terry L. Mayhugh for their helpful suggestions and support.

MILOŠ MILOŠEVIĆ

*The University of Texas at Austin*

*May 2003*

# Maximizing Data Rate of Discrete Multitone Systems using Time Domain Equalization Design

Publication No. \_\_\_\_\_

Miloš Milošević, Ph.D.

The University of Texas at Austin, 2003

Supervisor: Brian L. Evans

Asymmetric Digital Subscriber Line in its standardized versions G.DMT and G.Lite uses discrete multitone modulation (DMT) for data transmission. Orthogonal Frequency Division Multiplexing (OFDM) is a similar modulation standard for wireless transmission that has been adopted in IEEE 802.11a wireless local area network, Digital Video Broadcasting and HYPERLAN/2. The transmission channel induces inter-symbol (ISI) interference and other noise sources. The traditional DMT or OFDM equalizer is a cascade of a time domain equalizer (TEQ) as a single finite impulse response filter (FIR), a fast Fourier transform (FFT) multicarrier demodulator, and a frequency domain equalizer as a one-tap filter bank. The time domain equalizer shortens the transmission channel impulse response to mitigate ISI. Previous TEQ design methods optimize objective functions not directly tied to system bit rate.

I present the equalizer design that maximizes the bit rate of a DMT system at the output of the FFT demodulator. I develop a subchannel Signal-to-Noise

Ratio (SNR) model where the desired signal is formed as the circularly convolved data symbol and the channel impulse response at the input of the FFT and noise is the difference between the received and the desired signal. The received signal also includes the near-end crosstalk, additive white Gaussian noise, analog-to-digital converter quantization noise and the digital noise floor due to finite precision arithmetic. Using the subchannel SNR model, I arrive at the optimal time domain per-tone equalizer filter bank (TEQFB) that maximizes a measure of the ADSL system bit rate. I propose a novel receiver architecture that uses TEQFB and a Goertzel filter bank demodulator at the receiver during data transmission. I also present the design of single FIR equalizer that on average achieves more than 99% of the performance of the TEQFB for the tested standard ADSL carrier serving area loops. Simulation results show that the TEQFB and single FIR outperform the bit rate achieved by the minimum mean-squared error design methods, maximum bit rate approach, and minimum ISI design. The TEQFB also outperforms the least-squares initialized per-tone equalizer (LS PTE) method while the single FIR closely matches LS PTE performance.



# Contents

<b>Acknowledgments</b>	<b>v</b>
<b>Abstract</b>	<b>vii</b>
<b>List of Tables</b>	<b>xiii</b>
<b>List of Figures</b>	<b>xiv</b>
<b>Chapter 1 Introduction</b>	<b>1</b>
1.1 Wireline Communication Systems . . . . .	1
1.1.1 Voiceband transceivers . . . . .	2
1.1.2 Cable transceivers . . . . .	3
1.1.3 Digital subscriber line transceivers . . . . .	6
1.2 Multicarrier Modulation . . . . .	8
1.2.1 Discrete multitone modulation . . . . .	12
1.2.2 Orthogonal frequency division multiplexing . . . . .	16
1.3 Channel Equalization in Discrete Multitone Modulation . . . . .	18
1.4 Bit Rate in Discrete Multitone Modulation . . . . .	20
1.5 Notation . . . . .	21
1.6 Organization of Dissertation . . . . .	24

<b>Chapter 2</b>	<b>Previous Time Domain Equalization Designs</b>	<b>27</b>
2.1	Introduction . . . . .	29
2.2	Minimum Mean-squared Error Method . . . . .	30
2.3	Geometric Signal-to-noise Ratio Method . . . . .	39
2.4	Maximum Shortening Signal-to-noise Ratio Method . . . . .	42
2.5	Minimum Inter-symbol Interference Method . . . . .	51
2.6	Dual-path and Per-tone Equalizer Structures . . . . .	55
2.7	Alternative Channel Equalization Methods . . . . .	59
2.8	Conclusion . . . . .	64
<b>Chapter 3</b>	<b>Subchannel SNR Model</b>	<b>66</b>
3.1	Introduction . . . . .	67
3.2	Transmission Channel and Discrete Multitone Frames . . . . .	68
3.3	Sources of Noise and Interference . . . . .	70
3.3.1	Inter-symbol interference . . . . .	70
3.3.2	Near-end crosstalk, and additive white Gaussian noise . . . . .	72
3.3.3	Analog-to-digital conversion noise and digital noise floor . . . . .	74
3.4	Received and Desired Subchannel Signals . . . . .	76
3.5	Subchannel SNR . . . . .	77
3.5.1	Power of the desired subchannel signal . . . . .	77
3.5.2	Power of the subchannel noise signal . . . . .	78
3.6	Conclusion . . . . .	83
<b>Chapter 4</b>	<b>Efficient Computation of Subchannel SNR Model</b>	<b>85</b>
4.1	Introduction . . . . .	86
4.2	Subchannel SNR Model Numerator . . . . .	87
4.3	Subchannel SNR Model Denominator . . . . .	88
4.3.1	Transmission channel tail component . . . . .	89

4.3.2	Transmission channel head component . . . . .	90
4.3.3	Additive white Gaussian and analog-to-digital conversion noise component . . . . .	93
4.3.4	Near-end crosstalk component . . . . .	93
4.4	Implementation Complexity . . . . .	97
4.4.1	Matrix multiply-update . . . . .	97
4.4.2	Iterative time domain equalizer initialization methods . . . . .	98
4.5	Conclusion . . . . .	101
<b>Chapter 5 Optimal Time Domain Equalizer Design</b>		<b>102</b>
5.1	Introduction . . . . .	103
5.2	Bit Rate as Function of Time Domain Equalizer . . . . .	104
5.3	Impact of Transmission Delay on Time Domain Equalizer Design . . . . .	105
5.4	Time Domain Equalizer Filter Bank . . . . .	106
5.5	Single Time Domain Equalizer for Data-carrying Subchannels . . . . .	109
5.5.1	Solution space . . . . .	109
5.5.2	Fractional bit rate as function of the time domain equalizer taps	110
5.5.3	Single time domain equalizer design algorithm . . . . .	113
5.6	Computational Complexity . . . . .	117
5.6.1	Initialization cost . . . . .	117
5.6.2	Data transmission complexity . . . . .	117
5.7	Conclusion . . . . .	119
<b>Chapter 6 Multichannel Time Domain Equalizer Design</b>		<b>123</b>
6.1	Introduction . . . . .	123
6.2	Background . . . . .	125
6.3	Composite Shortening Signal-to-Noise Ratio . . . . .	126
6.4	Multichannel Time Domain Equalizer . . . . .	127

6.5 Conclusion . . . . .	128
<b>Chapter 7 Performance Evaluation</b>	<b>130</b>
7.1 Introduction . . . . .	131
7.2 Simulation Parameters . . . . .	132
7.3 Simulation Results . . . . .	136
7.4 Conclusion . . . . .	145
<b>Chapter 8 Conclusions</b>	<b>152</b>
8.1 Summary . . . . .	152
8.2 Future Work . . . . .	157
<b>Bibliography</b>	<b>162</b>
<b>Vita</b>	<b>176</b>

# List of Tables

1.1	xDSL Technologies [1] . . . . .	7
1.2	ADSL and VDSL DMT System Parameters . . . . .	16
1.3	IEEE 802.11a wireless LAN OFDM System Parameters [2] . . . . .	17
4.1	SNR Component Initialization Requirements Matrix Multiply-update Algorithm . . . . .	98
4.2	SNR Component Initialization Requirements . . . . .	99
4.3	Memory Requirements: Transmission Channel, Noise and FFT Pa- rameters . . . . .	99
4.4	Number of Multiply-accumulate Operations for Proposed Iterative Algorithms vs. Matrix Multiply-update . . . . .	101
5.1	Data Transmission Computational Complexity . . . . .	118
7.1	Highest Achieved Bit Rates for Time Domain Equalizer Filter Bank	139
7.2	Performance of Simulated Time Domain Equalizer Methods vs. Time Domain Equalizer Filter Bank . . . . .	140
7.3	Composite Shortening Signal-to-noise Ratio vs. Joint Maximum Signal- to-noise Ratio . . . . .	144

# List of Figures

1.1	Block Diagram of Cable Broadband Access . . . . .	5
1.2	Block Diagram of Digital Subscriber Line Broadband Access . . . . .	9
1.3	Twisted Copper Pair Technologies Spectral Compatibility . . . . .	10
1.4	Channel Bandwidth and Multicarrier Modulation [3] . . . . .	11
1.5	Multicarrier Modulation . . . . .	11
1.6	Discrete Multitone Modulation [3] . . . . .	13
1.7	Block Diagram of Discrete Multitone Transceiver Including Traditional Time Domain Equalizer Architecture and Alternative Per-Tone Equalizer Architecture . . . . .	14
2.1	Minimum Mean-squared Error Time Domain Equalizer Design Block Diagram . . . . .	30
2.2	Channel Impulse Response and Shortened Channel Impulse Response with Respect to the Target Window (adapted from [3]) . . . . .	43
2.3	Per-tone Equalizer Architecture . . . . .	57
3.1	Received Signals in DMT . . . . .	73
4.1	Algorithm for Efficient Computation of Subchannel SNR Numerator Hessian Matrix . . . . .	88

4.2	Algorithm for Efficient Computation of Subchannel SNR Denominator Hessian Matrix Contribution of Channel Tail Component . . . . .	91
4.3	Algorithm for Efficient Computation of Subchannel SNR Denominator Hessian Matrix Contribution of Channel Head Component . . . . .	92
4.4	Algorithm for Efficient Computation of Subchannel SNR Denominator Hessian Matrix Contributions of White Gaussian Noise and Analog-to-Digital Conversion Noise . . . . .	94
4.5	Algorithm for Efficient Computation of Subchannel SNR Denominator Hessian Matrix Contributions of Near-end Crosstalk . . . . .	96
4.6	General Matrix Multiply-update Algorithm . . . . .	97
4.7	Hermitian Symmetric Matrix Multiply-update Algorithm . . . . .	98
4.8	Computational Complexity of Proposed Iterative Initialization of Subchannel SNR Numerator and Denominator Hessian Matrices vs. Complexity of Straight Matrix Multiply-update . . . . .	100
5.1	Block Diagram of Discrete Multitone Receiver with Time Domain Equalizer Filter Bank Architecture . . . . .	108
5.2	Evaluation of Fractional and Integer Bit Rates for All Values of Time Domain Equalizer with Two Coefficients . . . . .	111
5.3	Evaluation of Fractional and Integer Bit Rates for All Values of Time Domain Equalizer with Three Coefficients . . . . .	112
5.4	Parametric Equation for Single-ratio Maximization . . . . .	115
5.5	Proposed Single Time Domain Equalizer Design Algorithm . . . . .	121
5.6	Memory Requirements of Proposed Time Domain Equalizer Design Methods During Data Transmission . . . . .	122
6.1	Proposed Maximum Composite Shortening Signal-to-Noise Ratio Multichannel Time Domain Equalizer Design Algorithm . . . . .	129

7.1	Standard Carrier Area Service Loops . . . . .	133
7.2	Phase and Magnitude Response of the Infinite Impulse Response Filter Modelling Discrete Multitone Transmit and Receive Filters . . .	134
7.3	Comparison of Measured Subchannel SNR and Subchannel SNR model on Carrier Service Area Loop 2 for Time Domain Equalizer Length $M = 32$ . . . . .	137
7.4	Simulation Data Rates Achieved on Carrier Service Area Loop 2 vs. the Length of Time Domain Equalizer . . . . .	138
7.5	Simulation Data Rates Achieved on Carrier Service Area Loop 5 vs. Length of Channel Prefix . . . . .	141
7.6	Simulation Data Rates of the Proposed Single Time Domain Equalizer Design Achieved on Carrier Service Area Loop 1 vs. Transmission Delay Design Parameter . . . . .	142
7.7	Signal-to-noise Ratio of Proposed Single Time Domain Equalizer Design vs. Maximum Bit Rate Method and Minimum-ISI Method for Carrier Area Service Loop 4 . . . . .	148
7.8	Maximization of Composite Shortening Signal-to-Noise Ratio vs. Iteration . . . . .	149
7.9	Simulation Data Rates per Channel for Multichannel Time Domain Equalizer for Standard Carrier Area Service Loops . . . . .	150
7.10	Maximum Composite Signal-to-noise Ratio Method Channel Shortening of Carrier Area Service Loops 1–8 . . . . .	151



# Chapter 1

## Introduction

### 1.1 Wireline Communication Systems

Today's customer has a variety of technologies to choose from to connect to a number of competing broadband access service providers. The telephone copper twisted pair network offers access to the Internet through the voiceband dial-up modems at rates up to 56 kbps and telephone voice service. In addition, the telephone network offers high-speed broadband access in the form of digital subscriber line (DSL) technologies, such as the high-speed DSL version 2 at 1.544 Mbps to and from the service provider and asymmetric DSL (ADSL) at up to 8 Mbps from and 1 Mbps to the service provider. A higher speed version of ADSL, known as very-high speed DSL, runs over much shorter line lengths and offers rates up to 23 Mbps from the service provider. Sections 1.1.1 and 1.1.3 describe voiceband and DSL modems in more detail.

Coaxial cable technologies enable cable TV services including TV interactive service, access to the Internet, voice-over Internet protocol (VoIP) and always-on service at connection speeds ranging from 0.5 to 1.5 Mbps. Cable companies have recently added video-on-demand services. Section 1.1.2 delves into cable technology

in greater detail.

DSL and voiceband modems provide a dedicated link from the customer's premises to the central office i.e. one-to-one connection, while the cable modem accesses a shared cable used simultaneously by many customers thus providing a many-to-one connection. Nonetheless, both access technologies support Transmission Control Protocol/Internet Protocol (TCP/IP) and allow deployment of a wireless local area network (LAN) in customer premises.

Wireless broadband access has been deployed early on using a two-way multichannel multipoint distribution service utilizing 150 MHz bandwidth centered at 2.5 GHz. The multichannel multipoint distribution systems available are based on technology used for the coaxial cable and as such are not specifically designed for the multipath channel. IEEE 802.16 standardized wireless systems in the 10 to 66 GHz range that are characterized by high data rates and a short access range. The systems are generally known as local multipoint distribution service. IEEE 802.11 standards reserve bandwidths centered at carrier frequencies of 2.4 and 5 GHz for the wireless local area networks targeting data rates from 6 to 54 Mbps. Wireless broadband access offers VoIP, TV programming and Internet access.

### **1.1.1 Voiceband transceivers**

The telephone network was designed to carry speech signals. The bandwidth needed for voice transmission is approximately 3.5 kHz. Through various modulation techniques it is possible to transmit data signals through the telephone network, as well. A number of standards ranging from V.21 to V.90 have been published dealing with data transmission over the telephone network with each successive standard enabling a higher data rate. Voiceband modems started with V.21 in the 1970s with a bit rate of less than 300 bps using frequency shift keying and had the ability to support

duplex<sup>1</sup> operations. V.22 and V.22 *bis* followed with the rate of 2400 bps using phase shift keying and 16 quadrature amplitude modulation (QAM), respectively, and also allowed duplex operation. V.26 *ter* was the first voiceband modem to employ separation of transmissions from the central office to the customer (downstream) and from the customer to the central office (upstream) using echo cancellation. V.27 doubled the rate to 4800 bps over a 4-wire telephone interface allowing duplex operation and including a 75 symbol/s feedback channel for error control. V.29 in 1976 again doubled the rate to 9600 bps using phase shift keying and amplitude modulation. V.29 also allowed rates of 7800 bps and 4800 bps as a backup if 9600 bps was not possible. As Drajić and Bajić [4] note, up to this point error control coding and modulation were designed separately. V.32 in 1984 allowed duplex operation and used Trellis coded modulation at the same rate of 9600 bps as V.29. V.32 utilized echo cancellation thus achieving upstream and downstream channel separation. V.33 in 1988 achieved 14400 bps using QAM with Trellis coded modulation and a 12000 bps option. V.34 communicated up to 33600 bps using QAM with Trellis coded modulation and allowed 14 data rate options starting from 2400 bps to 33600 bps that would be selected based on the channel conditions. V.34 allows full duplex or half-duplex transmission with echo cancellation. V.90 modem, which was standardized in 1998 allowed asymmetric connection, 56000 bps downstream and 33600 bps upstream. If a V.90 connection cannot be established, then a V.34 connection is attempted. A V.90 modem operates at 8000 symbols/s. Each symbol carries an eight-bit code word; however, only 7 bits carry information.

### 1.1.2 Cable transceivers

Cable television was first offered to the public in 1948 to provide TV service to viewers in remote rural areas [5]. The service was provided through a coaxial cable.

---

<sup>1</sup>A duplex system allows two-way simultaneous communication.

The number of United States households with access to the cable network is estimated at 99 million [6] as of 2001. The cable network allocates the bandwidth of 54-550 MHz for broadcasts (downstream) of programming content. The upstream is allocated the frequency band from 5-42 MHz. The allocated bandwidth for both upstream and downstream is divided further into 6 MHz-wide channels. In the standard cable TV architecture, the downstream provides the TV programming, while the upstream is used for interactive cable TV service where the subscribers can be up to 80 km away. Cable is a shared medium; that is, all users have to share the available bandwidth. The upstream path is the noisier of the two due to interference from poorly terminated subscriber equipment, household appliances, and strong radio transmitters [7]. This was not a concern in low data rate mode of interactive cable TV service using the upstream frequency band [8]; however, it becomes a concern for the cable modem technology that is using the same band at much higher data rate.

The existing coaxial cable TV network provided fertile ground for the development of a technology that multiplexes various types of content delivered over the same coaxial cable. Cable modem technology offers always-on access to the Internet, delivery of TV programming to the set-top box, and voice over the Internet protocol. The data rate available over a single downstream channel is approximately 30 Mbps and 1.5 Mbps upstream over a single upstream channel. The downstream is based on the 64-QAM and 256-QAM modulation where each symbol carries 6 bits and 8 bits, respectively. The upstream uses 16-QAM where each symbol carries 2 bits. The choice of modulation for upstream was dictated by the noise present in the upstream frequency band. Research cited in [6] based on statistical models predicts that up to 400 households can be connected to a single 6 MHz channel without traffic congestion caused by the shared cable medium.

Figure 1.1 shows a block diagram of a cable network connection where the

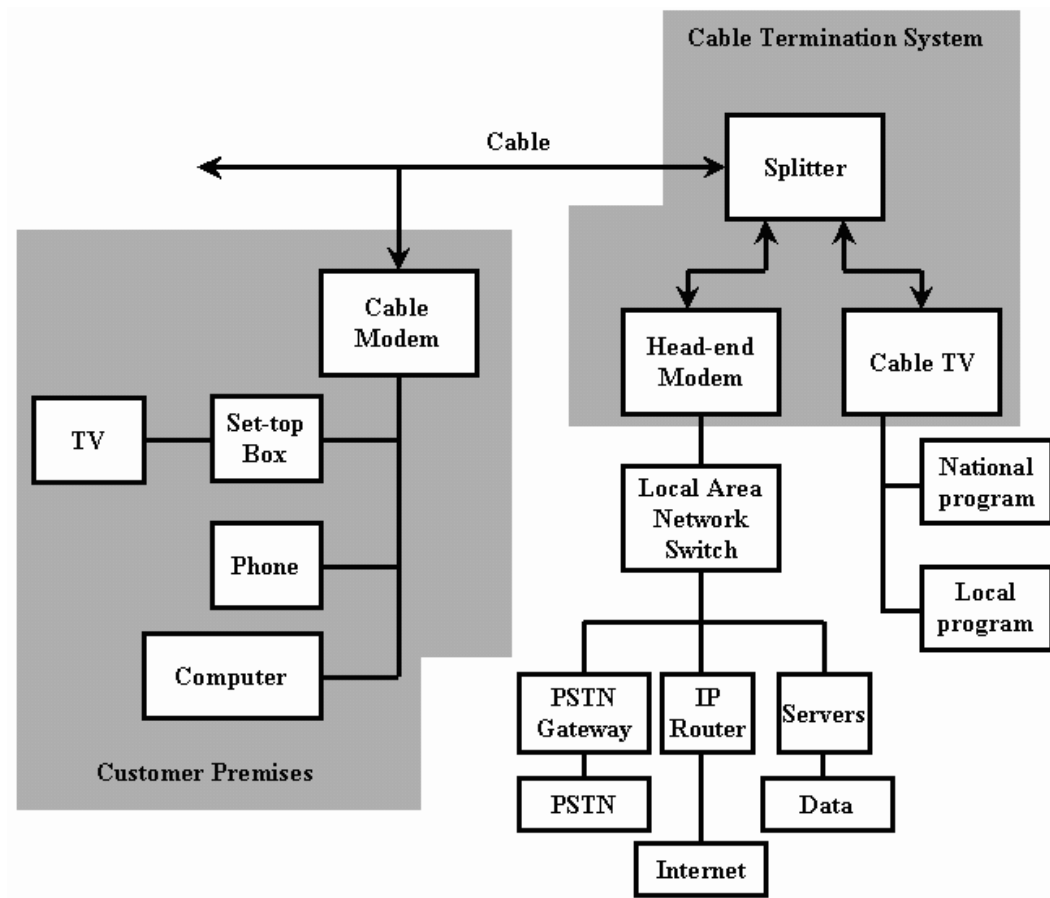


Figure 1.1: Block Diagram of Cable Broadband Access: PSTN - Public Switched Telephone Network

customer premises cable modem communicates with the head-end cable modem and at the same time receives TV programming and sends data from the customer. The standards work has proceeded in several international and corporate bodies. The European standard for set-top boxes and cable modems was produced by the Digital Audio Video Council (DAVIC). The IEEE 802.14 working group began the cable standards work in 1994. The Multimedia Cable Network System (MCNS) consortium also began cable standardization in 1995 and produced Data Over Cable Service Interface Specifications (DOCSIS) standards with versions 1.0 approved by

the International Communications Union in 1998 and 1.1 approved in 1999. DOCSIS 1.1 improved upon DOCSIS 1.0 mainly in the area of Quality of Service with the intent to enable VoIP [9]. By 2000 IEEE 802.14 had disbanded, thus leaving DOCSIS as the cable standard used by the cable industry. DOCSIS 2.0 was approved in December 2002, which adds a greater upstream bandwidth to the user with 30 Mbps achievable (shared) rate.

### 1.1.3 Digital subscriber line transceivers

Digital subscriber line (DSL) technologies are capable of utilizing the bandwidth of the copper twisted pair lines beyond the voice band (0-4 kHz) used by the voice telephone services. DSL bridges what is commonly called the “last mile” [10], to the optical fiber deployed close to the neighborhood. Although thought of as an interim solution, DSL will be of interest for a number of years as the deployment of the direct fiber optic link has been slow and limited to urban areas [1]. It was recently shown that the US local telephone carriers loose telephone customers at a rate of 5-6% per year to new cable services that include voice carried over the Internet in addition to TV entertainment content and Internet access [11]. In order to grow their customer base the telephone companies need to upgrade their copper network for high-bandwidth content with higher entertainment value. High bandwidth over the existing copper lines is what DSL can deliver to the telephone companies. Recent studies [12] suggest that in the United States at the end of the 3<sup>rd</sup> quarter of 2002, the market share for wireline broadband services is 2:1 in favor of cable modems; however, there are indications that the proportion changes to 5:1 in favor of DSL worldwide [13].

There are several versions of xDSL technologies where “x” stands for one of those technologies. The following listing traces the exposition on xDSL as given in [1, 14]. The predecessor of xDSL is the physical layer of ISDN (integrated services

Table 1.1: xDSL Technologies [1]: (NA) - North America, (E) - Europe, DS - downstream, US - upstream, #p - Number of copper twisted pairs, CAP - carrierless amplitude-phase modulation, PAM - pulse amplitude modulation, 2B1Q - two bit per quaternary modulation, DMT - discrete multitone modulation, QAM - Quadrature Amplitude Modulation

xDSL	Modulation	Data rates (Mbps)	Bandwidth (MHz)	#p
HDSL	2B1Q (4-PAM)	1.544 (NA)	0.193	2
		2.320 (E)	0.580	1
		2 x 1.168 (E)	0.292	2
		3 x 0.784 (E)	0.196	3
SDSL	16-PAM	$\leq 2.312$	$<0.386$	1
ADSL	DMT	$\leq 6.144$ (8.192) DS	1.104	1
	$< 256$ tones	$\leq 0.786$ (0.640) US		
ADSL lite	DMT with	$\leq 1.536$ DS	0.552	1
	$< 128$ tones	$\leq 0.512$ US		
VDSL	QAM/CAP or DMT $<4096$ tones	$\leq 13$ (NA) sym.	12	1
		$\leq 23/3$ (NA) asym.		
		$\leq 14.5$ (NA) sym.		
		$\leq 23/4$ (NA) asym.		

digital network) developed in 1980s with a data rate of 160 kbps at distances of up to 18,000 ft [15]. Subsequently, high-bit-rate DSL (HDSL) was developed with the data rate of 1.544 kbps and using the same signal processing techniques as ISDN but at 5 times the speed. The third xDSL system is called asymmetric DSL (ADSL). ADSL was standardized in 1998 and has been enjoying a rapid increase in worldwide deployment. A very-high-speed DSL (VDSL) is currently being standardized and it is intended to bridge short lengths (shorter than 4500 ft) at high speeds (up to 23 Mbps from the network to the residential customer). Symmetric DSL (SDSL) is a version of HDSL over a single pair achieving up to 800 kbps. Table 1.1 [1] summarizes different xDSL technologies.

Figure 1.2 shows the architecture of typical DMT DSL broadband access. The central office is connected to customer premises through a twisted copper pair

line. The function of a Digital Subscriber Line Access Multiplexer (DSLAM) is to queue data arriving from multiple DMT DSL connections to the network interface. Figure 1.3 shows the overlap of frequency bands assigned to different services that use the copper twisted pair. Different services operate on different copper twisted pairs emanating from the central office. The spectral overlap of different services leads to frequency domain interference on copper twisted pairs in close proximity and is a major source of noise.

## 1.2 Multicarrier Modulation

Multicarrier modulation (MCM) is a form of frequency division multiplexing used to transmit data through a physical medium, e.g. wires, air and water. The available bandwidth of a communication channel, such as the twisted-pair copper media or a wireless channel, is divided into numerous subchannels or bins as shown in Figure 1.4. Bingham [16] discusses the basics of the MCM and the reasons for its emergence as the modulation for broadband applications. I will use his notation here to introduce MCM. The serial data stream consists of  $Mf_{\text{symbol}}$  bits per second (bps); thus, every  $\frac{1}{f_{\text{symbol}}}$  seconds a block of  $M$  bits is being transmitted. This data stream would typically be provided by a higher protocol layer to the physical layer for modulation. The  $M$  bits are parallelized into  $N_c$  groups of  $m_n$  bits, which are coded and assigned to the carrier  $f_{c,n}$  for transmission. The carriers are spaced in increments of  $\Delta f$  up to the available bandwidth of the system. So,

$$f_{c,n} = n\Delta f \quad (1.1)$$

for  $n = [n_1, \dots, n_n]$  and

$$M = \sum_{n=n_1}^{n_n} m_n \quad (1.2)$$

where  $N_c = n_n - n_1 + 1$ . The modulated signals are summed together, passed through a spectral shaping transmit filter and sent to the physical medium for transmission.



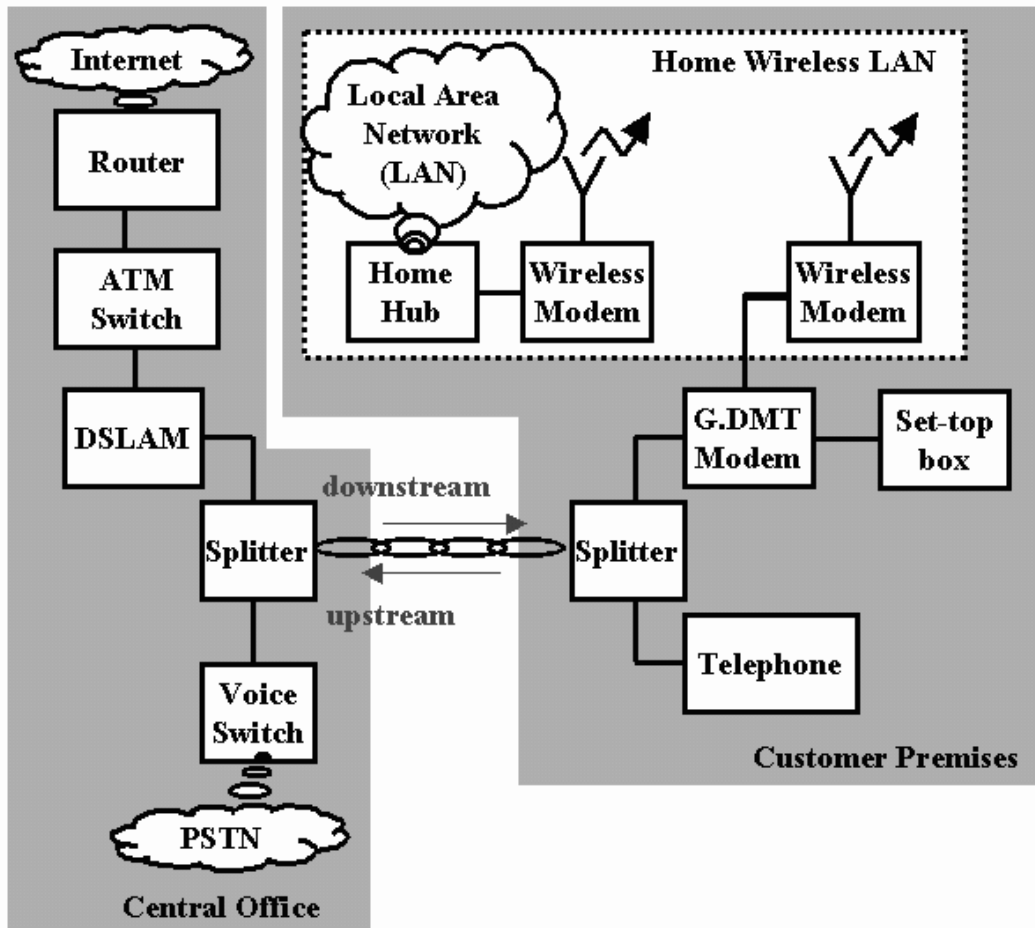


Figure 1.2: Block Diagram of Digital Subscriber Line Broadband Access: DSLAM - Digital Subscriber Line Access Multiplexer, PSTN - Public Switched Telephone Network, DMT - Discrete Multitone Modulation, ATM - Asynchronous Transfer Mode, ISDN - integrated services digital network,

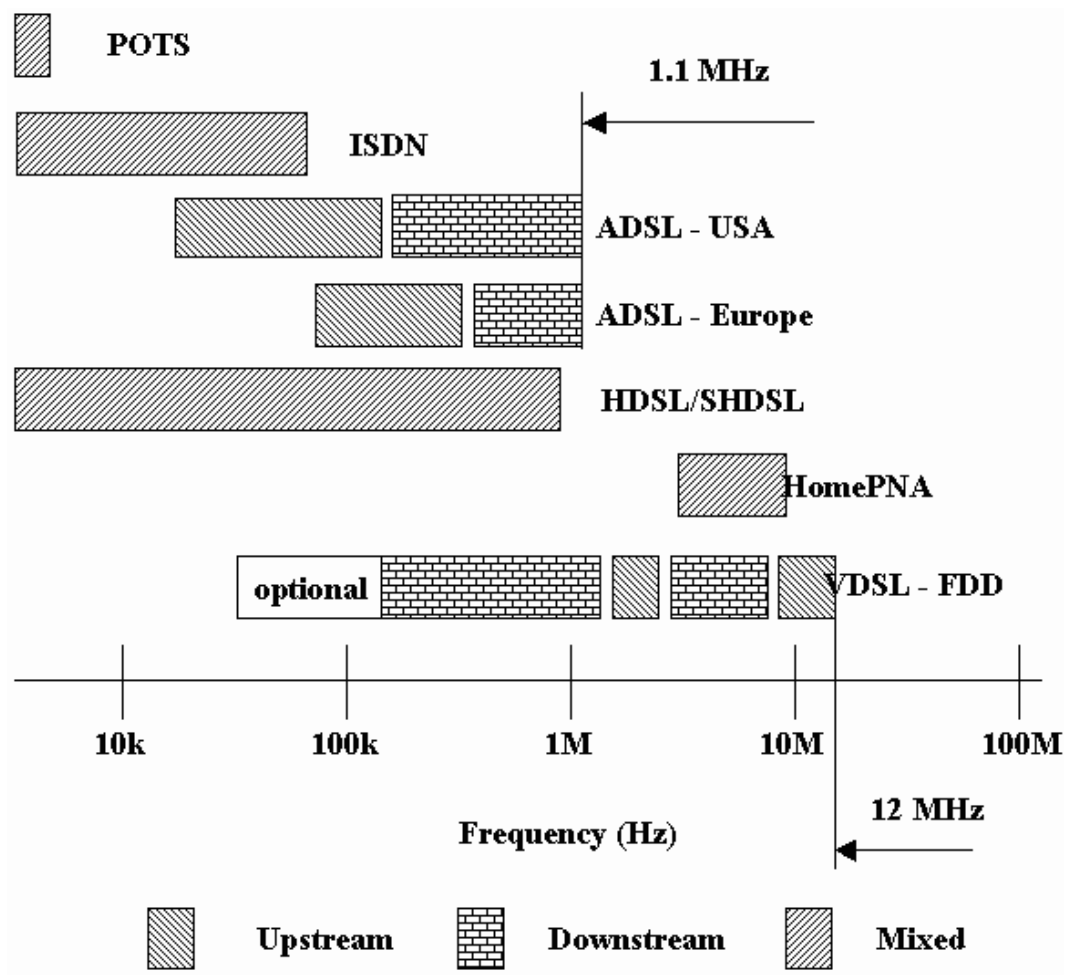


Figure 1.3: Twisted Copper Pair Technologies Spectral Compatibility: POTS - Plain Old Telephone Service, ADSL - Asymmetric Digital Subscriber Loop, VDSL - Very-high-speed Digital Subscriber Loop, HDSL - High-bit-rate Digital Subscriber Loop, SHDSL - Single-pair HDSL, FDD - Frequency Division Duplex, HomePNA - Home Phone Network Access

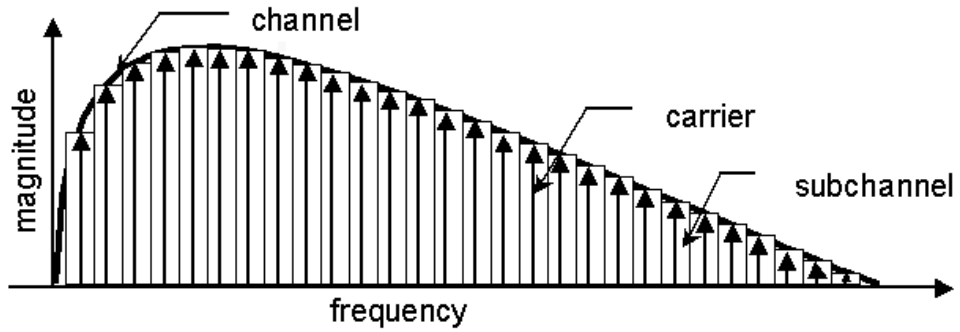


Figure 1.4: Channel Bandwidth and Multicarrier Modulation [3]

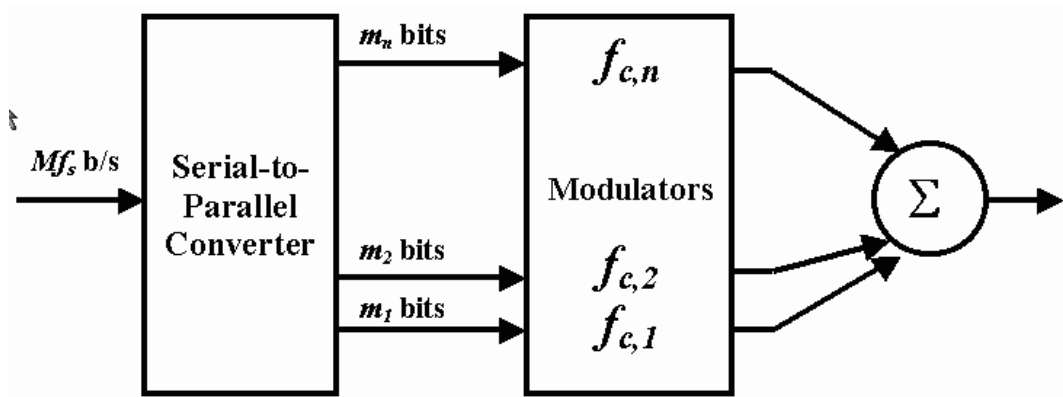


Figure 1.5: Multicarrier Modulation [16]

Decoding is performed at the receiver on each subchannel after they have been separated out of the received signal by the demodulator block. The separation of the subchannels at the receiver can be achieved in principle by a bank of sharp narrow-band filters. However, due to the difficulty of implementing sharp filters and the need to limit the time it takes to transmit  $M$  bits, the subchannel transmit filters overlap in the frequency domain. The subchannel transmit filters are designed such that they add to a flat transmit spectral profile, and under perfect demodulation one subchannel does not interfere with other subchannels. In some non-standard MCM implementations, successive symbols also overlap in the time domain such as discrete wavelet multitone (or discrete overlapped multitone) modulation [17]. The

reason to allow overlap of time domain symbols is to encourage the frequency domain containment of subchannels and reduce the leakage of energy into neighboring channels due to imperfections in receivers and transmitters and channel effects.

The reasons why the MCM has gained popularity are [1, 16, 18, 19]:

- With MCM it is relatively easy to shape the transmit spectrum according to the water-pouring algorithm.
- Channel equalization is significantly simpler when compared to single-tone systems like quadrature amplitude modulation.
- The long duration of a symbol in MCM technologies like DMT makes them more resistant to impulsive noise.
- Narrowband interferers affects only a limited number of subchannels that can be turned off according to a water-pouring algorithm. A similar disturbance in single-tone systems would require implementation of difficult notch filtering.
- Advancements in digital signal processing, e.g. in digital signal processor (DSP) computation and input/output capabilities and in higher precision analog-to-digital and digital-to-analog converters, made it possible to implement some variants of MCM.

In Section 1.2.1, I explore discrete multitone modulation used in ADSL, while in Section 1.2.2, I discuss the development and usage of orthogonal frequency division multiplexing used in wireless systems.

### **1.2.1 Discrete multitone modulation**

Discrete multitone (DMT) is a wireline multicarrier modulation method in which the available bandwidth of a communication channel, such as twisted-pair copper media, is divided into numerous subchannels or bins via a fast Fourier transform (FFT).

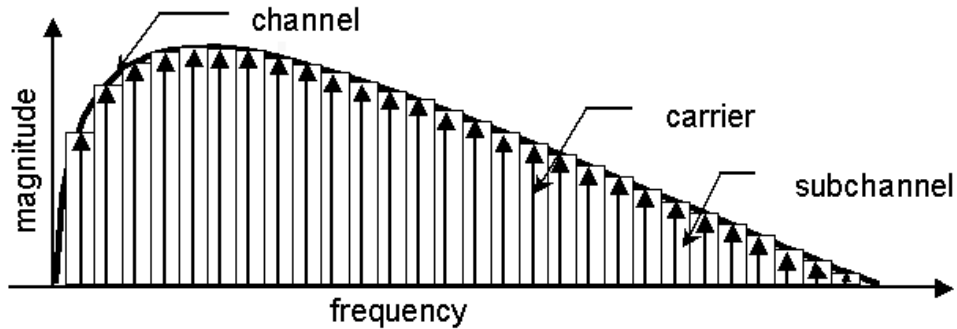


Figure 1.6: Discrete Multitone Modulation has subchannels that are 4.3125 kHz wide in Asymmetric and Very-high-rate Digital Subscriber Line [3].

DMT has been adopted for wireline applications in the US by the American National Standards Institute (ANSI) T1.413-1998 standard (Asymmetric Digital Subscriber Loop ADSL standard) [20], and internationally by the International Telecommunications Union G.DMT (G.992.1) [21] and G.Lite (G.992.2) [22] ADSL standards. DMT is figuring prominently in VDSL standard proposals [23, 24, 25].

G.DMT ADSL is a full duplex system, i.e. data simultaneously flows downstream from a central office to a remote terminal, and upstream in the opposite direction. In the G.DMT ADSL standard, FFT/IFFT is used to generate up to 256 separate 4.3125 kHz wide downstream subchannels from 0 to 1.1 MHz. The first six subchannels in the echo-cancelled ADSL and the first 32 channels in the frequency division multiplexed ADSL are not used for data transmission. Likewise, the FFT/IFFT is used to generate 26 upstream subchannels up to 138 kHz. Subchannels in the range 0 to 26 kHz are not used in ADSL so as not to interfere with the voiceband channel (0-4 kHz) and the ISDN band (4-26 kHz). Each DMT subchannel is nearly independent of the other subchannels, and the degree of independence increases with the number of subchannels [26].

Figure 1.7 shows a simplified block diagram of a DMT transceiver. The input bit stream on the transmitter is mapped into a  $\frac{N}{2} \times 1$  complex vector  $\mathbf{X}^i$  at time

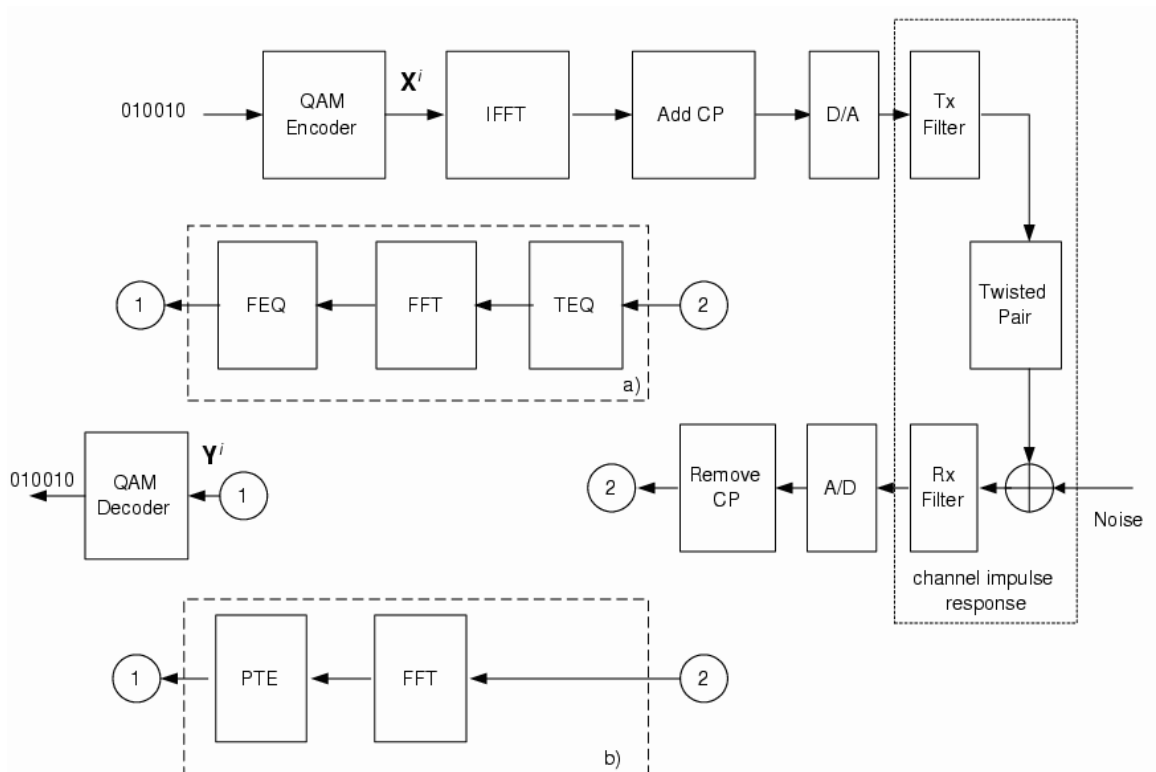


Figure 1.7: Block Diagram of Discrete Multitone Transceiver Including Traditional Time Domain Equalizer Architecture and Alternative Per-Tone Equalizer Architecture.

$i$  using Quadrature Amplitude Modulation (QAM). The bit stream is partitioned, mapped into complex values and assigned to subchannels based on the available SNR in each subchannel and the desired bit error rate. This process is called bit loading, and in G.DMT, it is designed with the  $10^{-7}$  bit error rate in mind. Vector  $\mathbf{X}^i$  is mirrored into its conjugate-symmetric copy  $\tilde{\mathbf{X}}^i$ , and both are jointly sent to the input of the IFFT block. Each input entry is modulated by the IFFT block into a different frequency band (subchannel) with the carrier frequency lying in the center of the band. The number of real-valued data obtained after the IFFT is  $N$ . A guard period of  $\nu$  samples is added before digital-to-analog (D/A) conversion and transmission. A spectrally shaped channel impulse response longer than  $\nu + 1$  causes inter-carrier interference (ICI) and inter-symbol interference (ISI). ISI refers to the mixing of energy belonging to neighboring symbols during transmission, whereas ICI refers to a similar process for the subchannels. If the length of the channel impulse response is less than or equal to  $\nu + 1$ , adding a guard period of  $\nu$  samples at the beginning of a DMT frame will prevent the occurrence of ISI. If the guard period is chosen to be the copy of the last  $\nu$  samples of a DMT frame and the length of the channel impulse response is less than or equal to  $\nu + 1$ , then ICI is eliminated as well. This choice of the guard period is also known as a cyclic prefix (CP) and is adopted in ADSL standards and proposed for DMT VDSL [27]. This grouping of  $N + \nu$  samples is referred to as a frame. Frames are sent sequentially one after the other. The CP of  $\nu$  samples lowers the data rate by a factor of  $N/(N + \nu)$ . For ADSL downstream transmission,  $N = 512$  and  $\nu = 32$  samples, whereas for ADSL upstream transmission,  $N = 64$  and  $\nu = 4$  samples. In VDSL,  $N$  is up to 8192 and  $\nu$  is the same fraction ( $\frac{1}{16}$ ) of  $N$  as in ADSL. In a conventional receiver, the specific cascade of operations is A/D conversion, time-domain equalization (TEQ) using a finite impulse response (FIR) filter, removal of the cyclic prefix, multicarrier demodulation using the FFT, QAM decoding of each used subchannel, and error

Table 1.2: ADSL and VDSL DMT System Parameters

	ADSL	VDSL
<b>Data Rate</b>	up to 8 Mbps	up to 22 Mbps
<b>Modulation</b>	DMT	DMT
<b>#subchannels</b>	256	up to 4096
<b>#pilots</b>	1	1
<b>Frame Duration</b>	246 $\mu$ s	246 $\mu$ s
<b>Cyclic Prefix</b>	14 $\mu$ s	14 $\mu$ s
<b>Subchannel spacing</b>	4.3125 kHz	4.3125 kHz
<b>Bandwidth</b>	1.104 MHz	12 MHz

correction. The TEQ is designed during modem initialization. The demodulation of the received DMT frame is done by the FFT block, after which the frequency domain equalizer (FEQ) completely removes the phase and frequency distortion of the channel. Subsequently, this fully equalized signal is decoded using a QAM decoder resulting in an estimate of the transmitted complex symbol  $\mathbf{Y}^i$ , which is further resolved into the corresponding bit stream. Table 1.2 summarizes some of the ADSL and VDSL system parameters.

### 1.2.2 Orthogonal frequency division multiplexing

Orthogonal Frequency Division Multiplexing (OFDM) is an MCM technology that similar to DMT. OFDM has been gaining acceptance for various wireless applications and has been adopted in IEEE 802.11a wireless LAN [28], Digital Video Broadcasting (DVB) [29] and HYPERLAN/2 [30] standards. OFDM is based on the principle of frequency division multiplexing whereby the available transmission bandwidth is divided into numerous nearly orthogonal subchannels. As in the DMT modulation, the OFDM modulation is efficiently achieved using an FFT/IFFT pair. An OFDM symbol consists of the data and the cyclic prefix. ISI/ICI are eliminated using the cyclic prefix defined similarly to the cyclic prefix of DMT. The signal pro-



Table 1.3: OFDM System Parameters ([2]):BPSK - Binary phase Shift Keying, QPSK - Quadrature Phase Shift Keying, QAM - Quadrature Amplitude Modulation

<b>Data Rate</b>	6, 9, 12, 18, 24, 36, 48, 52 Mbps
<b>Modulation</b>	BPSK, QPSK, 16-QAM, 64-QAM
<b>Coding rate</b>	$\frac{1}{2}, \frac{2}{3}, \frac{3}{4}$
<b>No. of subchannels</b>	52
<b>No. of pilot tones</b>	4
<b>Symbol Duration</b>	4 $\mu$ s
<b>Cyclic Prefix</b>	800 ns
<b>Subchannel spacing</b>	312.5 kHz
<b>3 dB bandwidth</b>	16.56 MHz
<b>Channel Spacing</b>	20 MHz

cessing operations in an OFDM system are very similar to those in a DMT system, although the order of operations is often different. As a wireless technique, OFDM confronts the multipath delay spread so the received symbol is a summation of time-shifted replicas of the transmitted symbol. As long as the delay spread (length of the multipath channel) is shorter than the cyclic prefix, ISI and ICI are not present [31]. The multipath fading channel present in wireless communications has deep nulls in certain frequency bands. The nulls render the OFDM subchannels in the same frequency band unable to carry data. In order to mitigate the effects of the nulls, OFDM requires forward error correction techniques and frequency-domain interleaving, which spread the information across various subchannels and thus, increasing the probability of correct data decoding [2]. An OFDM receiver employs time domain equalization (filtering) to reduce the channel state dimension, to simplify decoding and/or to reduce the delay spread of the multipath channel. The delay spread can also be mitigated by installing more base stations.

Table 1.3 [2] summarizes the parameters standardized for OFDM in [28]. The key parameter is the length of the cyclic prefix determined based on the desired resilience to ISI in various channel environments (homes, factories, etc.). The length

of the symbol is determined from the length of the cyclic prefix coupled with the requirement that the power of the cyclic prefix amounts to less than 1 dB of the total power of the symbol. Convolutional codes are used as appropriate with the desired coding rate. The 200 MHz spectrum centered at 5 GHz allows 8 channels with 20 MHz channel spacing.

### 1.3 Channel Equalization in Discrete Multitone Modulation

Figure 1.7 shows demodulation and equalization in a DMT receiver. Here I explain the signal path in Fig. 1.7(a), while the signal path Fig. 1.7(b) will be described as a part of the literature review in Chapter 2. The equalization in DMT is based on a two-step process. In the first equalization step, a time domain equalizer (TEQ) finite impulse response filter (FIR) is tasked with eliminating the ISI and ICI from the received DMT frame. The ISI and ICI will be present in the received frame if the channel impulse response is longer than  $\nu + 1$  samples. The convolution of the TEQ and channel impulse response results in a shortened channel impulse response that has an extent smaller than or equal to  $\nu + 1$  samples. Subsequently, the linear convolution of the shortened channel impulse response and a DMT frame is converted into their circular convolution by virtue of having repeated DMT frame samples present in the CP [20]. Demodulation, which is performed using an FFT, transforms this circular convolution into a multiplication of complex sequences in the frequency domain [32]. In the second equalization step, division by the frequency domain response of the shortened channel impulse response (known as frequency domain equalization or FEQ), fully equalizes the signal thus removing the phase and amplitude distortion imparted by the channel.

I will present a simplified example in order to illustrate the ISI/ICI creation

and removal. Let the useful data be  $\mathbf{x}^T = [1 \ 2 \ 3]^T$  and let the cyclic prefix have a length of one. Let the transmission channel impulse response be  $\mathbf{h}^T = [4 \ 5 \ 6]^T$ . Hence, the channel impulse response of length 3 is longer than the length of the cyclic prefix  $+1 = 2$  in this example. Let us also assume that the TEQ is not present in the receive path. The received frame is

$$\begin{aligned}
\mathbf{y} &= \underbrace{\begin{bmatrix} 0 & 1 & 0 & 0 \\ 0 & 0 & 1 & 0 \\ 0 & 0 & 1 & 1 \end{bmatrix}}_{\text{CP removal}} \underbrace{\begin{bmatrix} 4 & 0 & 0 & 0 \\ 5 & 4 & 0 & 0 \\ 6 & 5 & 4 & 0 \\ 0 & 6 & 5 & 4 \end{bmatrix}}_{\mathbf{H}} \underbrace{\begin{bmatrix} 0 & 0 & 1 \\ 1 & 0 & 0 \\ 0 & 1 & 0 \\ 0 & 0 & 1 \end{bmatrix}}_{\text{CP add}} \underbrace{\begin{bmatrix} 1 \\ 2 \\ 3 \end{bmatrix}}_{\mathbf{x}} \\
&= \underbrace{\begin{bmatrix} 4 & 0 & 5 \\ 5 & 4 & 6 \\ 6 & 5 & 4 \end{bmatrix}}_{\tilde{\mathbf{H}}} \underbrace{\begin{bmatrix} 1 \\ 2 \\ 3 \end{bmatrix}}_{\mathbf{x}} \tag{1.3}
\end{aligned}$$

where  $\mathbf{H}$  is the channel convolution matrix. The CP addition operation at the transmitter and CP removal operation at the receiver are represented using matrix operands. From (1.3) it is noticeable that  $\tilde{\mathbf{H}}$  is not a circulant matrix, thus, the linear convolution of the channel impulse response  $\mathbf{h}$  and the frame  $\mathbf{x}$  is  $\mathbf{y} = \mathbf{h} * \mathbf{x}$ , and it follows  $\mathcal{F}(\mathbf{y}) \neq \mathcal{F}(\mathbf{h})\mathcal{F}(\mathbf{x})$  where  $\mathcal{F}(\cdot)$  is a discrete Fourier transform operator. Hence, the channel distortions cannot be removed in the frequency domain using a 1-tap complex FEQ filter per complex value of  $\mathcal{F}(\mathbf{y})$ . If the channel impulse response was only two coefficients long, e.g.  $\mathbf{h} = [4 \ 5]$ , the matrix  $\tilde{\mathbf{H}}$  would be circulant therefore allowing equalization in the frequency domain using 1-tap FEQ filter for every complex value of  $\mathcal{F}(\mathbf{y})$ . This example only illustrates the effect of the ICI, but does not show the ISI as I have limited its scope to only one transmitted frame. If the example featured several successive transmitted symbols, then the ISI would also be present.

## 1.4 Bit Rate in Discrete Multitone Modulation

The achievable rate of a white Gaussian transmission channel [33] is given by its capacity in bits per real dimension per transmission

$$b_G = \frac{1}{2} \log_2 \left( 1 + \frac{P_s}{P_n} \right) \text{ (bits/s/Hz)} \quad (1.4)$$

Here,  $b_G$  is the number of bits per transmission,  $P_s$  is the signal power and  $P_n$  is the noise power. Define the signal-to-noise ratio (SNR) as  $\text{SNR} = P_s/P_n$ . Practical coding/modulation methods cannot achieve the rate given in (1.4). The difference between the rate in (1.4) and the best achievable rate in practice can be characterized by the SNR gap denoted by  $\Gamma$  and often expressed in decibels (dB) [26, 34]. SNR gap is a function of the modulation method and the target probability of bit error per dimension,  $P_e$ . For coded quadrature amplitude modulation (QAM),

$$\Gamma = 9.8 + \gamma_m - \gamma_c \text{ (dB)} \quad (1.5)$$

where  $\gamma_m$  is the desired system margin, and  $\gamma_c$  is the gain (efficiency) of the coding method. In G.DMT ADSL, typically,  $P_e = 10^{-7}$ ,  $\gamma_m = 6$  dB, and  $\gamma_c \approx 4.2$  dB; hence,  $\Gamma \approx 11.6$  dB. A DMT system has  $N/2$  subchannels, where  $N$  is the IFFT size. When  $N$  is large, the subchannels can be considered independent in the presence of Gaussian noise [26]. The data rate in bits per frame in the  $k^{\text{th}}$  subchannel becomes

$$b_k = \log_2 \left( 1 + \frac{\text{SNR}_k}{\Gamma_k} \right) \quad (1.6)$$

where  $\text{SNR}_k$  and  $\Gamma_k$  are expressed on a linear scale and not in dB. In DMT, data is modulated in the complex (two-dimensional) plane and every subchannel can have a different SNR gap  $\Gamma_k$ . We will assume that the target probability of error in all subchannels is the same. Thus, we can set  $\Gamma_k = \Gamma$  for all  $k$ .

A DMT system has  $N/2$  subchannels, but only a portion of those carry data. For instance, in ADSL, subchannels 0-5 are reserved for voice service and

ISDN compatibility, while subchannel 64 is reserved for the pilot tone used for synchronization [20, 21, 22]. Accordingly, we define a set of subchannels of interest,  $\mathcal{I}$ , such that

$$\mathcal{I} \subseteq \{0, 1, \dots, N/2 - 1\} \quad (1.7)$$

The number of bits per DMT frame that can be reliably transmitted for the target bit error rate is

$$b_{\text{DMT}}(\mathcal{I}) = \sum_{k \in \mathcal{I}} \log_2 \left( 1 + \frac{\text{SNR}_k}{\Gamma} \right) \quad (1.8)$$

Each DMT subchannel can support a specific number of bits given the power level of the signal, the desired bit error rate and the noise power. The total number of bits transmitted in a DMT frame is the sum of the bits transmitted in each subchannel.

Equation (1.8) could result in non-integer bit values, but G.DMT ADSL and VDSL DMT standards allow only integer bit loading on subchannels. A non-integer number of bits could be loaded if constellations of dimensionality higher than two are considered. This situation arises when Trellis coding is used [35]. The number of bits per frame in a G.DMT-compliant system is

$$b_{\text{DMT}}^{\text{int}}(\mathcal{I}) = \sum_{k \in \mathcal{I}} \left\lfloor \log_2 \left( 1 + \frac{\text{SNR}_k}{\Gamma} \right) \right\rfloor \quad (1.9)$$

where  $\lfloor \cdot \rfloor$  means the closest smaller integer. Equation (1.8) is a monotonically increasing function with respect to  $\text{SNR}_k$  and (1.9) is a monotonically non-decreasing function of  $\text{SNR}_k$ . The expressions  $\text{SNR}_k$  are a function of the time domain equalizer coefficients as the TEQ is placed in the receiving path of the signal. Designing a good TEQ can significantly increase the data rate. Thus, I need to model (1.9) as a function of TEQ filter coefficients and then design an efficient optimization method that can maximize data rate of DMT systems.

## 1.5 Notation

**ADSL** : Asymmetric Digital Subscriber Line

<b>ANSI</b>	: American National Standards Institute
<b>ATM</b>	: Asynchronous Transfer Mode
<b>AWGN</b>	: Additive White Gaussian Noise
<b>CAP</b>	: Carrierless Amplitude-phase
<b>CP</b>	: Cyclic Prefix
<b>CSA</b>	: Carrier Service Area
<b>DAVIC</b>	: Digital Audio Video Council
<b>DFT</b>	: Discrete Fourier Transform
<b>DMT</b>	: Discrete Multitone
<b>DOCSIS</b>	: Data Over Cable Service Interface Specification
<b>DSL</b>	: Digital Subscriber Loop
<b>DSLAM</b>	: Digital Subscriber Line Access Multiplexer
<b>DVB</b>	: Digital Video Broadcast
<b>FEQ</b>	: Frequency-domain Equalizer
<b>FEXT</b>	: Far-end Crosstalk
<b>FFT</b>	: Fast Fourier Transform
<b>FIR</b>	: Finite Impulse Response
<b>FSK</b>	: Frequency Shift Keying
<b>ETSI</b>	: European Telecommunication Standards Institute
<b>GSNR</b>	: Geometric Signal-to-Noise Ratio
<b>HDSL</b>	: High-speed Digital Subscriber Loop
<b>HomePNA</b>	: Home Phone Network Access
<b>ICI</b>	: Inter-carrier Interference
<b>IEEE</b>	: Institute of Electrical and Electronic Engineers
<b>IFFT</b>	: Inverse Fast Fourier Transform
<b>IIR</b>	: Infinite Impulse Response
<b>IP</b>	: Internet Protocol

<b>ISDN</b>	: Integrated Services Digital Network
<b>ISI</b>	: Inter-symbol Interference
<b>ITU</b>	: International Telecommunication Union
<b>LAN</b>	: Local Area Network
<b>LMS</b>	: Least Mean Squared
<b>LU</b>	: Lower Upper
<b>LS</b>	: Least Squares
<b>MAC</b>	: Multiply Accumulate
<b>MBR</b>	: Maximum Bit Rate
<b>MCM</b>	: Multicarrier Modulation
<b>MCNS</b>	: Multimedia Cable Network System
<b>MCSSNR</b>	: Maximum Composite Signal-to-Noise Ratio
<b>MGSNR</b>	: Maximum Geometric Signal-to-Noise Ratio
<b>Min-ISI</b>	: Minimum Inter-symbol Interference
<b>MMSE</b>	: Minimum Mean Squared Error
<b>MSE</b>	: Mean Squared Error
<b>MSSNR</b>	: Maximum Shortening Signal-to-Noise Ratio
<b>NEXT</b>	: Near-end Crosstalk
<b>OFDM</b>	: Orthogonal Frequency Division Multiplexing
<b>PAM</b>	: Pulse Amplitude Modulation
<b>PSTN</b>	: Public Switched Telephone Network
<b>PTE</b>	: Per-tone Equalizer
<b>Rx</b>	: Receive
<b>QAM</b>	: Quadrature Amplitude Modulation
<b>SDSL</b>	: Single-line Digital Subscriber Loop
<b>SNR</b>	: Signal-to-Noise Ratio
<b>SSNR</b>	: Shortening Signal-to-Noise Ratio

<b>TEQ</b>	: Time Domain Equalizer
<b>TEQFB</b>	: Time Domain Equalizer Filter Bank
<b>TCP</b>	: Transmission Control Protocol
<b>TV</b>	: Television
<b>Tx</b>	: Transmit
<b>UEC</b>	: Unit Energy Constraint
<b>UTC</b>	: Unit Tap Constraint
<b>VDSL</b>	: Very-high-speed Digital Subscriber Loop
<b>VoIP</b>	: Voice over the Internet Protocol

Lower case bold letters denote vectors, e.g. **t**, while upper case bold letters denote matrices, e.g. **A**. Subscript  $[\cdot]_k$  is used to signify that the variable is relevant to a single subchannel  $k$  and that there are  $0 < k < \|I\|$  such variables. Superscripts  $[\cdot]^{i,j}$  or  $[\cdot]^i$  denote the element  $(i, j)$  of a matrix or the  $i^{\text{th}}$  element of a vector, respectively. Superscripts  $[\cdot]^{i,k:p}$  or  $[\cdot]^{k:p,j}$  signify elements  $k$  through  $p$  of the row  $i$  or column  $j$ , respectively. Superscript  $[\cdot]^H$  denotes Hermitian conjugate of a matrix or a vector, while  $[\cdot]^*$  is a conjugation operator. Functions  $\min(\cdot, \cdot)$  and  $\max(\cdot, \cdot)$  designate the minimum and the maximum of the enclosed arguments, respectively.

## 1.6 Organization of Dissertation

This dissertation focuses on time domain equalizer architecture and filter design that maximize the bit rate achievable in discrete multitone systems. The contributions of this dissertation are:

- A new model for the subchannel signal-to-noise ratio at the FFT output that includes inter-symbol interference, near-end crosstalk, white Gaussian noise, analog-to-digital converter quantization noise and the digital noise floor. The subchannel SNR model explores the DMT frame structure to arrive at the



composition of the signal needed for perfect demodulation - the circular convolution of the transmission channel and the transmitted frame. The subchannel SNR model defines as noise the difference between this perfect signal at the output of the FFT and the actual received signal at the output of the FFT. The new subchannel SNR model is a nonlinear function of the time domain equalizer coefficients.

- Optimal time domain equalizer filter bank structure in which each subchannel is assigned a separate time domain equalizer designed to maximize the data rate in the given subchannel. The subchannel time domain equalizer is obtained by maximizing the subchannel bit rate equation expressed as a function of the proposed subchannel SNR model that also includes the dependency on the time domain equalizer coefficients. The proposed modification of a DMT receiver is fully compliant with the G.DMT standard and its performance defines the achievable bit rate upper bound for a linear equalizer.
- Single data rate maximization time domain equalizer design that benefits from the low complexity of the traditional time domain equalizer block compared to the time domain equalizer filter bank design algorithm. The algorithm does not guarantee optimality of the solution as it will find the local maximum of the DMT system bit rate equation closest to the initial point. Simulation results suggest that due to a prudent choice of the initial point the algorithm arrives at a single time domain equalizer that achieves more than 99% of the optimal performance of the time domain equalizer filter bank.
- Single time domain equalizer design that compresses channel impulse responses of multiple transmission channels based on a maximization of a novel composite cost function.

The presented contributions were published in [36, 37] and submitted in [38].

This dissertation is organized as follows. Chapter 2 discusses previously published literature dealing with time domain equalizer design and the issue of inter-symbol/inter-carrier interference removal in multicarrier systems. Chapter 3 derives the proposed subchannel SNR model after the FFT demodulator. Chapter 4 presents computationally efficient algorithm for the calculation of the matrices in the subchannel SNR definition. Chapter 5 proposes a time domain equalizer filter bank and its optimal initialization as well as a method for the near-optimum design of a single time domain equalizer and discusses the computational complexity of both approaches. Chapter 6 arrives at a single time domain equalizer that will simultaneously shorten multiple channels. The presented method does not maximize the bit rate of multiple channels, as its objective function only aims to shorten the channels in a joint manner. Chapter 7 presents simulation parameters, assumptions and final results. Chapter 8 concludes this dissertation with a summary of the presented contributions and future work suggestions.

## Chapter 2

# Previous Time Domain Equalization Designs

Chapter 1 describes high-speed broadband wireline and wireless technologies, introduces multicarrier modulation concept and analyzes two implementations of it: discrete multitone modulation and orthogonal frequency division multiplexing.

In a discrete multitone transceiver, which is depicted in Figure 1.7, the design of the equalizer has a profound impact on the achievable bit rate. The time domain equalizer is traditionally designed to remove inter-symbol and inter-carrier interference. This chapter surveys three equalizer structures that are currently shipping in commercial modems: (1) conventional, (2) dual-path, and (3) per-tone. This chapter also surveys alternative approaches to time domain equalization that do not necessarily conform to the aforementioned three structures. The conventional equalizer includes a single finite impulse response (FIR) filter that performs the time domain equalization. The two key TEQ design methods - the minimum mean squared error (1992) and the maximum shortening SNR (1996) methods - seek to optimize a convenient objective function instead of a measure of bit rate. The geometric SNR method (1996) was an early attempt to include a measure of bit rate in the objective

function. Unfortunately, the geometric SNR requires manual intervention, is based on invalid assumptions, and does not offer much improvement over the minimum mean squared error method. The maximum bit rate design method (2000) uses an objective function that is a measure of bit rate and yields high bit rates; however, it does not offer a closed-form solution. This dissertation will improve further on the maximum bit rate method in Chapter 5 by generalizing the dependency of the bit rate on time domain equalizer.

The dual-path equalizer (2002) consists of two parallel time domain equalizers. Dual-path design approach optimizes one time domain equalizer across the multiple subchannels and the other over a subset of subchannels e.g. using the minimum inter-symbol interference method (2000) thus allowing improved equalization for subchannels in that subset. This equalizer structure would enable a company to reuse their previous time domain equalizer designs and still improve on the performance of the conventional methods.

The per-tone equalizer structure (2001) shifts the burden of time domain equalization to the frequency domain. The time domain equalizer is moved across the fast Fourier transform and combined with frequency domain equalizer. The frequency domain equalizer becomes multi-tap complex-valued linear combiner, in which a different linear combiner is assigned to each subchannel. The linear combiner taps can be trained using a minimum mean squared error method. This dissertation takes a complementary approach to the per tone equalizer structure in developing a time-domain equalizer filter bank to assign a different FIR filter to each subchannel (Chapter 5). A number of alternative methods that are not compliant with DMT ADSL standards attempt to eliminate the time domain equalizer and the cyclic prefix. These frequency domain methods exploit DMT subchannels that are not carrying data for signal equalization; however, the objective functions lead to a zero forcing equalizer with its noise enhancement properties.

The time domain equalizer significantly influences the achievable bit rate of a DMT system. The design of the time domain equalizer should be directly related to the DMT system bit rate equation. This casts the time domain equalizer as not only a filter to reduce the ISI/ICI but also as a tool to increase the bit rate by balancing the influence of all considered noise sources present in a DMT system. This approach to time domain equalization is presented in this dissertation.

## 2.1 Introduction

The transmission channel provided by the copper twisted pair is generally longer than the length of the cyclic prefix (guard band) placed between DMT symbols. The excess channel energy beyond the cyclic prefix leads to inter-symbol interference and destroys the orthogonality of DMT subchannels thus introducing inter-carrier interference. Time domain equalizer at the receiver is traditionally tasked with compressing the channel energy into a window of at most  $\nu + 1$  samples where  $\nu$  is the number of samples in the cyclic prefix. Perfect compression of the channel energy would remove the inter-symbol interference and inter-carrier interference. There is a number of time domain equalizer design methods published that can be separated in different classes depending on the cost function leading to TEQ design or the receiver architecture they impose. Section 2.2 discusses the minimum mean-squared error TEQ design methods. Section 2.3 analyzes the geometric signal-to-noise ratio methods. Section 2.4 summarizes the shortening signal-to-noise ratio methods. Section 2.5 delves into explanation of the minimum inter-symbol interference method and maximum bit rate approach. Section 2.6 presents dual-path and per-tone equalizer structures. Section 2.7 explains several alternatives to the major design approaches of previous sections. Finally, Section 2.8 concludes this chapter.

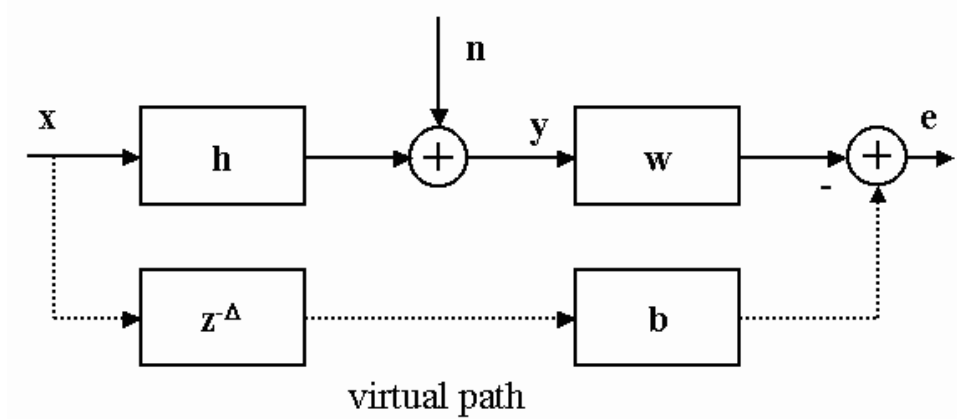


Figure 2.1: Minimum Mean-squared Error Time Domain Equalizer Design Block Diagram:  $\mathbf{x}$  - the transmitted signal,  $\mathbf{h}$  - the channel impulse response,  $\mathbf{y}$  - the received signal,  $\mathbf{n}$  - additive noise,  $z^\Delta$  - transmission delay of  $\Delta$  samples,  $\mathbf{b}$  - target impulse response, and  $\mathbf{e}$  - error signal

## 2.2 Minimum Mean-squared Error Method

Chow, Tu and Cioffi [39] discuss the need to perform time domain equalization so that the impulse response of the channel is shortened to  $\nu + 1$  samples. The channel is modelled in [39] as an infinite impulse response (IIR) filter. The time domain equalizer is set to the value of the denominator of the IIR model. The equalizer is identified through the estimation of the channel model using a known pseudo-random transmission sequence. Chow and Cioffi in [40] propose the minimum mean-squared error (MMSE) TEQ design algorithm. Minimum mean-squared error TEQ design is one of the earliest, widely used, and mathematically tractable solutions. Figure 2.1 shows the diagram used in the MMSE TEQ design where  $\mathbf{h}$  is the  $N$ -tap long transmission channel,  $\mathbf{w}$  is the  $M$ -tap long TEQ filter,  $N_b$ -tap long  $\mathbf{b}$  is the target impulse response delayed by the transmission channel  $\Delta$ , all modelled as FIR filters;  $\mathbf{x}$  is the transmitted data sequence;  $\mathbf{y}$  is the received sequence and  $\mathbf{e}$  is the error sequence. The target impulse response  $\mathbf{b}$  is defined for design purposes and is not present in the receiver. The MMSE TEQ design finds the equalizer  $\mathbf{w}$  that

minimizes the mean squared error between the signal path and the virtual path. DMT frames are sent successively at times  $0, T_f, 2T_f, \dots, pT_f, (p+1)T_f$  where each frame lasts  $T_f = 232\mu s$ . The error resulting from the difference in the virtual path and actual path at frame index  $p$  is

$$e_p = \mathbf{x}_{p-\Delta} \mathbf{b} - \mathbf{w} \mathbf{y}_p \quad (2.1)$$

where  $\mathbf{y}_p$  is a block of  $D$  successively received DMT symbols starting from frame  $p$  and  $\mathbf{x}_{p-\Delta}$  is the transmitted DMT frame at time  $p$ . Chow and Cioffi set a unit-tap constraint on the  $i^{\text{th}}$  tap of  $\mathbf{b}$  to avoid the trivial solution  $\mathbf{w} = \mathbf{0}$ . Under the unit time constraint, the error given by (2.1) becomes

$$e_p = \mathbf{x}_{p-\Delta-1} - \mathbf{v} \mathbf{u}_p \quad (2.2)$$

where

$$\mathbf{v} = [\mathbf{w} \ \mathbf{b}_i] \quad (2.3)$$

$$\mathbf{u}_p^T = [\mathbf{y}_p^T \ \mathbf{x}_{p-\Delta|i}^T] \quad (2.4)$$

$$\mathbf{x}_{p-\Delta|i}^T = [x_{p-\Delta}, \dots, x_{p-\Delta-i+1}, x_{p-\Delta-i-1}, \dots, x_{p-\Delta-\nu}] \quad (2.5)$$

$$\mathbf{b}_i = [-b_0, \dots, -b_{i-1}, -b_{i+1}, \dots, -b_\nu] \quad (2.6)$$

Chow and Cioffi use the orthogonality principle which states that the optimal error will be uncorrelated with the observed data and set  $E[e_p \mathbf{u}_p] = 0$  where  $E[\cdot]$  is the expectation operator. The target impulse response is also unknown and is obtained from the algorithm with the only parameter specified being the length of the target impulse response which is set to  $\nu + 1$  or less. Chow, Cioffi and Bingham [41, 42] define a popular iterative algorithm for the implementation of Chow and Cioffi's MMSE algorithm in [40] that avoids costly matrix inversion and does not require channel identification.

Bladel and Moeneclaey [43] further investigate MSE equalization and generalize the results of [40]. Bladel and Moeneclaey also include the correlation of the

input and noise sequences that were not used in [40]. They define the mean squared error as

$$\begin{aligned} E[e^2] &= E[\mathbf{w}^T \mathbf{y} - \mathbf{b}^T \mathbf{x}] \\ &= \mathbf{w}^T \mathbf{R}_{yy} \mathbf{w} + \mathbf{b}^T \mathbf{R}_{xx} \mathbf{b} + 2\mathbf{w}^T \mathbf{R}_{yx} \mathbf{b} \end{aligned} \quad (2.7)$$

where  $\mathbf{R}_{yy}$  is the autocorrelation of the un-equalized received signal,  $\mathbf{R}_{yx}$  is the cross-correlation with the transmit signal and  $\mathbf{R}_{xx}$  is the autocorrelation of the transmit signal. The equalizer  $\mathbf{w}$  minimizing the MSE satisfies

$$\mathbf{w} = \mathbf{R}_{yy}^{-1} \mathbf{R}_{yx} \mathbf{b} \quad (2.8)$$

The target impulse response  $\mathbf{b}$  is the eigenvector corresponding to the minimum eigenvalue of the matrix  $\mathbf{R}_{xx} - \mathbf{R}_{xy}^T (\mathbf{R}_{yy}^{-1})^T \mathbf{R}_{xy}$  under the unit energy constraint on  $\mathbf{b}$ . Then, the corresponding equalizer is found from (2.8).

Nafie and Gatherer [44] suggest a numerically less expensive method to do MMSE TEQ design than proposed in [41] that will result in the minimum eigenvalue and corresponding eigenvector. They propose using the inverse power method in conjunction with LU matrix factorization to converge to the minimum eigenvalue and corresponding eigenvector in several iterations. In the same paper, they propose an off-line least mean square (LMS) based iterative approach to MMSE TEQ design assuming that they have the knowledge of the transmission channel.

Lee, Chow and Cioffi [45] propose a fast implementation of the MMSE TEQ design that relies on the approximation of Toeplitz matrices present in the MMSE TEQ by circulant matrices. This approximation allows the use of the FFT block as the eigenvalues of a circulant matrix are found in the discrete Fourier transform of its first column. The validity of the approximation suffers until the equalizer length becomes large (longer than 60 taps).

Al-Dhahir and Cioffi [46] repeat and formalize the work in [43] formulating the MSE as a quadratic form of the equalizer taps. The received and transmitted



symbols in Figure 2.1 are related through

$$\begin{bmatrix} \mathbf{y}_{k+N_f-1} \\ \mathbf{y}_{k+N_f-2} \\ \vdots \\ \mathbf{y}_k \end{bmatrix} = \mathbf{H} \begin{bmatrix} \mathbf{x}_{k+N_f-1} \\ \mathbf{x}_{k+N_f-2} \\ \vdots \\ \mathbf{x}_{k-T-1} \end{bmatrix} + \mathbf{n} \quad (2.9)$$

where  $N_f$  is the number of transmitted and received  $(N + \nu)$ -long frames starting with frame  $k$ ,  $\mathbf{H}$  is the transmission channel convolution matrix and  $\mathbf{n}$  is the signal-independent noise vector. The mean squared error  $e_k$  is

$$\text{MSE} = \text{E}[e_k^2] = \tilde{\mathbf{b}}^H \mathbf{R}_{xx} \tilde{\mathbf{b}} - \tilde{\mathbf{b}}^H \mathbf{R}_{xy} \mathbf{w} - \mathbf{w}^H \mathbf{R}_{yx} + \mathbf{w}^H \mathbf{R}_{yy} \mathbf{w} \quad (2.10)$$

where  $\tilde{\mathbf{b}}^T = [\mathbf{0}_{1 \times \Delta} \quad \mathbf{b} \quad \mathbf{0}_{1 \times N_f + \nu - \Delta - N_b - 1}]$ . Al-Dhahir and Cioffi note that the solution  $\mathbf{w}$  that will minimize MSE will satisfy the orthogonality principle resulting in

$$\tilde{\mathbf{b}}^H \mathbf{R}_{xy} = \mathbf{w}^H \mathbf{R}_{yy} \quad (2.11)$$

The equalizer taps are designed to minimize the mean-square of the residual error between the shortened channel impulse response and a desired target impulse response of length  $\nu + 1$ . Taking (2.11) into account, the MSE given by (2.10) can be rewritten as

$$\text{MSE} = \mathbf{b}^H \mathbf{R}_\Delta \mathbf{b} \quad (2.12)$$

where  $\mathbf{R}_\Delta$  encompasses the contributions of  $\mathbf{R}_{xx}$ ,  $\mathbf{R}_{xy}$  and  $\mathbf{H}$ .

$$\mathbf{R}_\Delta = \mathbf{P}^T (\mathbf{R}_{xx} - \mathbf{R}_{xy} \mathbf{R}_{yy}^{-1} \mathbf{R}_{yx}) \mathbf{P} \quad (2.13)$$

where

$$\mathbf{P} = \begin{bmatrix} \mathbf{0}_{(N_b+1) \times \Delta} & \mathbf{I}_{(N_b+1)} & \mathbf{0}_{(N_b+1) \times (N_f + \nu - \Delta - N_b - 1)} \end{bmatrix} \quad (2.14)$$

such that  $\mathbf{I}_{N_b+1}$  is the identity matrix of size  $N_b + 1$ . Al-Dhahir and Cioffi discuss TEQ solutions under two constraints on the resulting equalized channel: unit-tap

constraint and unit-energy constraint. The unit tap constraint is  $\tilde{\mathbf{b}}^H \mathbf{e}_i = 1$  where  $\mathbf{e}_i$  is the  $i^{\text{th}}$  unit vector. The solution minimizing (2.12) under the unit tap constraint is

$$\mathbf{b}^{\text{opt}} = \frac{\mathbf{R}_{\Delta}^{-1} \mathbf{e}_i^{\text{opt}}}{\mathbf{R}_{\Delta}^{(i_{\text{opt}}, i_{\text{opt}})}} \quad (2.15)$$

where  $i_{\text{opt}}$  is the index that achieves the solution with the smallest MSE. Then, the resulting TEQ is

$$\mathbf{w}_{\text{opt}}^H = \tilde{\mathbf{b}}_{\text{opt}}^H \mathbf{R}_{xy} \mathbf{R}_{yy}^{-1} \quad (2.16)$$

Under the unit energy constraint where  $\mathbf{b}^H \mathbf{b} = 1$  the optimal target impulse response becomes the eigenvector of the Hermitian positive definite matrix  $\mathbf{R}_{\Delta}$  that corresponds to the smallest eigenvalue. Again the optimal TEQ vector is found by using (2.16). The TEQ taps obtained by using MMSE do not necessarily increase the data rate because minimizing MSE is not tightly coupled with increasing data rate. MMSE solutions tend to have a narrow spectral profile where the subchannels with high SNR are not attenuated as severely as the subchannels with low SNR. To minimize the MSE, the TEQ needs to suppress the subchannels with higher noise content and does it by placing the deep nulls<sup>1</sup> in the DMT passband. Seemingly, the nulls should have no effect on the SNR as both the channel induced noise and the signal are experiencing the same filter. However, in the presence of spectral leakage noise (not affected by TEQ) due to the use of rectangular windowing inherent in discrete Fourier transform and the noise due to finite precision signal processing, the subchannels experiencing TEQ nulls are not able to carry data as this noise becomes dominant.

Van Kerchove and Spruyt [47] point out that time domain equalization of frequency division multiplexed (FDM) ADSL poses unique challenges. In FDM ADSL the upstream and downstream transmission is allocated separate frequency bands but use the same channel, i.e. the copper twisted pair. This is opposed to the echo-

---

<sup>1</sup>Null in this paper refers to a region of high attenuation in the spectrum of the signal

cancelled ADSL that partially overlaps the spectra of upstream and downstream transmission in order to increase the usable bandwidth. Echo cancelled ADSL has to rely on sophisticated echo cancellation techniques ([48, 49, 50]) in order to utilize the overlapped spectrum. The separation of upstream and downstream frequency bands in FDM ADSL is achieved using sharp filters in the analog front-end of the modem that minimize the near-end echo from the local transmitter (transmitting downstream) into the local receiver (receiving upstream). The sharp filters have significant influence on the shape of the channel impulse response as seen by the receiver. Van Kerchove and Spruyt show an example where an MMSE TEQ exhibits low MSE (thus satisfying MMSE design objective) and negligible channel energy outside of the desired window (thus, minimizing ISI); however, it results in poor performance. This is due to the fact that although the TEQ spectrally shapes the signal and the noise equally, the shaping happens before the FFT block. The discrete Fourier transform has relatively high spectral sidelobes [18] and it leaks amplified noise energy from the upstream spectrum into the downstream spectrum due to the high magnitude response of the downstream TEQ in the upstream frequency band. Van Kerchove and Spruyt remedy the problem by modifying the MSE objective function to take into account the desired spectral shaping of the TEQ magnitude response. This is achieved by presenting high “virtual” noise content in the band where the energy of the TEQ should be suppressed (in this case the upstream band as the downstream TEQ is being designed). The resulting TEQ tries to suppress this noise source in order to minimize the modified MSE cost function thus resulting in a desired spectral shape of the TEQ.

Farhang-Boroujeny and Ding [51] follow up on Van Kerchove and Spruyt [47] by noticing that the nulls of the MMSE TEQ correspond to the subchannels that during data transmission carry low number of bits compared to the surrounding subchannels. In the presence of system imperfections such as sampling jitter, the

leakage of energy due to the DFT sidelobes can significantly effect the SNR in the subchannel that was affected by a TEQ null. Other subchannels that have not experienced a TEQ null would be less effected by the spectral energy leakage. Farhang-Boroujeny and Ding propose an MMSE-based DMT TEQ design procedure where the TEQ is designed using a linear combination of the eigenvectors of the matrix  $\mathbf{R}_\Delta$  defined in (2.13). Eigenvector weights are chosen heuristically so that the MSE is kept low. Farhang-Boroujeny and Ding report that the bit rates obtained through the use of their proposed technique are comparable to the bit rates achieved by Al-Dhahir and Cioffi [52]. Both methods use bandwidth optimization algorithms in which the power of the subchannels not able to carry data is distributed to the subchannels that can carry data. Farhang-Boroujeny and Ding also propose a method to design a TEQ for a large number or a class of transmission channels [53]. They identify 20 classes of channels through carrier service area loop simulation and measurement in the Singapore carrier service area. The modem measures the transmission channel impulse response during the initialization sequence. It then uses the measured impulse response to find the best match among the magnitude responses of the representative channel class members. The classification process retrieves the matching target impulse response and the transmission delay. The target impulse response and transmission delay for each class is saved off-line as a by-product of MMSE TEQ design for the representative members of each class. After classification, the TEQ coefficients are calculated online using the MMSE design method on the retrieved target impulse response and the transmission delay.

Wang and Adalı [54] propose a TEQ design algorithm that modifies the cost function of [46] to

$$\begin{aligned}
 E(\Theta) &= \frac{1}{2} \sum_{k=0}^{N/2} A_k \left( |H_k W_k - B_k|^2 + |H_k^* W_k^* - B_k^*|^2 \right) \\
 &= \Theta^T \Phi \Theta
 \end{aligned} \tag{2.17}$$

where  $H_k$ ,  $W_k$  and  $B_k$  are the frequency domain values in subchannel  $k$  of the channel impulse response, TEQ and target impulse response, respectively,  $A_k$  is the frequency weighting in subchannel  $k$ ,  $\Theta^T = [\mathbf{w}_0, \dots, \mathbf{w}_{M-1}, \mathbf{b}_0, \dots, \mathbf{b}_{L-1}]$  and  $\Phi$  contains the contributions of the transmission channel and frequency weighting. The weighting  $A_k$  is intended to influence the TEQ frequency domain shape; however, the choice of weights is not explicitly given and is assumed to be set heuristically. The cost function is minimized under the unit energy constraint condition on  $\Theta$  and the resulting TEQ taps are found as the eigenvector corresponding to the minimum eigenvalue of  $\Phi$ . Given the reported results, the design tends to put nulls in the frequency response of the TEQ.

Lashkarian and Kiaei [55] propose an MMSE-based algorithm that obtains the minimum eigenvalue and the corresponding eigenvector of the Rayleigh quotient [56, p.408] required by the MMSE TEQ design under the unit energy constraint through an approximation of the matrix  $\mathbf{R}_\Delta$  defined in (2.13). The algorithm allows the use of the FFT and approaches the performance of the MSEE TEQ in [43] with the increase in the size of the equalizer as the approximation of  $\mathbf{R}_\Delta$  becomes more accurate.

Al-Dhahir [57] expands the single-input single-output (SISO) MMSE TEQ design of [46] appropriate for wireline channels with its multi-input multi-output (MIMO) version appropriate for wireless channels. In the MIMO TEQ design intended for discrete matrix multitone, the time domain equalizer becomes a matrix with the channel matrix having block matrix structure that describes the channel from any transmitter to any receiver. The design procedure follows the one shown in [46].

Warke *et al.* [58] address the issue of the flatness of the TEQ frequency domain response. The motivation is found in the poor performance of the conventional TEQ design methods when applied to an FDM ADSL system. Warke *et al.*

show the measurements of the performance of the conventional TEQ designs which produce deep nulls near the FDM transition band and in the passband. Thus, to mitigate the nulls in the TEQ response Warke *et al.* propose a design criterion that encourages spectral flatness of the equalizer. They demonstrate their approach on the MSE criterion but note that other criteria can be used, as well. The MSE criterion is augmented with a flatness measure given by  $(\mathbf{w} - \mathbf{u}_i)^T(\mathbf{w} - \mathbf{u}_i)$  where  $\mathbf{u}_i$  is the unit magnitude vector of the same length as the equalizer with tap  $i$  equal to 1. The added term relies on the fact that  $\mathbf{u}_i$  is flat in the frequency domain. Thus, the augmented MSE measures also the deviation of the spectral response of the equalizer from the flat spectral response. The augmented MSE cost function is

$$J(\mathbf{w}) = \text{MSE} + \mu(\mathbf{w} - \mathbf{u}_i)^T(\mathbf{w} - \mathbf{u}_i) \quad (2.18)$$

where  $\mu$  balances the tradeoff between minimizing the MSE and deviating from the flat response. The cost function is minimized using MMSE TEQ design techniques with the note that the unit energy constraint is not necessary due to the constraint imposed by the flatness term.

Martin *et al.* [59] offer an analysis of the performance of MMSE and maximum shortening signal-to-noise ratio (MSSNR) TEQ design (discussed in Section 2.4) with respect to the length of the TEQ. This analysis also gives the reasons why the MMSE and MSSNR TEQ design place nulls in the transfer function of the shortened channel impulse response. These nulls as pointed in [51, 58] severely attenuate the signal before the demodulating FFT block and make the noise induced during the FFT operation a dominant noise source that renders the subchannels affected by the nulls unable to carry data. Martin *et al.* show that a TEQ designed using the MMSE or the MSSNR in the infinite equalizer length case has  $\nu$  zeros on the unit circle thus the shortened channel impulse response can have up to  $\nu$  zeros on the unit circle. Thus, up to  $\nu$  subchannels would not be able to carry data due to the placement of nulls at the subchannel carrier frequencies. Beyond the decrease

in the data rate, a null affects the stability of the entire system if it lies in the pilot subchannel used for synchronization. For the finite length TEQ, which can be implemented in practice, Martin *et al.* offer empirical results where they show that the distance of the nulls from the unit circle decreases with the length of the TEQ designed using MMSE or MSSNR. This implies that the bit rate of a DMT system will decrease with the increase in the length of the MMSE or MSSNR designed TEQ. This conclusion demonstrates the non-optimality of MMSE or MSSNR as the achieved bit rate of the system should not decrease with an increase in the length of the time domain equalizer.

### 2.3 Geometric Signal-to-noise Ratio Method

Al-Dhahir and Cioffi [52, 60, 61, 62] define the geometric SNR (GSNR) and attempt to maximize the bit rate achievable in a DMT system using GSNR. Al-Dhahir and Cioffi note in [60] that MMSE TEQ design although easy to analyze, is not the optimal TEQ design method. They define  $B_k$ ,  $W_k$  and  $H_k$  to be the complex valued frequency domain representations of the  $N_b \times 1$  target impulse response  $\mathbf{b}$ , the  $T \times 1$  TEQ  $\mathbf{w}$  and the  $N \times 1$  transmission channel  $\mathbf{h}$  in subchannel  $k$ . Then the signal-to-noise ratio in subchannel  $k$  assuming equal power distribution in all subchannels is

$$\begin{aligned} \text{SNR}_k &= \frac{S_x |H_k|^2}{S_{nn,k}} \\ &= \frac{S_x |H_k|^2 |W_k|^2}{S_{nn,k} |W_k|^2} \\ &= \frac{S_x |B_k|^2}{S_{nn,k} |W_k|^2} \end{aligned} \tag{2.19}$$

where  $S_{nn,k}$  and  $S_x$  are the power spectral densities of the noise and of the signal, respectively. The geometric SNR algorithm is then defined as

$$\text{SNR}_{geom} = \Gamma \prod_{k \in \mathcal{I}} \left[ \left( 1 + \frac{\text{SNR}_k}{\Gamma} \right)^{\frac{1}{N}} - 1 \right]$$

$$\begin{aligned}
&\approx \prod_{k \in \mathcal{I}} (\text{SNR}_k)^{\frac{1}{N}} \\
&= S_x \left[ \prod_{k \in \mathcal{I}} \left( \frac{|B_k|^2}{S_{nn,k} |W_k|^2} \right)^{\frac{1}{N}} \right]
\end{aligned} \tag{2.20}$$

Thus (2.20) approximates (1.8) as

$$b_{\text{DMT}}(\mathcal{I}) = \frac{N}{2} \log_2 \left( 1 + \frac{\text{SNR}_{\text{geom}}}{\Gamma} \right) \tag{2.21}$$

Maximizing (2.20) maximizes (2.21) as the logarithmic function is monotonically increasing. Maximizing (2.20) is equivalent to maximizing

$$\begin{aligned}
L(\mathbf{b}) &= \frac{1}{N} \sum_{k=1}^{N/2} \ln |B_k|^2 \\
&= \frac{1}{N} \sum_{k=1}^{N/2} \mathbf{b}^H \mathbf{G}_k \mathbf{b}
\end{aligned} \tag{2.22}$$

where  $\mathbf{G}_k$  is the matrix of FFT coefficients related to subchannel  $k$ . The dependence of (2.20) on  $\Gamma$  and independence of noise and time domain equalizer  $\mathbf{w}$  on  $\mathbf{b}$  is assumed in (2.22).

The unit energy constraint is imposed on  $\mathbf{b}$ ; however, with this constraint it follows that  $|B_k|^2 = 1$  which leads to a zero forcing solution for the time domain equalizer  $\mathbf{w}$ . A zero forcing solution is not necessary in DMT since it uses a guard band. To avoid the zero forcing solution a constraint is imposed that the MSE resulting from the solution needs to be less than some value  $\text{MSE}_{\text{max}}$ . The optimal target impulse response  $\mathbf{b}$  in terms of the maximum geometric SNR (MGSSNR) algorithm is then found by

$$\begin{aligned}
\mathbf{b}_{\text{GSSNR}}^{\text{opt}} &= \arg \max \{ L(\mathbf{b}) : \mathbf{b} \} \\
\text{s. t. } \mathbf{b}^H \mathbf{b} &= 1, \text{ and} \\
\mathbf{b}^H \mathbf{R}_\Delta \mathbf{b} &< \text{MSE}_{\text{max}}
\end{aligned} \tag{2.23}$$

where  $\mathbf{R}_\Delta$  is defined in (2.13). This non-linear optimization problem can only be solved using numerical methods. Once the optimal target impulse response is found,



the corresponding TEQ  $\mathbf{w}$  follows from (2.16). Several simplifying assumptions are made, notably that the input SNR is high enough that the dependence of the geometric SNR on  $\Gamma$  and the unity terms in (2.20) can be ignored. These assumptions tend to design a TEQ that ignores the subchannels with lower SNR (which contain ISI and ICI that the TEQ is to remove) in favor of the subchannels with higher SNR, thus not achieving the maximization of the data rate [63]. This comes about due to the fact that the unity terms in (2.20) are not negligible in the subchannels with low SNR. Also, the definition of the subchannel SNR does not include the effects of the ISI in the denominator, but instead only the effects of the equalizer and the noise. The definition of (2.22) incorrectly assumes that the time domain equalizer  $\mathbf{w}$  and the target impulse response  $\mathbf{b}$  are independent. The time domain equalizer  $\mathbf{w}$  is found from  $\mathbf{b}_{\text{GSNR}}^{\text{opt}}$  using (2.16). The definition of GSNR (2.19) also assumes

$$\mathcal{F}_k(\mathbf{w} * \mathbf{h}) \equiv \mathcal{F}_k(\mathbf{w})\mathcal{F}_k(\mathbf{h}) = W_k H_k \quad (2.24)$$

where  $*$  is the time domain linear convolution,  $\equiv$  is the equivalence operator and  $\mathcal{F}_k$  is the DFT operator for subchannel  $k$ . Linear convolution may not be equal to the product in the frequency domain and the difference appears as a noise source. Al-Dhahir and Cioffi [52] change the subchannel SNR model to include the effects of the ISI but only when evaluating the TEQ designed using (2.19). The subchannel SNR is

$$\text{SNR}_k = \frac{S_x |B_k|^2}{S_x |B_k - W_k H_k|^2 + S_{nn,k} |W_k|^2} \quad (2.25)$$

Lashkarian and Kiaei [64, 65] propose an iterative equalization algorithm based on GSNR that uses projection on convex sets to maximize GSNR and solve (2.23). They note that the constraint  $\mathbf{b}^H \mathbf{R}_\Delta \mathbf{b} < \text{MSE}_{\text{max}}$  is a convex set due to the positive definite property of  $\mathbf{R}_\Delta$ ; however, unit energy constraint is not. Lashkarian and Kiaei note that the unit energy constraint can be removed because the trivial solution does not satisfy the  $\text{MSE}_{\text{max}}$  constraint. GSNR is maximized using a gradient projection method where in each iteration a step is taken along the

negative gradient of the objective function followed by a projection on the convex constraint set. Lashkarian and Kiaei note that the objective function lacks convexity thus, the stationary point of the algorithm depends on the choice of the initial point. As a suitable starting point they suggest the solution obtained from MMSE TEQ design under the unit energy constraint.

Milisavljevic and Verriest [66] point out that optimizing GSNR as a function of the target impulse response results in a cost function with many local minima and maxima and possibly discontinuous gradients. They propose to maximize GSNR using an algorithm that is a hybrid of simulated annealing and genetic algorithms. Milisavljevic and Verriest initialize the algorithm with a random population of column vectors  $\mathbf{z}^T = [\mathbf{b} \ \mathbf{w} \ \Delta]^T$  where  $\Delta$  is the transmission delay. For each vector they compute the bit rate and rank the vectors accordingly. A new population of vectors (child population) is created by random change in the coefficients of the parent. If the bit rate achieved using a child equalizer  $\mathbf{w}$  is higher than that of a parent, then the child takes the place of the parent (together with corresponding target impulse response  $\mathbf{b}$  and transmission delay  $\Delta$ ). Milisavljevic and Verriest show that for the test carrier area service (CSA) 6 channel their algorithm surpasses the data rate achieved by the mean squared error time domain equalizer design by the 8<sup>th</sup> generation and reaches the maximum data rate afforded by the GSNR objective function around the 40<sup>th</sup> generation.

## 2.4 Maximum Shortening Signal-to-noise Ratio Method

Melsa, Younce, and Rohrs in [67] define the shortened channel impulse response as

$$\mathbf{h}_{\text{eff}} = \mathbf{h} * \mathbf{w} \tag{2.26}$$

where  $*$  is the linear convolution operator,  $\mathbf{h}$  is the channel impulse response and  $\mathbf{w}$  is the time domain equalizer. The Maximum Shortening Signal-to-noise Ratio

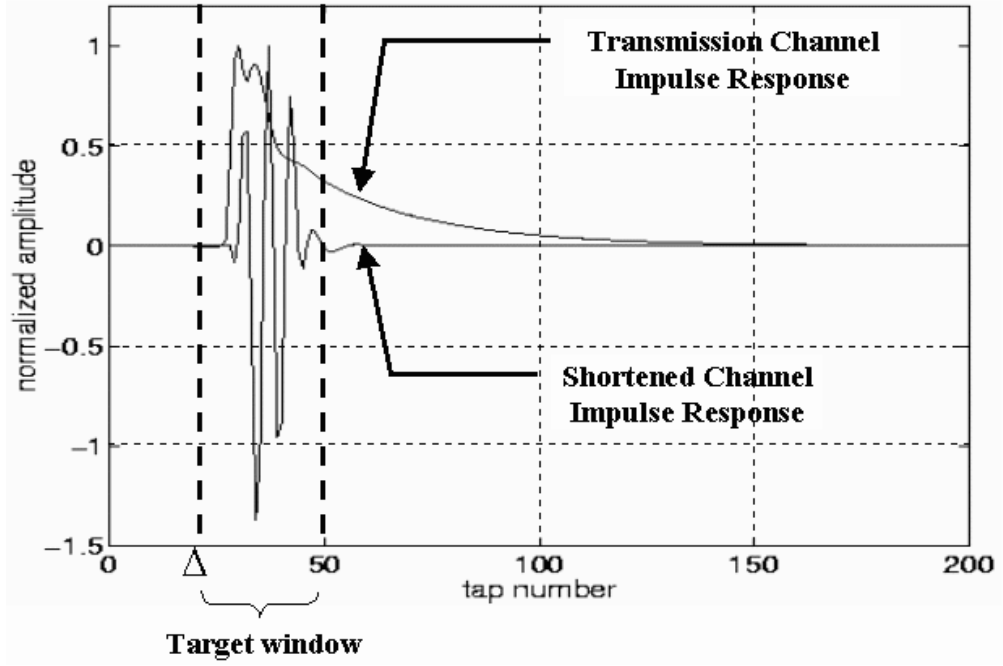


Figure 2.2: Channel Impulse Response and Shortened Channel Impulse Response with Respect to the Target Window (adapted from [3]):  $\Delta$  - channel transmission delay.

(MSSNR) TEQ design method of Melsa, Younce, and Rohrs [67, 68, 69] maximizes the ratio of the shortened channel impulse response energy within a target window length  $\nu + 1$  samples to the energy of the channel outside of the window. This TEQ design method is based on an observation that reducing the energy of shortened channel impulse response outside the target window will reduce ISI and ICI. Figure 2.2 shows the relationship of the channel impulse response and the shortened impulse response to each other with respect to the target window. Melsa, Younce, and Rohrs partition the shortened channel  $\mathbf{h}_{\text{eff}}$  into two channels: (1)  $\mathbf{h}_{\text{win}}$ , which consists of samples of  $\mathbf{h}_{\text{eff}}$  lying within the desired  $\nu + 1$  window, and (2)  $\mathbf{h}_{\text{wall}}$ , which consists of the remaining samples of  $\mathbf{h}_{\text{eff}}$ . Then,  $\mathbf{h}_{\text{eff}} = \mathbf{H}\mathbf{w}$  where  $\mathbf{H}$  is the  $(N + M - 1) \times M$  convolution matrix of  $\mathbf{h}$ . So, the signal is defined as the portion of the channel within the window  $\mathbf{h}_{\text{win}} = \mathbf{H}_{\text{win}}\mathbf{w}$  and the ISI-causing part of the channel is  $\mathbf{h}_{\text{wall}} = \mathbf{H}_{\text{wall}}\mathbf{w}$

where  $\mathbf{H}_{\text{win}}$  consists of  $\nu + 1$  rows of  $\mathbf{H}$  starting from position  $\Delta$ , where  $\Delta$  is the transmission delay, and  $\mathbf{H}_{\text{wall}}$  consists of the remaining rows of  $\mathbf{H}$ . The SSNR is defined as

$$SSNR(\mathbf{w}) = \frac{\mathbf{w}^T \mathbf{H}_{\text{win}}^T \mathbf{H}_{\text{win}} \mathbf{w}}{\mathbf{w}^T \mathbf{H}_{\text{wall}}^T \mathbf{H}_{\text{wall}} \mathbf{w}} = \frac{\mathbf{w}^T \mathbf{B} \mathbf{w}}{\mathbf{w}^T \mathbf{A} \mathbf{w}} \quad (2.27)$$

MSSNR seeks to minimize the energy of the distortion (denominator of SSNR) while keeping the energy of the signal (numerator of SSNR) equal to 1.

Matrix  $\mathbf{B}$  is positive definite and Melsa, Younce, and Rohrs use Cholesky decomposition [70, p. 77] to define

$$\begin{aligned} \mathbf{B} &= \mathbf{Q} \mathbf{\Lambda} \mathbf{Q}^T = (\mathbf{Q} \mathbf{\Lambda}^{1/2}) (\mathbf{\Lambda}^{1/2} \mathbf{Q}^T) \\ &= (\mathbf{Q} \mathbf{\Lambda}^{1/2}) (\mathbf{Q} \mathbf{\Lambda}^{1/2})^T \\ &= \mathbf{B}^{1/2} (\mathbf{B}^T)^{1/2} \end{aligned} \quad (2.28)$$

where  $\mathbf{\Lambda}$  is a diagonal matrix of the eigenvalues of  $\mathbf{B}$  and  $\mathbf{Q}$  is a matrix of orthogonal eigenvectors. Define

$$\mathbf{z} = (\mathbf{B}^T)^{1/2} \mathbf{w} \quad (2.29)$$

from which

$$\mathbf{w} = (\mathbf{B}^T)^{-1/2} \mathbf{z} \quad (2.30)$$

Now substituting (2.30) into (2.27), the SSNR becomes

$$SSNR(\mathbf{z}) = \frac{\mathbf{z}^T \mathbf{z}}{\mathbf{z}^T \mathbf{C} \mathbf{z}} \quad (2.31)$$

where  $\mathbf{C} = \mathbf{B}^{-1/2} \mathbf{A} (\mathbf{B}^T)^{-1/2}$ . Melsa, Younce, and Rohrs minimize  $\mathbf{z}^T \mathbf{C} \mathbf{z}$  subject to the constraint that  $\mathbf{z}^T \mathbf{z} = 1$ , which yields the MSSNR TEQ design method. The solution of the minimization is the eigenvector  $\mathbf{z}_{\text{min}}$  corresponding to the minimum eigenvalue of  $\mathbf{C}$ . The constraint is necessary in order to prevent the trivial solution at  $\mathbf{w} = \mathbf{0}$ . The resulting TEQ taps are

$$\mathbf{w} = (\mathbf{B}^T)^{-1/2} \mathbf{z}_{\text{min}} \quad (2.32)$$

Although the method maximizes the SSNR measure, which is related to the ISI, the method does not maximize bit rate directly and does not take into account the noise induced by the channel. Thus, SSNR maximization will not yield the data-maximization TEQ design as also concluded by Melsa, Younce, and Rohrs [67].

Melsa, Younce, and Rohrs in [67, 68, 69] also propose a method for jointly shortening two channels, which I refer to as Joint MSSNR. This method jointly shortens the channel impulse response and the near-end echo channel impulse response <sup>2</sup> using a single TEQ FIR, thus reducing ISI and simplifying the removal of near-end echo. Joint MSSNR uses previously defined  $\mathbf{H}_{\text{wall}}$  and  $\mathbf{H}_{\text{win}}$  matrices and introduces equivalently defined matrices  $\mathbf{H}_{\text{wall,e}}$  and  $\mathbf{H}_{\text{win,e}}$  derived from the near-end echo impulse response  $\mathbf{h}_e$ . Matrices  $\mathbf{A}$  and  $\mathbf{B}$  are defined in terms of the real-valued parameter  $\alpha$ , where  $0 < \alpha < 1$ , as follows:

$$\mathbf{B}(\alpha) = \alpha \mathbf{H}_{\text{win}}^T \mathbf{H}_{\text{win}} + (1 - \alpha) \mathbf{H}_{\text{win,e}}^T \mathbf{H}_{\text{win,e}} \quad (2.33)$$

$$\mathbf{A}(\alpha) = \alpha \mathbf{H}_{\text{wall}}^T \mathbf{H}_{\text{wall}} + (1 - \alpha) \mathbf{H}_{\text{wall,e}}^T \mathbf{H}_{\text{wall,e}} \quad (2.34)$$

Joint MSSNR seeks to solve

$$\mathbf{w}_{\text{opt}} = \min_{\mathbf{w}: \mathbf{w}^T \mathbf{A}(\alpha) \mathbf{w} = 1} \mathbf{w}^T \mathbf{B}(\alpha) \mathbf{w} \quad (2.35)$$

Djokovic [71] defines a similar ratio to SSNR; however, he adds the contribution of the additive noise, which is not considered in [67]. Thus, the proposed signal-to-noise ratio measure is

$$\text{SNR}_{\text{ISI+noise}} = \frac{\mathbf{w}^T \mathbf{B} \mathbf{w}}{\mathbf{w}^T (\mathbf{A} + \mathbf{R}_n) \mathbf{w}} \quad (2.36)$$

where  $\mathbf{w}^T \mathbf{R}_n \mathbf{w}$  is the additive noise energy. Djokovic also proposes a least mean squares iterative method and includes the contribution of the additive noise to arrive at the TEQ taps.

---

<sup>2</sup>Near-end echo results from the leakage of the signal transmitted on a local transmitter into the local receiver.

Yin and Yue [72] point out that the MSSNR method minimizes the energy outside of the window, i.e.  $\mathbf{w}^T \mathbf{A} \mathbf{w}$ , while keeping the energy of the channel inside the window constant, i.e.  $\mathbf{w}^T \mathbf{B} \mathbf{w} = 1$ . However, when the length of  $\mathbf{w}$  exceeds  $\nu$  samples, i.e. the length of the cyclic prefix, matrix  $\mathbf{B}$  becomes singular and  $\mathbf{B}^{-1/2}$  does not exist. They propose instead to maximize the energy of the channel inside the window, i.e.  $\mathbf{w}^T \mathbf{B} \mathbf{w}$  while keeping the energy outside the window constant, i.e.  $\mathbf{w}^T \mathbf{A} \mathbf{w} = 1$ . The advantage of this approach is that matrix  $\mathbf{A}$  is always positive definite regardless of the length of the desired equalizer. The resulting equalizer in this case is the eigenvector corresponding to the largest generalized eigenvalue of the matrix pair  $(\mathbf{B}, \mathbf{A})$ . Schur, Spidel and Angerbauer [73] investigate further the work of Yin and Yue by testing their method in the presence of white Gaussian noise and near- and far-end crosstalk.

Chiu *et al.* [74] propose the inverse power method to find the the necessary minimum eigenvalue and corresponding eigenvector in an iterative variation of the MSSNR method. They conclude that the convergence properties of the power method are not sufficient for the MSEE TEQ design due to the possibility of slow convergence. The proposed variation of the inverse power method has super-linear convergence rate. The algorithm iteration is

$$\mathbf{A} \mathbf{w}_i = \mathbf{B} \mathbf{w}_{i-1} \quad (2.37)$$

where  $[\cdot]_i$  is the  $i^{\text{th}}$  iteration. Hence, there is no need for Cholesky decomposition or matrix inversion. Each iteration becomes a problem of solving a linear system of equations, i.e.  $\mathbf{A} \mathbf{w}_i = \mathbf{b}_i$  followed by  $\mathbf{B} \mathbf{w}_{i-1} = \mathbf{b}_i$ . Also, the equalizer taps are computed directly without the need of computing either the target impulse response or the minimum eigenvalue.

Lu, Clark, Arslan and Evans [75] and Lu in [76] present a low-complexity sub-optimal divide and conquer TEQ design algorithm. Divide and conquer TEQ separates the problem of designing an  $M$ -tap long TEQ into a problem of iteratively

designing a series of two-tap TEQ filters by optimizing a cost function that is at each iteration changed by the previously designed two-tap TEQ. The cost function minimized at each step is the energy in the transmission channel outside of the window of interest, i. e. the denominator of the SSNR. The two-tap filter in the  $i^{\text{th}}$  iteration is  $(\mathbf{w}^i)^{\text{T}} = [1 \ g]^{\text{T}}$  where the first tap is set to one to prevent the trivial solution. Setting the first tap to 1 amounts to re-normalization of the TEQ taps that does not affect the SSNR. After every iteration  $i$ , the new transmission channel is  $\mathbf{h}^i = \mathbf{h}^{i-1} * \mathbf{w}^{i-1}$ . Notice that the length of the channel increases with every iteration while hopefully the energy is compacted in fewer taps. The energy outside the target window is

$$(\mathbf{h}_{\text{wall}}^i)^{\text{T}} \mathbf{h}_{\text{wall}}^i = \sum_{s \in D} (\mathbf{h}_s^{i-1} + g \mathbf{h}_{s-1}^{i-1})^2 \quad (2.38)$$

where  $D = \{1, 2, \dots, \Delta, \Delta + \nu + 2, \dots, |\mathbf{h}^{i-1}|\}$ . Equation (2.38) is quadratic in  $g$  and its minimization is performed by setting the first derivative to zero. Then

$$g = - \frac{\sum_{s \in D} \mathbf{h}_{s-1}^{i-1} \mathbf{h}_s^{i-1}}{\sum_{s \in D} (\mathbf{h}_{s-1}^{i-1})^2} \quad (2.39)$$

The final TEQ is obtained by convolving all of the computed  $\mathbf{w}^i$ . This procedure does not require matrix inversion or Cholesky composition and is less complex than MSSNR.

Daly, Heneghan and Fagan [77] compare the MMSE and MSSNR TEQ design. Daly, Heneghan and Fagan are able to show that the matrices used in both methods are the same under the unit-energy constraint. They conclude (assuming that the input signal is white) that two methods are:

- equivalent if there is no noise present in the system,
- equivalent even when noise is present (white or colored) if the MSEE is implemented non-adaptively, and
- not equivalent if MMSE is implemented adaptively.

MSSNR in the presence of noise estimates the channel using the procedure in [45] by generating an average of the channel estimates obtained from each received DMT frame. With the additive noise, the problem is transformed from  $\mathbf{B}\mathbf{w} = \lambda\mathbf{A}\mathbf{w}$  to  $\mathbf{B}\mathbf{w} = \lambda[\mathbf{A} + (p+\nu)\sigma_n^2\mathbf{I}]\mathbf{w}$  where  $p$  is the index beyond which the energy of the shortened transmission channel is insignificant,  $\sigma_n^2$  is the variance of the noise (assuming white noise) and  $\mathbf{I}$  is the identity matrix. In the adaptive implementation of the MMSE in the presence of noise the problem is transformed to  $\mathbf{B}\mathbf{w} = \lambda[\mathbf{A} + \sigma_n^2\mathbf{I}]\mathbf{w}$ . Hence, the noise is lower in the adaptive MMSE implementation and theoretically we may expect better results from MMSE than from MSSNR.

Schur and Speidel [78] propose a new cost function

$$D = \frac{\mathbf{w}^T \mathbf{H}^T \mathbf{Q} \mathbf{H} \mathbf{w}}{\mathbf{w}^T \mathbf{H}^T \mathbf{H} \mathbf{w}} \quad (2.40)$$

where  $\mathbf{Q}$  is a diagonal matrix containing the squared distances of the coefficients of the shortened transmission channel from the “time center”  $\tilde{n}$  proportional to  $\sum_{n=-\infty}^{\infty} n |\mathbf{h}_n * \mathbf{w}_n|^2$ . Minimization of  $D$  results in a Rayleigh quotient problem. Schur and Speidel also take into account additive noise imparted by the transmission channel but only to evaluate and compare their algorithm to the previous work. Presented results show better channel shortening than the MSSNR and thus increased resistance to frame synchronization issues. However, there is no explicit dependency on the length of the cyclic prefix or the inclusion of the channel-induced additive noise into the design framework. The method does not establish the relationship between the TEQ design and the bit rate of the system.

Tkancenko and Vaidyanathan [79, 80] generalize the algorithm presented by Schur and Speidel [78] to include the effects of the noise and propose new penalizing functions to control the channel spread. A new objective function  $J$  is presented that is a convex combination of the channel shortening objective and a noise-to-signal ratio.

$$J = \alpha J_{\text{short}} + (1 - \alpha) J_{\text{noise}}$$



$$= \alpha \frac{\sum_n f(n - n_{\text{mid}}) |\mathbf{h}_{\text{eff}}|^2}{\sum_n |\mathbf{h}_{\text{eff}}|^2} + (1 - \alpha) \frac{\sigma_{\text{noise}}^2}{\sigma_{\text{signal}}^2 \sum_n |\mathbf{h}_{\text{eff}}|^2} \quad (2.41)$$

where  $\mathbf{h}_{\text{eff}} = \mathbf{h} * \mathbf{w}$ ,  $n_{\text{mid}}$  is the desired centroid or time center of  $\mathbf{h}_{\text{eff}}$ ,  $f(n)$  is a non-negative function penalizing the coefficients of  $\mathbf{h}_{\text{eff}}$  away from  $n_{\text{mid}}$ ,  $0 \leq \alpha \leq 1$ ,  $\sigma_{\text{noise}}^2$  is the noise power and  $\sigma_{\text{signal}}^2$  is the transmitted signal power. The proposals for  $f(n)$  are  $n^2$  as in [78] or  $|n|$ . The algorithm leads to a Rayleigh quotient and corresponding eigenvalue problem. Again, the cost function does not establish the relationship between the TEQ design and the bit rate of the system. Moreover, the shortening cost function penalizes all of the channel samples and not only the samples outside of the window that cause ISI. Tkancenko and Vaidyanathan [81] extend their approach from [79, 80] to include multiple-in multiple-out channels in which the equalizer becomes a matrix equalizing a channel that is a matrix in itself. This work changes the penalizing function of [79, 80] to penalize only the values outside of the window of interest.

Troulis and Sesia [82] notice that TEQ nulls introduce severe attenuation in the subchannels with high SNR and cause a decrease in data rate (see [51] for insight on the influence of the shape of the TEQ on bit rate). Troulis and Sesia incorporate a measure of TEQ flatness into the SSNR criterion and minimize the modified SSNR cost function with the flatness included. Their choice of the flatness measure is given by  $|\mathbf{h}_{\text{eff}} - \alpha \mathbf{h}_{n-t}|^2$  where  $\alpha = \mathbf{h}_t^T \mathbf{h}_{\text{eff}}$ . The measure of flatness is the distance of the shortened channel impulse response  $\mathbf{h}_{\text{eff}}$  (convolution of the transmission channel impulse response and the equalizer) from the transmission channel impulse response  $\mathbf{h}$ . The choice of the flatness measure is somewhat surprising because one can not expect that the shortened channel will be similar in shape to the original channel. The flatness measure is added to the MSSNR denominator as a source of noise and then minimized under the MSSNR constraint that the power of the channel in the target window is equal to 1. This method shows improvement over the original Melsa design and recognizes the importance of avoiding nulls in the

frequency response of the TEQ.

Martin *et al.* [83] propose a blind, iterative, globally convergent channel shortening algorithm that is related to MSSNR. The algorithm is called MERRY (or Multicarrier Equalization by Restoration of RedundancY) and it uses the fact that the cyclic prefix is a repetition of the last  $\nu$  samples of a DMT frame. Due to the cyclic prefix the following is true

$$\mathbf{x}_{(N+\nu)k+i} = \mathbf{x}_{(N+\nu)k+i+N} \quad (2.42)$$

for  $i \in \{1, 2, \dots, \nu\}$  where  $\mathbf{x}$  is the  $k^{\text{th}}$  transmitted  $(N + \nu)$ -long time domain frame. The ISI destroys the relationship in (2.42) because a channel that is longer than  $\nu + 1$  samples will introduce energy into the sample  $\mathbf{x}_{(N+\nu)k+i}$  at the receiver that is not equal to the energy received by its dual at the end of the DMT frame. The cost function is defined as

$$J_{\Delta} = E[|\mathbf{y}_{\nu+\Delta} - \mathbf{y}_{\nu+\Delta+N}|^2] \quad (2.43)$$

where  $\Delta$  is the transmission delay and  $\mathbf{y}$  is the received frame after the TEQ given by

$$\mathbf{y}_i = \sum_{j=0}^{M-1} \mathbf{w}_j \underbrace{\sum_{l=0}^{L-1} (\mathbf{h}_l \mathbf{x}_{i-j-l} + \mathbf{n}_{i-j})}_{\mathbf{r}_{i-j}} \quad (2.44)$$

MERRY is a stochastic gradient descent algorithm with a constraint that avoids  $\mathbf{w} = 0$  and that iterates once every frame. The iteration is

$$\mathbf{w}_j^{k+1} = \mathbf{w}_j^k + \mu[\mathbf{y}_{(N+\nu)k+\nu+\Delta} - \mathbf{y}_{(N+\nu)k+\nu+\Delta+N}][\mathbf{r}_{\nu+\Delta-j}^* - \mathbf{r}_{\nu+\Delta-j+N}^*] \quad (2.45)$$

Martin *et al.* show that MERRY finds a solution similar to [67]; however, MERRY shortens the channel to  $\nu$  coefficients instead of  $\nu + 1$  coefficient.

Martin *et al.* [84] researches the structure of the MSSNR matrices  $\mathbf{B}$  and  $\mathbf{A}$  (the energy of the channel within the window and the energy of the channel outside

of the window of interest) respectively defined in [67]. Martin *et al.* look at a class of matrices called centrosymmetric symmetric matrices defined as members of the set  $V_N = \{\mathbf{C} : \mathbf{C}^T = \mathbf{C}, \mathbf{J}\mathbf{C}\mathbf{J} = \mathbf{C}\}$  where  $\mathbf{J}$  is a square  $N \times N$  matrix with ones on the cross diagonal. If matrices  $\mathbf{P}$  and  $\mathbf{Z}$  are centrosymmetric symmetric and  $\mathbf{P}$  is invertible, then the eigenvectors of  $\mathbf{P}^{-1}\mathbf{Z}$  can always be chosen to be symmetric or skew-symmetric. Also if all of the eigenvalues of  $\mathbf{P}^{-1}\mathbf{Z}$  are distinct, all of the eigenvectors are symmetric or skew-symmetric. Martin *et al.* mark that matrices  $\mathbf{A}$  and  $\mathbf{B}$  are nearly centrosymmetric symmetric and thus the resulting solution TEQ filter (eigenvector corresponding to the minimum generalized eigenvalue) is also nearly symmetric or skew-symmetric. The simulation results show that the MSSNR TEQ becomes increasingly more symmetric with the increase in the length of the TEQ. Also presented is the method to force the MSSNR TEQ to be perfectly symmetric by a rewrite of the  $\mathbf{A}$  to take into account the desired properties of a centrosymmetric symmetric metric. Forcing symmetry on TEQ coefficients reduces the complexity found of MSSNR TEQ design by 75%. Ribeiro, Silva and Diniz [85] also suggest time domain equalizers with linear phase by modifying the MSSNR method to include the constraint that the equalizer be either symmetric or anti-symmetric.

## 2.5 Minimum Inter-symbol Interference Method

Arslan, Evans and Kiaei [63] and Arslan in [86] propose the Maximum Bit Rate (MBR) and Minimum ISI (Min-ISI) TEQ design algorithms. MBR and Min-ISI follow the methods of separating the transmission channel impulse response of [67] and the subchannel SNR definition used in [52, 60, 62] to define a new model for

the subchannel SNR. The new model of the subchannel SNR is

$$\text{SNR}_k = \frac{\overbrace{S_{x,k}|H_{\text{win},k}|^2}^{\text{signal}}}{\underbrace{S_{n,k}|W_k|^2}_{\text{AWGN}} + \underbrace{S_{x,k}|H_{\text{wall},k}|^2}_{\text{ISI}}} \quad (2.46)$$

where  $H_{\text{win},k}$  and  $H_{\text{wall},k}$  are the  $k^{\text{th}}$  FFT coefficients of  $\mathbf{h}_{\text{win}}$  and  $\mathbf{h}_{\text{wall}}$ , respectively and  $S_{n,k}$  and  $S_{x,k}$  are the  $k^{\text{th}}$  subchannel power spectral densities of the noise and the signal. The difference with the subchannel SNR model defined in MGSNR (2.25) is that the numerator now contains only the portion of the resulting transmission channel that contributes to the useful signal as opposed to (2.25) where the numerator contains the contribution of the entire channel. The denominator includes the contribution of the ISI noise of the shortened channel impulse response outside of the desired window as opposed to (2.25) which also includes shortened channel impulse response inside the desired window. The improvement over the MSSNR method that pioneered the idea of separation of the channel into the portion inside the window and the portion outside of the window is that the subchannel SNR is defined in the frequency domain, thus enabling the design of a TEQ for particular frequency band as opposed to MSSNR which cannot discriminate between subchannels or tailor the TEQ design for a particular frequency band. It seems that (2.46) is defined in terms of the magnitude of the frequency response  $W_i$  of the time domain equalizer FIR; however, [63] shows that the design is in terms of the impulse response of the TEQ,  $\mathbf{w}$ .

Arslan, Evans and Kiaei define the following

$$\mathbf{h}^{\text{signal}} = \mathbf{G}\mathbf{H}\mathbf{w} \quad (2.47)$$

$$\mathbf{h}^{\text{ISI}} = \mathbf{D}\mathbf{H}\mathbf{w} \quad (2.48)$$

$$\mathbf{h}^{\text{noise}} = \mathbf{F}\mathbf{w} \quad (2.49)$$

where the  $N \times T$  matrix  $\mathbf{H}$  is the first  $N$  rows of the convolutional matrix of the transmission channel,  $N \times N$  matrices  $\mathbf{G}$  and  $\mathbf{D}$  “pick off” the rows of the vector  $\mathbf{H}\mathbf{w}$  corresponding to the desired  $\nu + 1$  window and outside of it, respectively, and  $N \times T$  matrix  $\mathbf{F}$  accounts for the effects of the removal of cyclic prefix. Then, if the multiplication with the vector  $\mathbf{q}_k^H$  gives the  $k^{\text{th}}$  FFT coefficient of the vector, the following holds

$$H_k^{\text{signal}} = \mathbf{q}_k^H \mathbf{G} \mathbf{H} \mathbf{w} \quad (2.50)$$

$$H_k^{\text{ISI}} = \mathbf{q}_k^H \mathbf{D} \mathbf{H} \mathbf{w} \quad (2.51)$$

$$H_k^{\text{noise}} = \mathbf{q}_k^H \mathbf{F} \mathbf{w} \quad (2.52)$$

The subchannel SNR model becomes

$$\begin{aligned} \text{SNR}_k &= \frac{\mathbf{w}^T \mathbf{H}^T \mathbf{G}^T \mathbf{q}_k S_{x,k} \mathbf{q}_k^H \mathbf{G} \mathbf{H} \mathbf{w}}{\mathbf{w}^T \mathbf{F}^T \mathbf{q}_k S_{n,k} \mathbf{q}_k^H \mathbf{F} \mathbf{w} + \mathbf{w}^T \mathbf{H}^T \mathbf{D}^T \mathbf{q}_k S_{x,k} \mathbf{q}_k^H \mathbf{D} \mathbf{H} \mathbf{w}} \\ &= \frac{\mathbf{w}^T \mathbf{A}_k \mathbf{w}}{\mathbf{w}^T \mathbf{B}_k \mathbf{w}} \end{aligned} \quad (2.53)$$

The subchannel SNR model in (2.46) includes ISI and additive white Gaussian noise (AWGN) and is substituted in (2.54) to determine the bit rate (same as (1.8)):

$$b_{\text{DMT}}(\mathcal{I}) = \sum_{k \in \mathcal{I}} \log_2 \left( 1 + \frac{\text{SNR}_k}{\Gamma} \right) \quad (2.54)$$

MBR tries to maximize the nonlinear bit rate equation (2.54) by using the Broyden-Fletcher-Goldfarb-Shanno quasi-Newton algorithm in Matlab’s optimization toolbox. The subchannel SNR model used in MBR and Min-ISI fails to incorporate other noise sources present such as near-end crosstalk or the digital noise floor imparted by the finite precision arithmetic used in digital signal processors. Arslan, Evans and Kiaei in [63] conclude that the MBR procedure is computationally expensive and therefore not well suited for real-time implementation on a programmable digital signal processor. Nevertheless, the procedure does maximize the bit rate at the TEQ output for the traditional receiver architecture as it achieves the matched filter bound.

Henkel *et al.* [87] analyze the ISI and ICI and show that the ICI and ISI are separate noise sources with the same power spectral density. The ISI is “pulling in” the energy of the previous and the next received frame into the current received frame, and this energy causes a distortion. The ICI is caused by the inability of the cyclic prefix to force the linear convolution of the channel and the frame to look like their circular convolution thus destroying subchannel orthogonality after the FFT. ICI would not be present even if the channel impulse response was longer than the cyclic prefix but the samples in the previous frame looked like an extension of the cyclic prefix. The absence of those samples is causing ICI. Henkel *et al.* show that ICI and ISI have the same power spectral densities and have to be accounted for separately. The subchannel SNR model in MBR only includes the contribution of the ISI to the noise. The subchannel SNR model presented in this dissertation (Chapter 3) improves on the subchannel SNR model in MBR by integrating both ISI and ICI into the model, as well as the contribution of other noise sources not accounted for in MBR.

Arslan, Evans and Kiaei in [63] also define lower complexity non-optimal Min-ISI TEQ design method. Min-ISI generalizes the MSSNR method with the additional benefit of frequency weighting in the form of the subchannel SNR (matched filter bound). This choice of weights then results in the minimization of the ISI noise in the subchannels with the high SNR when compared to the subchannels with lower SNR. The weighting allows Min-ISI to shape the frequency response of the TEQ.

$$\mathbf{w}_{\text{Min-ISI}} = \arg \min_{\mathbf{w}: \mathbf{w}^T \mathbf{H}^T \mathbf{G}^T \mathbf{G} \mathbf{H} \mathbf{w} = 1} \left[ \mathbf{w}^T \mathbf{H}^T \mathbf{D}^T \sum_{k \in \mathcal{I}} \left( \mathbf{q}_k \frac{S_{x,k}}{S_{n,k}} \mathbf{q}_k^H \right) \mathbf{D} \mathbf{H} \mathbf{w} \right] \quad (2.55)$$

In simulation, the Min-ISI method achieved more than 95% of the bit rate of the MBR method [63]. The Min-ISI method has been implemented on several fixed-point programmable digital signal processors [63].

## 2.6 Dual-path and Per-tone Equalizer Structures

Acker *et al.* [88, 89, 90] propose an alternate DMT receiver architecture shown in Figure 1.7 under b). Since the traditional equalizer equalizes all subchannels “in a combined fashion,” which may limit equalization performance, Acker *et al.* [90] propose to transfer the TEQ operations to the frequency domain by moving the TEQ into the FEQ. The combined TEQ-FEQ would yield a multi-tap FEQ structure in which each subchannel (tone) could be separately equalized. The optimality of the per-tone equalizer (PTE) structure was shown in [90]. This per-tone equalizer could be implemented as a vector dot product of the sliding FFT coefficients for that subchannel and the vector of complex-valued FEQ coefficients. Acker *et al.* define the received signal as

$$\begin{bmatrix} \mathbf{y}_{ks+\nu-T+2+\delta} \\ \vdots \\ \mathbf{y}_{(k+1)s+\delta} \end{bmatrix} = \mathbf{H} \begin{bmatrix} \mathbf{X}_{1:N}^{(k-1)} \\ \mathbf{X}_{1:N}^{(k)} \\ \mathbf{X}_{1:N}^{(k+1)} \end{bmatrix} + \mathbf{n} \quad (2.56)$$

where  $\nu$  is the length of the cyclic prefix,  $s = N + \nu$  is the length of the frame including the cyclic prefix,  $T$  is the length of the time domain equalizer,  $\mathbf{X}_{1:N}^{(c)}$  is the complex  $N$ -long frame to be transmitted at time  $k$ ,  $H$  is a matrix that includes the convolution matrix of the transmission channel  $\mathbf{h}$ , the IFFT transform and the addition of cyclic prefix,  $\mathbf{n}$  is the channel-induced additive noise vector and  $\delta$  is a design parameter denoting the transmission delay.

The demodulated and equalized  $N \times 1$  complex frame vector of the transmitted  $N \times 1$  complex frame at time  $k$  is obtained from the traditional single FIR architecture as

$$\begin{bmatrix} \mathbf{z}_1^{(k)} \\ \vdots \\ \mathbf{z}_N^{(k)} \end{bmatrix} = \mathbf{H} \begin{bmatrix} D_1 & 0 & \cdots \\ 0 & \cdots & 0 \\ \cdots & 0 & D_N \end{bmatrix} \mathcal{F}_N(\mathbf{Y}\mathbf{w}) \quad (2.57)$$

where  $\mathbf{w}$  is the real-valued  $T \times 1$  TEQ finite impulse response filter,  $\mathcal{F}_N$  is the

$N \times N$  FFT matrix,  $D_i$  is the 1-tap complex frequency domain equalizer tap for the subchannel  $i$  and  $N \times T$  received samples matrix  $\mathbf{Y}$  is

$$\begin{bmatrix} \mathbf{y}_{ks+\nu+1} & \mathbf{y}_{ks+\nu} & \cdots & \mathbf{y}_{ks+\nu-T+2} \\ \mathbf{y}_{ks+\nu+2} & \mathbf{y}_{ks+\nu+1} & \cdots & \mathbf{y}_{ks+\nu-T+3} \\ \vdots & \vdots & \ddots & \vdots \\ \mathbf{y}_{(k+1)s} & \mathbf{y}_{(k+1)s-1} & \cdots & \mathbf{y}_{(k+1)s-T+1} \end{bmatrix} \quad (2.58)$$

The equation (2.57) utilizes the time domain equalizer  $\mathbf{w}$ ; however, Acker *et al.* notice that given the linearity of operations, vector  $\mathbf{w}$  can be transferred after the FFT matrix. Thus, the operations in (2.57) can be rewritten as follows

$$\mathbf{z}_i^{(k)} = D_i[\text{row}_i(\mathcal{F}_N)](\mathbf{Y}\mathbf{w}) = [\text{row}_i(\mathcal{F}_N\mathbf{Y})] \underbrace{\mathbf{w}D_i}_{\mathbf{w}_i} \quad (2.59)$$

where  $\mathbf{w}_i$  is a complex  $T \times 1$  vector that performs the functions of the frequency domain equalizer and time domain equalizer in the (2.57). Now each subchannel has its own complex  $T$ -tap frequency domain TEQ. It seems that the new structure requires  $T$  FFT operations per DMT frame instead of one as is the case in the standard architecture, Acker *et al.* point out that due to the Toeplitz structure of  $\mathbf{Y}$  only one “full” FFT needs to be calculated (for the first column of  $\mathbf{Y}$ ) and the other FFTs can be efficiently computed from the first column using sliding FFT procedure. The resulting receiver structure is shown in Figure 2.3. Per tone equalizer initialization can assume the knowledge of the transmission channel and noise parameters or the lack of that knowledge. If the channel parameters are known the equalizers are found by minimizing the following functional

$$J(\mathbf{w}_i) = \left\| \left[ \begin{array}{c} \mathbf{R}_{\mathbf{X}}^{1/2} \mathbf{H}^H \mathbf{F}_i^H \\ \mathbf{R}_{\mathbf{n}}^{1/2} \mathbf{F}_i^H \end{array} \right] \mathbf{w}_i^* - \left[ \begin{array}{c} \mathbf{R}_{\mathbf{X}}^{1/2} \mathbf{e}_i^{(k)H} \\ \mathbf{0} \end{array} \right] \right\|_2^2 \quad (2.60)$$

where  $\mathbf{R}_{\mathbf{X}}$  and  $\mathbf{R}_{\mathbf{n}}$  are the autocorrelations of the transmitted frame  $\mathbf{X}$  and noise vector  $\mathbf{n}$ , respectively, and  $\mathbf{F}_i$  is the FFT-operation dependant matrix for each subchannel  $i$ . The other way to initialize the PTE is not to assume the knowledge of



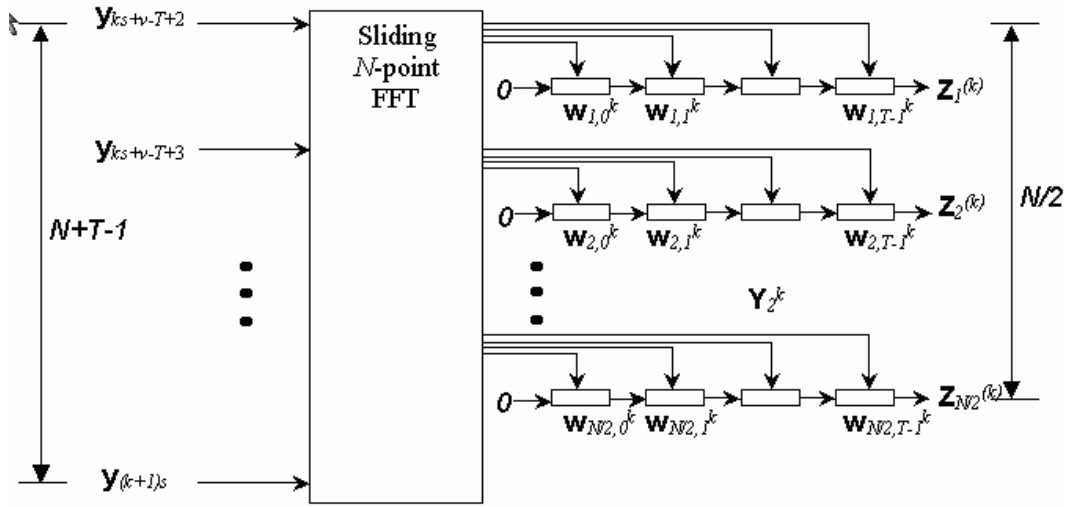


Figure 2.3: Per-tone Equalizer Architecture where  $k$  denotes the  $k^{\text{th}}$  received frame and  $\mathbf{w}_i$  is the  $T$ -tap complex equalizing filter for each subchannel  $i$

the channel and to approach the solution by minimizing the mean squared error between the transmitted value in subchannel  $i$  denoted by  $\mathbf{X}_i^k$  and the value after the PTE in the same subchannel given by  $\mathbf{Z}_i^k$ . This scheme uses a known training sequence and can be implemented using the least-squares iteration (the method used to initialize PTE in the simulations presented in Chapter 7). The new receiver structure exhibits reduced sensitivity to synchronization delay and smaller equalizer size for the same performance compared to earlier methods. In [89, 90], Acker *et al.* also propose various groupings of subchannels, in which each group has a complex equalizing filter assigned to it. However, in that case they are not able to take advantage of the sliding FFT and have to resort to costly full FFTs to design the PTE.

Martin and Johnson [91] propose an application of the traditional blind adaptive algorithms to train the per tone equalizer structure proposed in [90]. The use of the Constant Modulus Algorithm (CMA) (see [92] for a review of CMA) and

Direction-Directed LMS (DD-LMS) is more readily applicable to the PTE architecture than to the traditional TEQ/FEQ DMT receiver architecture. The DD-LMS algorithm performs stochastic gradient descent of the cost function  $E[|\mathbf{z}_k^i - Q[\mathbf{z}_k^i]|^2]$  for each subchannel  $k$  and iteration  $i$ , where  $\mathbf{z}_k^i$  is the equalized estimate of the QAM constellation point and  $Q[\cdot]$  is the decision device. The DD-LMS algorithm is then

$$\begin{aligned}\mathbf{z}_k^i &= [\mathbf{v}_k^i]^\text{T} \mathbf{F}_k \mathbf{y}^i \\ \mathbf{e}^i &= Q[\mathbf{z}_k^i] - \mathbf{z}_k^i \\ \mathbf{v}_k^{i+1} &= \mathbf{v}_k^i + \mu \mathbf{e}^i \mathbf{F}_k^* [\mathbf{y}^i]^* \end{aligned} \quad (2.61)$$

where  $\mathbf{v}_k^i$  is the frequency domain equalizer for subchannel  $k$ ,  $\mathbf{F}_k$  is the DFT for subchannel  $k$ ,  $\mathbf{y}$  is the received time domain frame and  $\mathbf{e}$  is the estimation error. The CMA algorithm performs stochastic gradient descent of the cost function  $E[(|\mathbf{z}_k^i|^2 - \gamma^i)^2]$ . The resulting algorithm is

$$\begin{aligned}\mathbf{z}_k^i &= [\mathbf{v}_k^i]^\text{T} \mathbf{F}_k \mathbf{y}^i \\ \mathbf{v}_k^{i+1} &= \mathbf{v}_k^i - \mu \mathbf{z}_k^i (|\mathbf{z}_k^i|^2 - \gamma^i) \mathbf{F}_k^* [\mathbf{y}^i]^* \end{aligned} \quad (2.62)$$

Martin and Johnson suggest that both algorithms can be used during PTE training; first, use the CMA while the distortion is still strong and the equalizer is still not producing fairly accurate results, and second, use DD-LMS that depends on the accurate decision making to finish the training as it has faster convergence rate. Both algorithms converge asymptotically to the performance of the MMSE initialization in [90].

Ding, Redfern and Evans [93] propose an alternative TEQ block structure, which bridges the gap between the standard single TEQ architecture and PTE architecture of [90]. They propose a dual-path TEQ block where each signal path has a separate TEQ followed an FFT and then by the FEQ. After the FEQ, the complex value from  $i^{\text{th}}$  subchannel is present from both paths, and the subchannel with

higher SNR is chosen for further processing. Two TEQ filters are designed such that one TEQ equalizes over the entire bandwidth while the other one optimizes over a selected frequency band. The selective band TEQ is focused on the subchannels with higher initial pre-TEQ SNR. Ding, Redfern and Evans point to their simulation results that show that the high SNR subchannels have the largest potential to increase the data rate with improved equalization. The TEQ that equalizes over the entire bandwidth can be designed using any of the TEQ design methods such as MMSE or MSSNR. The selective band TEQ would need to be designed using a method that allows frequency selective weighting such as Min-ISI.

## 2.7 Alternative Channel Equalization Methods

De Courville, Duhamel, Madec and Palicot [94] propose an equalization method for OFDM systems where the unused subchannels are used to fully equalize the channel thus removing the need for a cyclic prefix. The unused subchannels are known in advance at the transmitter and the receiver. This equalization architecture removes the traditional TEQ-FEQ pair and replaces it with zero-forcing equalizer after the FFT block. The optimization problem is

$$\begin{aligned} \min_{\mathbf{w}: \mathbf{w}^T \mathbf{w}} (J_z) &= \min_{\mathbf{w}: \mathbf{w}^T \mathbf{w}} \left( \sum_{k=N_u}^{N/2-1} E[|\mathbf{Y}_k|^2] \right) \\ &= \min_{\mathbf{w}: \mathbf{w}^T \mathbf{w}} (\mathbf{W}^T (\mathbf{P} + \mathbf{Q}) \mathbf{W}) \end{aligned} \quad (2.63)$$

where  $\mathbf{Y}_k$  is the received signal in subchannel  $k$ ,  $\mathbf{W}$  is the frequency domain zero-forcing equalizer and  $\mathbf{P}$  and  $\mathbf{Q}$  are matrices capturing the signal and noise components after the FFT block. The zero-forcing criterion tends to enhance noise in the nulls of the transmission channel frequency response.

Cheong and Cioffi [95] propose that the ISI be removed not at the receiver using some form of time domain equalizer, but by pre-coding (distorting) of the signal at the transmitter. The transmitter implements a feedback loop whereby

the frame at time  $i$  is filtered and added to the frame at time  $i + 1$ . The filtering operation assumes the knowledge of the transmission channel as the filters depend on the ISI-causing parts of the channel. The feedback spans the IFFT operation at the transmitter because a time domain frame at time  $k$  is being added to the frequency domain frame at time  $k + 1$ . The algorithm increases the energy of a transmitted frame and requires  $O(N^2)$  operations.

Djokovic [96] follows on the approach in [94] and proposes a method that relies on the redundancy present in a DMT frames where the subchannels not used for data transmission are known and the position of the ISI-corrupted samples in any frame is also known (i. e. the channel has been identified). Djokovic defines

$$\mathbf{y} = \begin{bmatrix} \mathbf{y}_c \\ \mathbf{y}_{nc} \end{bmatrix} \quad \mathbf{Y} = \begin{bmatrix} \mathbf{Y}_z \\ \mathbf{Y}_u \end{bmatrix} \quad \mathbf{F} = \begin{bmatrix} \mathbf{F}_{11} & \mathbf{F}_{12} \\ \mathbf{F}_{21} & \mathbf{F}_{22} \end{bmatrix} \quad (2.64)$$

where  $\mathbf{y}_c$  is the  $n_I \times 1$  vector of ISI-corrupted samples,  $\mathbf{y}_{nc}$  is the  $N - 1 - n_I \times 1$  vector of non-corrupted samples,  $\mathbf{Y}_z$  is the  $n_z \times 1$  vector of zero subchannels,  $\mathbf{Y}_u$  is the  $N/2 - n_z \times 1$  vector of used subchannels,  $\mathbf{F}$  is the FFT operator and  $n_I$  is the number of channel samples beyond the cyclic prefix. From  $\mathbf{Y} = \mathbf{F}\mathbf{y}$  it follows that

$$\mathbf{Y}_z = \mathbf{F}_{11}\mathbf{y}_c + \mathbf{F}_{12}\mathbf{y}_{nc} = 0 \quad (2.65)$$

and

$$\mathbf{Y}_u = \mathbf{F}_{21}\mathbf{y}_c + \mathbf{F}_{22}\mathbf{y}_{nc} \quad (2.66)$$

Now, substituting (2.65) into (2.66) the values of  $\mathbf{Y}_u$  become

$$\mathbf{Y}_u = (\mathbf{F}_{22} - \mathbf{F}_{21}\mathbf{F}_{22}^{-1}\mathbf{F}_{12})\mathbf{y}_{nc} \quad (2.67)$$

Djokovic shows that the approach is practical for the channel length of up to two samples  $n_I = 2$  beyond the length of the cyclic prefix as the  $l_\infty$ -norm of the matrices involved grows with  $n_I$  and noise enhancement becomes more pronounced. Also

new transform loses the properties of the FFT that made it amenable to low-cost implementation.

Trautmann, Karp and Fliege [97] follow on the work by Djokovic ([96]) and introduce a new frequency domain equalizer, which in the absence of the cyclic prefix or guard interval utilizes redundancy in the DMT frame given by the unused subchannels to eliminate the ISI and ICI. In multicarrier modulation, usually, it is not possible to use all of the subchannels due to the spectral compatibility constraints or due to the inability of some subchannels to support at least two bits of data because of high noise. Trautmann, Karp and Fliege use the extra redundancy provided by the unused subchannels to equalize the channel, effectively to “push” the distortion into the unused subchannels without sacrificing useful bandwidth or increasing system latency with the introduction of a cyclic prefix. The equalizer has to remove the phase and magnitude distortion induced by the channel (in standard architecture function of FEQ) and remove the ISI/ICI (in standard architecture function of TEQ). The final equalizer is non-diagonal complex matrix that multiplies the complex  $N/2$ -tap FFT output at the receiver, thus forming a linear combination of the un-equalized FFT output. The equalizer matrix  $\mathbf{E}$  can be split in two sections

$$\begin{aligned} \mathbf{E} &= \mathbf{E} \underbrace{(\mathbf{S}_0 + \mathbf{S}_1)}_{\mathbf{I}_{N/2}} \\ &= \underbrace{\mathbf{E}\mathbf{S}_0}_{\mathbf{E}_0} + \underbrace{\mathbf{E}\mathbf{S}_1}_{\mathbf{E}_1} \end{aligned} \quad (2.68)$$

where  $\mathbf{S}_0$  and  $\mathbf{S}_1$  are subchannel selection matrices of used and unused subchannels, respectively,  $\mathbf{I}_{N/2}$  is a unity matrix,  $\mathbf{E}_0$  contains all linear combinations with unused subchannels, while  $\mathbf{E}_1$  contains all linear combinations with used subchannels. Matrix  $\mathbf{E}_1$  is a diagonal matrix of inverse frequency domain channel coefficients at the frequencies of the used subchannels. Matrix  $\mathbf{E}_0$  is not a diagonal matrix but it also only depends on the channel frequency characteristics in the used subchannels. Trautmann, Karp and Fliege note that with every additional unused subchannel

that can be employed for equalization, the channel impulse response can be one coefficient longer and still allow perfect equalization. However, they also calculate that due to the presence of zero forcing equalizer in  $\mathbf{E}_1$  and the inversion of channel related matrices needed to obtain  $\mathbf{E}_0$ , this equalizer suffers from a 3 dB noise enhancement compared to the standard equalizer structure (TEQ followed by FEQ). Nonetheless, this work explores an interesting idea of utilizing the unused carriers and elimination of the cyclic prefix all together. Trautmann and Fliege [98, 99] follow on this work and consider in their equalizer design both the tail and the head ISI-causing sections of the transmission channel impulse response.

Redfern [100] also considers a new frame structure where the guard band would be created at the transmitter not in the time domain but in the frequency domain by imposing the necessary structure on the unused subchannels. The frequency domain data dependent signal is chosen such that the last  $P$  samples of the  $N$ -long time domain DMT frame are zero. So, in effect, the guard band is present still but instead of being added as  $\nu$  samples to the  $N$  sample long frame, the guard band is incorporated within the  $N$  samples. The difference to the method of Trautmann and Fliege [98, 99] is that the redundancy is being added at the transmitter instead of being “extracted” at the receiver by a multichannel FEQ described by Trautmann and Fliege. The result is that the loss of performance due to noise enhancement is not present. The drawback of Redfern’s approach is that the channels that are not able to carry data will now require power allocation. The usage of the unused carriers to create a guard band does not solve the problem of ISI in case when the channel is longer than  $P$  and Redfern does not propose a way of designing a TEQ that would take advantage of the new frame structure. However, the author does point out that the method can be used with the standard G.DMT to enhance the equalization properties of TEQ filters by essentially extending the guard band between the symbols; i.e. the new guard band consists of the standard cyclic prefix

and  $P$  trailing zeros.

Lu and Evans [101] propose channel equalization using feedforward neural networks. The equalizer performs the full equalization of the channel by compensating for non-linear, linear and additive distortions of the channel. As a non-linear equalization approach, this method can hope to remove the non-linear distortions that cannot be removed using linear filtering. The neural network model is adaptive and does not require a training sequence.

Henkel and Kessler [102] investigate a novel adaptive TEQ design algorithm that maximizes the bit rate achievable in a DMT system by defining a new SNR measure that takes into account the contributions of the crosstalk noise, ISI and energy leakage due to the time domain rectangular windowing imposed by the FFT. The algorithm requires oversampling in the frequency domain by a factor of two thus doubling the required FFT block during the TEQ training. The design alternates between the time and frequency domain representations of the variables during the adaptation. Henkel and Kessler define the following steps:

1. Determine the additive noise power spectral density,  $(N_k^a)^2$  for the subchannel  $k = (0, \dots, 2N - 1)$ ,
2. Let  $H_k$  be proportional to the frequency domain representation of the transmission channel,
3. Let  $S_k = H_k W_k$ ,
4. Determine  $\mathbf{s} = \text{IFFT}(\mathbf{S})$ , where  $\mathbf{S} = [S_0, S_1, \dots, S_{2N-1}]$ ,
5. Determine the power spectral density  $(N_k^s)^2$  of the part of  $\mathbf{s}$  beyond the cyclic prefix,
6. Compute  $(N_k^n)^2 = (N_k^a)^2 W_k^2$ ,
7. Add noise components  $N_k^2 = (N_k^s)^2 + (N_k^n)^2$ ,

8. Compute the autocorrelation function  $\mathbf{n} = \text{IFFT}(\mathbf{N})$ , where  $\mathbf{N} = [N_0, N_1, \dots, N_{2N-1}]$ ,
9. Account for the energy leakage effect introduced by the rectangular windowing of the FFT so that  $\lambda_k = n_k t_k$  where  $\mathbf{t}$  is the triangular function resulting from the convolution of rectangular windows,
10. Find  $\mathbf{\Lambda} = \text{FFT}(\lambda)$ ,
11. Define subchannel  $\text{SNR}_k = \frac{S_k^2}{\Lambda_k}$ ,
12. Substitute the SNR into the bit rate equation (1.8), and
13. Use a numerical algorithm to arrive at the next value of  $\mathbf{w}$  and repeat.

There is no guarantee that the algorithm will converge. The algorithm is the first one to take into account the effect of the energy leakage due to the nature of the DFT and design a TEQ with this noise source included. The resulting TEQ may not shorten the channel so that its length is within the length of the cyclic prefix as the TEQ is designed to maximize the bit rate and balance the effect on all noise sources. Unfortunately, the algorithm requires oversampling and numerous FFTs, not counting the optimization step in 13. Also, in step 4, the assumption is that the linear convolution of the channel and the TEQ is equivalent to the multiplication in the frequency domain of their frequency domain representations which may not be true.

## 2.8 Conclusion

The TEQ block in a DMT receiver should be used to maximize the DMT system bit rate, thus its design should be directly tied to the maximization of the bit rate equation. MSSNR and MMSE TEQ design methods fail to tie their objective to the bit rate of the system thus designing suboptimal time domain equalizers.



The MGSNR attempt to maximize the bit rate makes large approximations thus designing TEQ filters that do not truly maximize the bit rate. MBR defines the bit rate as a function of TEQ coefficients at the output of the TEQ; however, it only considers ISI and white Gaussian noise and it does not propose a closed form solution. PTE maximizes the signal-to-noise ratio by shifting the equalization to the frequency domain where each subchannel is assigned an complex equalizer calculated through a mean-squared error minimization. PTE eliminates TEQ and requires additional complexity in the implementation of the FFT block called “sliding FFT”.

TEQ design should take into account the various noise sources present in a DMT system such as near-end crosstalk, white Gaussian noise, the effects of finite-precision arithmetic, the effects of signal quantization and inter-carrier interference and include these in the SNR measure. This approach is not fully followed in the previous work. The optimal TEQ will balance the effect of all noise sources on the bit rate and not only the effect of ISI/ICI. In the following chapter, I define a subchannel SNR model that follows the aforementioned guidelines and continue by discussing its efficient computation in Chapter 4. I proceed to define a new optimal G.DMT-compliant TEQ architecture and also apply the method to the traditional single TEQ receiver architecture in Chapter 5. Chapter 6 discusses a TEQ that shortens multiple channels simultaneously but its design is based on the MSSNR and not on the bit rate maximization model. Chapter 7 presents simulations results followed by conclusions and future work in Chapter 8.

## Chapter 3

# Subchannel SNR Model

Chapter 1 describes high-speed broadband wireline and wireless technologies, introduces multicarrier modulation concept and analyzes two implementations of it: discrete multitone modulation and orthogonal frequency division multiplexing. Chapter 2 focuses on the impact of the time domain equalizer on the system data rate and surveys existing time domain equalizer design methods. In this chapter, I derive a subchannel signal-to-noise ratio model to establish the functional dependency of the bit rate on time domain equalizer coefficients and enable the formulation of bit rate maximization time domain equalizer designs. The time domain equalizer should maximize the bit rate achievable in a discrete multitone modulation/ orthogonal frequency division multiplexing system. I develop a subchannel signal-to-noise ratio model where the desired signal is formed as the circularly convolved data symbol and the channel impulse response at the input of the FFT and noise is the difference between the received and the desired signal. The received signal also includes the near-end crosstalk, additive white Gaussian noise, analog-to-digital converter quantization noise and the digital noise floor due to finite precision arithmetic.

### 3.1 Introduction

The TEQ block is available to the DMT receiver designer to use to change the received signal in such a way that the SNR in each data-carrying subchannel is increased. A good model of the subchannel SNR that will show the dependence on the TEQ coefficients is a prerequisite for a successful TEQ design as it establishes a direct link between the TEQ design and the bit rate which depends on the subchannel SNR. The proposed subchannel SNR is a ratio of the desired signal power to the power of the noise present in the received signal. The noise sources included in the model are: ISI and ICI, additive white Gaussian noise, near-end crosstalk, analog-to-digital conversion noise and the digital noise floor. The model is flexible so that additional noise sources such as far-end crosstalk, near-end echo or far-end echo can be included. The SNR model is defined after the receiver's demodulating FFT block and the TEQ block. Although the SNR model is defined for all subchannels in the frequency domain it is still a function of the time domain equalizer coefficients.

In the subchannel SNR definition, the numerator is the power of the desired signal that results in a particular subchannel when a DMT frame is circularly convolved with the channel impulse response. This is the desired signal in the particular subchannel of interest. In DMT, the ability to write the circular convolution of the frame and the channel impulse response as the multiplication of their discrete Fourier transform representations in the frequency domain simplifies the removal of the channel distortion as explained in Chapter 1. If all of the ISI and ICI are removed from the received signal, it is possible to use this property as the channel has been shortened enough so that the CP has converted the linear convolution of the DMT frame and the transmission channel into their circular convolution. Thus, the desired signal will exhibit this property. The power of the noise in the particular subchannel of interest (the denominator of the subchannel SNR) is then the power

of the difference of the actual received signal (before the TEQ is designed and placed in the receive path) and this desired signal. The received signal carries with it all of the noise mentioned above.

In this chapter, Section 3.2 defines the transmission channel and DMT frame parameters. Section 3.3 analyzes the noise sources considered being the inter-symbol and inter-carrier interference, additive white Gaussian noise, near-end crosstalk, analog-to-digital conversion noise and digital noise floor. Section 3.4 defines the concepts of the signal desired in a subchannel carrying data and the signal received in that subchannel. Section 3.5 presents a new model of the signal-to-noise ratio in a subchannel based on the definitions of Section 3.4. Section 3.6 concludes this chapter.

## 3.2 Transmission Channel and Discrete Multitone Frames

Let  $\nu$  be the length of the CP and  $\mathbf{h} = [h_0, h_1, \dots, h_{N-1}]^T$  be the  $N \times 1$  channel impulse response. G.DMT provides for frame-length identification of the channel impulse response at a sampling rate of  $f_s = 2.208$  MHz which amounts to roughly  $232 \mu\text{s}$  for a symbol length,  $N$ , of 512 samples. The frame rate  $f_{\text{frame}}$  is 4 kHz. Let  $\mathbf{w} = [w_0, w_1, \dots, w_{M-1}]^T$  be an  $M \times 1$  TEQ, where  $M$  is some predetermined length. Let  $\mathbf{H}$  be the  $(N + M - 1) \times M$  convolution matrix of the channel impulse

response and the TEQ.

$$\mathbf{H} = \begin{bmatrix} h_0 & 0 & 0 & \cdots & 0 \\ h_1 & h_0 & 0 & \cdots & 0 \\ \vdots & & & & \vdots \\ h_{M-1} & \cdots & & \cdots & h_0 \\ \vdots & & & & \vdots \\ h_{N-1} & \cdots & & \cdots & h_{N-1-M} \\ 0 & h_{N-1} & \cdots & \cdots & h_{N-M} \\ \vdots & & & & \vdots \\ 0 & 0 & 0 & \cdots & h_{N-1} \end{bmatrix} \quad (3.1)$$

Let  $\Delta$  be the transmission delay incurred by the signal from the transmitter to the receiver FFT block. Let  $\mathbf{u}_i$  be the  $i^{\text{th}}$   $N \times 1$  sample DMT frame to be decoded. Preceding and following this frame are  $\mathbf{u}_{i-1}$  and  $\mathbf{u}_{i+1}$  DMT frames, respectively. DMT time domain samples are a superposition of a number of sinusoids (up to 256 in ADSL and up to 4096 in VDSL) with “random” amplitudes and phase shifts of varying frequencies. DMT time domain samples can therefore be approximated using the Central Limit Theorem (CLT) [103] as being independent, identically distributed (i.i.d.) according to  $\mathcal{N}(0, \sigma_s^2)$ , where  $\mathcal{N}$  represents normal distribution and  $\sigma_s^2$  is the transmit signal variance, which is measured by the transmit power with respect to  $100\Omega$  resistance. Define the vector

$$\mathbf{q}_k = \left[ 1, e^{j2\pi k/N}, \dots, e^{j2\pi(N-1)k/N} \right]^T \quad (3.2)$$

such that the inner product of  $\mathbf{q}_k^H$  with an  $N$ -point vector gives the  $k^{\text{th}}$  FFT coefficient of that vector, where  $(\cdot)^H$  means the Hermitian (conjugate transpose) operator.

### 3.3 Sources of Noise and Interference

#### 3.3.1 Inter-symbol interference

Inter-symbol interference refers to the mixing of energies of DMT frames  $i - 1$  and  $i + 1$  into the DMT frame  $i$  due to their passage through a transmission channel whose energy is spread over a time longer than the length of the CP. This mixing of energy makes proper detection of the data transmitted in frame  $i$  less likely and is therefore a source of noise. Using the above define

$$\mathbf{U}_{\text{ISI}}^{\Delta} = \mathbf{U}_{i-1}^{\Delta} + \mathbf{U}_i^{\Delta} + \mathbf{U}_{i+1}^{\Delta} \quad (3.3)$$

to be the  $N \times (N + M - 1)$  convolution matrix of the DMT frames  $i - 1$ ,  $i$  and  $i + 1$  and the transmission channel  $\mathbf{h}$  that will capture the ISI noise in the SNR model. Let  $\mathbf{U}_i^{\Delta}$

$$\mathbf{U}_i^{\Delta} = \left[ \left( \mathbf{U}_i^{\Delta} \right)_L \left( \mathbf{U}_i^{\Delta} \right)_R \right] \quad (3.4)$$

be  $N \times (N + M - 1)$  convolution matrix of the DMT frame  $i$  with the transmission channel, where for notational convenience I define

$$\left( \mathbf{U}_i^{\Delta} \right)_L = \begin{bmatrix} u_i^{\Delta} & u_i^{\Delta-1} & \dots & u_i^0 & u_i^{N-1} & \dots & u_i^{N-\nu} \\ u_i^{\Delta+1} & u_i^{\Delta} & \dots & \dots & u_i^0 & u_i^{N-1} & \dots \\ \vdots & \vdots & & & & \vdots & \vdots \\ u_i^{N-1} & u_i^{N-2} & \dots & \dots & \dots & u_i^0 & u_i^{N-1} \\ 0 & u_i^{N-1} & u_i^{N-2} & \dots & \dots & u_i^1 & u_i^0 \\ \vdots & & & & & \vdots & \vdots \\ 0 & \dots & \dots & \dots & \dots & 0 & u_i^{N-1} \\ \vdots & & & & & \vdots & \vdots \\ 0 & \dots & \dots & \dots & \dots & 0 & 0 \end{bmatrix} \quad (3.5)$$

and

$$\left( \mathbf{U}_i^\Delta \right)_R = \begin{bmatrix} 0 & \cdots & \cdots & \cdots & \cdots & 0 \\ u_i^{N-\nu} & \cdots & \cdots & \cdots & \cdots & 0 \\ \vdots & & \vdots & \vdots & & \vdots \\ u_i^{N-2} & \cdots & u_i^{N-\nu} & 0 & \cdots & 0 \\ u_i^{N-1} & \cdots & u_i^{N-\nu-1} & 0 & \cdots & 0 \\ \vdots & & \vdots & \vdots & & \vdots \\ u_i^{N-2} & \cdots & u_i^0 & u_i^{N-1} & \cdots & u_i^{N-\nu} \\ \vdots & & \vdots & \vdots & & \vdots \\ 0 & \cdots & 0 & u_i^{N-1} & \cdots & u_i^{\Delta-M-1} \end{bmatrix} \quad (3.6)$$

Let  $\mathbf{U}_{i-1}^\Delta$  be the  $N \times (N + M - 1)$  convolution matrix of the DMT frame  $i - 1$  with the transmission channel.

$$\mathbf{U}_{i-1}^\Delta = \begin{bmatrix} 0 & \cdots & 0 & u_{i-1}^{N-1} & u_{i-1}^{N-2} & \cdots & u_{i-1}^{\nu+\Delta-M+1} \\ \vdots & & & & & & \vdots \\ 0 & \cdots & \cdots & 0 & u_{i-1}^{N-1} & \cdots & u_{i-1}^{N+\nu-M+1} \\ \vdots & & & & & & \vdots \\ 0 & \cdots & \cdots & 0 & \cdots & 0 & u_{i-1}^{N-1} \\ 0 & \cdots & 0 & 0 & \cdots & \cdots & 0 \\ \vdots & & & & & & \vdots \\ 0 & \cdots & 0 & 0 & \cdots & \cdots & 0 \end{bmatrix} \quad (3.7)$$

be  $N \times (N + M - 1)$  convolution matrix of the DMT frame  $i + 1$  with the transmission channel

$$\mathbf{U}_{i+1}^\Delta = \begin{bmatrix} 0 & 0 & \cdots & 0 & 0 & \cdots & 0 \\ 0 & 0 & \cdots & \cdots & 0 & 0 & 0 \\ \vdots & & & & & & \vdots \\ 0 & 0 & \cdots & 0 & 0 & \cdots & 0 \\ u_{i+1}^{N-\nu} & 0 & \cdots & \cdots & 0 & \cdots & \cdots \\ \vdots & & & & & & \vdots \\ u_{i+1}^0 & u_{i+1}^{N-1} & \cdots & u_{i+1}^{N-\nu} & 0 & \cdots & 0 \\ \vdots & & & & & & \vdots \\ u_{i+1}^{\Delta-\nu-1} & \cdots & u_{i+1}^0 & u_{i+1}^{N-1} & \cdots & u_{i+1}^{N-\nu} & 0 \end{bmatrix} \quad (3.8)$$

### 3.3.2 Near-end crosstalk, and additive white Gaussian noise

The near-end crosstalk results from the unwanted reception of neighboring transmitter's signal into the local receiver. The unshielded copper twisted pair used for communication between the customer premises and the central office allows cross-coupling of signals on adjacent twisted pair links through electromagnetic induction. Figure 3.1 depicts the near-end crosstalk noise among other noise sources. The figure shows two transceiver pairs linked through a copper twisted pair. The individual transceivers are numbered 1 through 4 where Rx indicates a receiver and Tx indicates a transmitter. The receiver of interest is numbered with 3. Lettered links indicate signals received by the number 3 receiver. Letter a) indicates near-end crosstalk noise, letter b) shows near-echo noise, letter c) marks the additive white Gaussian noise, letter d) denotes the desired far-end signal and letter e) indicates the far-end crosstalk. Signals a), b), c) and d) are some of the noise sources for the number 3 receiver.



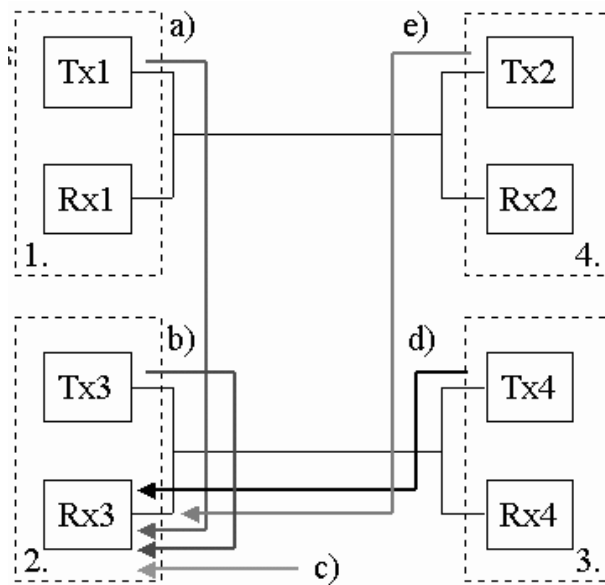


Figure 3.1: Received signals in DMT. The figure shows 2 transceiver pairs linked through a copper twisted pair. The individual transceivers are numbered 1. through 4 where Rx indicates a receiver and Tx indicates a transmitter. The receiver of interest is numbered with 3. Lettered links indicate signals received by the number 3 receiver. Letter a) indicates near-end crosstalk noise, letter b) shows near-echo noise, letter c) marks the additive white Gaussian noise, letter d) denotes the desired far-end signal and letter e) indicates the far-end crosstalk. Signals a), b), c) and d) are some of the noise sources for the number 3 receiver.

Let the NEXT, and AWGN noise vectors be of the form

$$\mathbf{n}^{\text{xx}} = \{n_{-M+1}^{\text{xx}}, n_{-M+2}^{\text{xx}}, \dots, n_0^{\text{xx}}, \dots, n_{N-1}^{\text{xx}}\}^T \quad (3.9)$$

where the subscript  $(\cdot)_{\text{xx}}$  is equal to either NEXT or AWGN. Then the  $(N+M-1) \times M$  AWGN, and NEXT convolution matrices with the TEQ,  $\mathbf{G}_{\text{AWGN}}$ , and  $\mathbf{G}_{\text{NEXT}}$  are

$$\mathbf{G}_{\text{xx}} = \begin{bmatrix} n_0^{\text{xx}} & n_{-1}^{\text{xx}} & \dots & n_{-M+1}^{\text{xx}} \\ n_1^{\text{xx}} & n_0^{\text{xx}} & \dots & n_{-M+2}^{\text{xx}} \\ \vdots & & & \vdots \\ n_{M-1}^{\text{xx}} & \dots & \dots & n_0^{\text{xx}} \\ \vdots & & & \vdots \\ n_{N-1}^{\text{xx}} & \dots & & n_{N-1-M}^{\text{xx}} \\ \vdots & & & \vdots \\ n_{N+M}^{\text{xx}} & n_{N+M-1}^{\text{xx}} & \dots & n_{N-1}^{\text{xx}} \end{bmatrix} \quad (3.10)$$

The samples of AWGN are i.i.d. according to  $\mathcal{N}(0, \sigma_{\text{AWGN}}^2)$  where  $\sigma_{\text{AWGN}}^2$  is the noise variance, which is measured by the power of the noise with respect to  $100\Omega$  resistance. Samples of the NEXT have spectrally shaped power spectral density (PSD) as defined in [20] for various types of interferers and denoted using the Toeplitz variance matrix  $\Sigma_{\text{NEXT}}$ .

### 3.3.3 Analog-to-digital conversion noise and digital noise floor

The signals presented to a DMT receiver will be sampled and quantized using an analog-to-digital converter (ADC). The samples of the received signal are then processed using either a digital signal processor (DSP) or application-specific integrated circuits. The quantization process imparts noise on the received signal. Starr, Cioffi and Silverman [33, p. 299] recommend using 14-bit ADC, while ADSL transceivers commonly use 16-bit ADCs. This source of noise is treated here as ADC noise and is considered an additive noise source. Processing of samples is commonly performed

in fixed-point arithmetic, which also imparts noise onto the signal. Fixed-point DSPs commonly use a 16-bit word length, have 16 x 16 bit multipliers on chip, and accumulate the 32-bit result of multiplication result at a precision of 32 bits or higher. Some of the Motorola DSPs use a 24-bit word length, and accumulate the result of the multiplication at a resolution of 56 bits. Gersho and Gray [104, p. 152] point out that in a high resolution case one can approximate the probability density function of the quantization noise to be uniform. The fixed-point arithmetic thus defines another noise source that is called here digital noise floor (DNF) and is treated as an additive noise source. The following derives the sources of both ADC noise and DNF in terms of the input signal and shows the dependency (or lack thereof) on the TEQ coefficients. Let  $\bar{\mathbf{w}} = \mathbf{w} + \mathbf{n}_w$ , where  $\mathbf{w}$  is the TEQ in infinite precision,  $\bar{\mathbf{w}}$  is the TEQ in fixed-point representation, and  $\mathbf{n}_w$  the corresponding quantization noise. Let  $\bar{\mathbf{y}} = \mathbf{y} + \mathbf{n}_y$ , where  $\mathbf{y}$  is the received signal before the ADC,  $\bar{\mathbf{y}}$  is the received signal after the ADC, and  $\mathbf{n}_y$  the corresponding quantization noise. After some algebra, the convolution of  $\bar{\mathbf{w}}$  and  $\bar{\mathbf{y}}$  can be written as

$$\bar{\mathbf{w}} * \bar{\mathbf{y}} = \mathbf{w} * \mathbf{y} + \underbrace{\mathbf{w} * \mathbf{n}_y}_{\mathbf{e}_1} + \underbrace{\bar{\mathbf{y}} * \mathbf{n}_w}_{\mathbf{e}_2} \quad (3.11)$$

where the error terms are the loss incurred by performing operations using digital processing. Here,  $\mathbf{e}_1$  depends on the TEQ, while  $\mathbf{e}_2$  does not.

Thus, I define  $\mathbf{G}_{\text{ADC}}$  as the ADC noise  $(N + M - 1) \times M$  convolution matrix with the TEQ defined analogously to  $\mathbf{G}_{\text{AWGN}}$ . ADC noise samples are i.i.d. according to  $\mathcal{U}(0, \sigma_{\text{ADC}}^2)$ , where  $\mathcal{U}$  stands for uniform distribution and  $\sigma_{\text{ADC}}^2 = 2^{-2p}/12$ , where  $p$  is the number of bits in the ADC.

The vector  $\mathbf{e}_2$  captures the fixed-point noise (DNF) and whose value in sub-channel  $k$  is  $D_k$ . DNF does not depend on the TEQ but it does effect the subchannel SNR terms,  $\text{SNR}_k(\mathbf{w})$ . DNF  $D_k$  distribution is Gaussian by Central Limit Theorem with  $\mathcal{N}(0, \sigma_{\text{DNF}}^2(k))$  where  $\sigma_{\text{DNF}}^2$  is the noise variance <sup>1</sup>.

---

<sup>1</sup>Assuming that the samples of  $\mathbf{n}_w$  are i.i.d. according to  $\mathcal{U}(0, \sigma_{\text{FP}}^2)$  and independent of  $\bar{\mathbf{y}}$ , then

### 3.4 Received and Desired Subchannel Signals

Using the variables defined in previous sections, I write the received data point in the  $k^{\text{th}}$  subchannel as

$$Y_{\text{R}}^k(\mathbf{w}) = \mathbf{q}_k^{\text{H}} \mathbf{U}_{\text{ISI}}^{\Delta} \mathbf{H} \mathbf{w} + \mathbf{q}_k^{\text{H}} \mathbf{G}_{\text{AWGN}} \mathbf{w} + \mathbf{q}_k^{\text{H}} \mathbf{G}_{\text{NEXT}} \mathbf{w} + \mathbf{q}_k^{\text{H}} \mathbf{G}_{\text{ADC}} \mathbf{w} + D_k \quad (3.12)$$

where  $k \in \{0, \dots, \frac{N}{2} - 1\}$ . The received data contains the noise due to the ISI, ICI, AWGN, NEXT, ADC quantization and DNF.

The desired signal has no noise present. It is “formatted” to the modulation scheme and the strength of the signal is much higher than the DNF. The desired circular convolution of the  $i^{\text{th}}$  frame and the channel impulse response in the  $k^{\text{th}}$  subchannel, after the TEQ and FFT, can be written as

$$Y_{\text{D}}^k(\mathbf{w}) = \mathbf{q}_k^{\text{H}} \left[ \mathbf{U}_i^{\Delta} \right]_{\text{circ}} \mathbf{H} \mathbf{w}, \quad k \in \{0, \dots, N/2 - 1\} \quad (3.13)$$

where  $(N + M - 1) \times M$  convolution matrix with the TEQ is

$$\left[ \mathbf{U}_i^{\Delta} \right]_{\text{circ}} = \begin{bmatrix} u_i^{\Delta} & \dots & u_i^0 & u_i^{N-1} & \dots & u_i^{\Delta-M+2} \\ \vdots & & & & \vdots & \\ u_i^{N-1} & \dots & u_i^{\Delta} & u_i^{\Delta-1} & \dots & u_i^{N-M+1} \\ u_i^0 & \dots & u_i^{\Delta+1} & u_i^{\Delta} & \dots & u_i^{N-M+2} \\ \vdots & & & & \vdots & \\ u_i^{\Delta-1} & \dots & u_i^0 & u_i^{N-1} & \dots & u_i^{\Delta-M-1} \end{bmatrix} \quad (3.14)$$

Thus, having defined the desired signal, I express the received signal as the sum of the desired signal and the noise. The received signal in subchannel  $k$  is  $Y_{\text{R}}^k(\mathbf{w})$  given by

$$Y_{\text{R}}^k(\mathbf{w}) = Y_{\text{D}}^k(\mathbf{w}) + \underbrace{(Y_{\text{R}}^k(\mathbf{w}) - Y_{\text{D}}^k(\mathbf{w}))}_{\text{ISI, ICI, AWGN, NEXT, DNF, ADCnoise}} \quad (3.15)$$

---

$\sigma_{\text{DNF}}^2(k)$  can be approximated as  $\sigma_{\text{DNF}}^2(k) = N \sigma_{\text{FP}}^2 (\sigma_s^2 |H(k)|^2 + \sigma_{\text{ADC}}^2)$ ; where  $H(k) = \mathbf{q}_k^{\text{H}} \mathbf{h}$  and  $\sigma_{\text{FP}}^2 = 2^{-2r}/12$  for a fixed-point (FP) mapping with  $r$  bits.

### 3.5 Subchannel SNR

I define the subchannel SNR<sup>Model</sup><sub>*k*</sub>(**w**) for each subchannel *k* as

$$\text{SNR}_k^{\text{Model}}(\mathbf{w}) = \frac{E \left\{ \left[ Y_D^k(\mathbf{w}) \right]^H Y_D^k(\mathbf{w}) \right\}}{E \left\{ \left[ Y_R^k(\mathbf{w}) - Y_D^k(\mathbf{w}) \right]^H \left[ Y_R^k(\mathbf{w}) - Y_D^k(\mathbf{w}) \right] \right\}} \quad (3.16)$$

where  $E[\cdot]$  is the statistical expectation operator and  $[\cdot]^{\text{Model}}$  stands for model.

I have defined the proposed SNR model as the ratio of the desired signal, which excludes the effects of the noise including the ISI and ICI, to the difference between the received signal and the desired signal. If there were no noise due to ISI and ICI, then the denominator would be reduced to the contributions of the AWGN, NEXT, ADC quantization noise and DNF. After several algebraic steps (shown in the following sections) I derive the SNR model of the numerator and the denominator and the model of the SNR (3.16) has the familiar form

$$\text{SNR}_k^{\text{Model}}(\mathbf{w}) = \frac{\mathbf{w}^T \tilde{\mathbf{A}}_k \mathbf{w}}{\mathbf{w}^T \tilde{\mathbf{B}}_k \mathbf{w}} \quad (3.17)$$

SNR<sup>Model</sup><sub>*k*</sub>(**w**) is a ratio of quadratic functions of the vector of the time domain equalizer coefficients, **w**. Matrices  $\tilde{\mathbf{A}}_k$  and  $\tilde{\mathbf{B}}_k$  are Hermitian symmetric. A similar quadratic form has been derived in [63]. The proposed SNR model becomes equivalent to the SNR that could be measured at the output of the FFT in an ADSL system when the ISI and ICI have been removed from the received signal.

#### 3.5.1 Power of the desired subchannel signal

I now proceed through several algebraic steps to derive the power of both the desired signal and noise in subchannel *k* which constitute the nominator and the denominator of the SNR model, respectively. I will start with the numerator of (3.17).

$$E \left[ \left( Y_D^k \right)^H Y_D^k \right] = E \left[ \mathbf{w}^T \mathbf{H}^T \left[ \mathbf{U}_i^\Delta \right]_{\text{circ}}^T \mathbf{q}_k \mathbf{q}_k^H \left[ \mathbf{U}_i^\Delta \right]_{\text{circ}} \mathbf{H} \mathbf{w} \right]$$

$$\begin{aligned}
&= \mathbf{w}^T \mathbf{H}^T \mathbf{Q}_k^{\text{circ}} E \left[ \mathbf{u}_i \mathbf{u}_i^T \right] \left[ \mathbf{Q}_k^{\text{circ}} \right]^H \mathbf{H} \mathbf{w} \\
&= \sigma_s^2 \mathbf{w}^T \mathbf{H}^T \mathbf{Q}_k^{\text{circ}} \left[ \mathbf{Q}_k^{\text{circ}} \right]^H \mathbf{H} \mathbf{w} \\
&= \mathbf{w}^T \tilde{\mathbf{A}}_k \mathbf{w}
\end{aligned} \tag{3.18}$$

where

$$\mathbf{Q}_k^{\text{circ}} = \begin{bmatrix} q_k^{ND+1} & \dots & \dots & q_k^{N1} & q_0 & \dots & q_k^{ND} \\ q_k^{ND+2} & \dots & q_k^{N1} & q_0 & \dots & \dots & q_k^{ND+1} \\ \vdots & & & & & & \vdots \\ q_k^0 & q_k^1 & \dots & \dots & \dots & \dots & q_k^{N1} \\ \vdots & & & & & & \vdots \\ q_k^{MD-3} & q_k^{MD-2} & \dots & q_0 & \dots & \dots & q_k^{N-MD-2} \end{bmatrix} \tag{3.19}$$

is a  $N + M - 1 \times N$  matrix and  $ND = N - \Delta$ ,  $MD = M + \Delta$  and  $N1 = N - 1$ .

Thus,

$$\tilde{\mathbf{A}}_k = \sigma_s^2 \mathbf{H}^T \mathbf{Q}_k^{\text{circ}} \left[ \mathbf{Q}_k^{\text{circ}} \right]^H \mathbf{H} \tag{3.20}$$

### 3.5.2 Power of the subchannel noise signal

Noise is defined using the difference between the received and desired signals for every subchannel.

$$\begin{aligned}
Y_R^k - Y_D^k &= \mathbf{q}_k^H \left( \mathbf{U}_{i-1}^\Delta + \mathbf{U}_{i+1}^\Delta + \underbrace{\mathbf{U}_i^\Delta - [\mathbf{U}_i^\Delta]_{\text{circ}}}_{\mathbf{P}} \right) \mathbf{H} \mathbf{w} \\
&+ \mathbf{q}_k^H \mathbf{G}_{\text{AWGN}} \mathbf{w} \\
&+ \mathbf{q}_k^H \mathbf{G}_{\text{NEXT}} \mathbf{w} + D_k
\end{aligned} \tag{3.21}$$

In order to easily deal with matrix  $\mathbf{P}$ , we are going to break it into two matrices containing the non-zero entries. Define

$$\mathbf{P} = \left[ \mathbf{U}_{i,L}^\Delta \right] + \left[ \mathbf{U}_{i,U}^\Delta \right] \tag{3.22}$$

where

$$\left[ \mathbf{U}_{i,L}^\Delta \right] = \begin{bmatrix} 0 & \cdots & \cdots & \cdots & \cdots & \cdots & 0 \\ \vdots & & & & & & \vdots \\ u_i^0 & 0 & \cdots & \cdots & \cdots & \cdots & 0 \\ u_i^1 & u_i^0 & 0 & \cdots & 0 & \cdots & 0 \\ \vdots & \vdots & \vdots & & \vdots & & \vdots \\ u_i^{\Delta-1} & u_i^{\Delta-2} & \cdots & u_i^0 & 0 & \cdots & 0 \end{bmatrix} \quad (3.23)$$

and

$$\left[ \mathbf{U}_{i,U}^\Delta \right] = \begin{bmatrix} 0 & \cdots & 0 & u_i^{NV1} & u_i^{NV1-1} & \cdots & u_i^{DM+2} \\ 0 & \cdots & 0 & 0 & u_i^{NV1} & \cdots & u_i^{DM+3} \\ \vdots & & \vdots & \vdots & \vdots & & \vdots \\ 0 & \cdots & 0 & \cdots & 0 & 0 & u_i^{NV1} \\ 0 & \cdots & 0 & 0 & \cdots & 0 & 0 \\ \vdots & & \vdots & \vdots & \vdots & & \vdots \\ 0 & \cdots & 0 & 0 & \cdots & 0 & 0 \end{bmatrix} \quad (3.24)$$

where we define  $NV1 = N - \nu - 1$  and  $DM = \Delta - M$ . Notice that non-zero entries come about because of the contributions of DMT frame  $i - 1$  and  $i + 1$  present in the matrix  $\left[ \mathbf{U}_{ISI}^\Delta \right]$ .

For notational convenience define  $Z_k$  as

$$Z_k = Y_R^k - Y_D^k \quad (3.25)$$

Then the power in  $Z_k$  is

$$\begin{aligned} P_Z &= E \left[ Z_k^H Z_k \right] \quad (3.26) \\ &= \mathbf{w}^T E \left[ \mathbf{S} \right] \mathbf{w} + \mathbf{w}^T E \left[ \underbrace{\mathbf{G}_{AWGN}^T \mathbf{q}_k \mathbf{q}_k^H \mathbf{G}_{AWGN}}_{\mathbf{P}_{Z1}} \right] \mathbf{w} + \mathbf{w}^T E \left[ \underbrace{\mathbf{G}_{NEXT}^T \mathbf{q}_k \mathbf{q}_k^H \mathbf{G}_{NEXT}}_{\mathbf{P}_{Z2}} \right] \mathbf{w} \\ &+ \mathbf{w}^T E \left[ \underbrace{\mathbf{G}_{ADC}^T \mathbf{q}_k \mathbf{q}_k^H \mathbf{G}_{ADC}}_{\mathbf{P}_{Z3}} \right] \mathbf{w} + E \left[ D_k^H D_k \right] \end{aligned}$$

Where

$$\begin{aligned}
\mathbf{S} &= \underbrace{\mathbf{H}^T [\mathbf{U}_{i-1}^\Delta]^\text{H} \mathbf{q}_k \mathbf{q}_k^\text{H} \mathbf{U}_{i-1}^\Delta \mathbf{H}}_{\mathbf{S1}} \\
&+ \underbrace{\mathbf{H}^T [\mathbf{U}_{i+1}^\Delta]^\text{H} \mathbf{q}_k \mathbf{q}_k^\text{H} \mathbf{U}_{i+1}^\Delta \mathbf{H}}_{\mathbf{S2}} \\
&+ \underbrace{\mathbf{H}^T \mathbf{P}^\text{H} \mathbf{q}_k \mathbf{q}_k^\text{H} \mathbf{P} \mathbf{H}}_{\mathbf{S3}}
\end{aligned} \tag{3.27}$$

Notice that now we can transform the parts of (3.27) as follows

$$[\mathbf{U}_{i+1}^\Delta]^\text{H} \mathbf{q}_k = \begin{bmatrix} \mathbf{V}_k^\text{b} & \mathbf{0} & \mathbf{V}_k^\text{u} \\ \mathbf{0} & \mathbf{0} & \mathbf{0} \end{bmatrix}_{(N+M-1) \times N} \mathbf{u}_{i+1} \tag{3.28}$$

where  $\mathbf{V}_k$  is an upper diagonal matrix defined as

$$\mathbf{V}_k = \begin{bmatrix} q_k^{N-\Delta} & q_k^{N-\Delta+1} & \dots & q_k^{N-2} & q_k^{N-1} \\ q_k^{N-\Delta+1} & q_k^{N-\Delta} & \dots & q_k^{N-1} & 0 \\ \vdots & & & \vdots & \vdots \\ q_k^{N-1} & 0 & \dots & 0 & 0 \end{bmatrix}_{\Delta \times \Delta} \tag{3.29}$$

Also define  $\mathbf{V}_k = [\mathbf{V}^\text{u} | \mathbf{V}^\text{b}]$  where  $\mathbf{V}^\text{u}$  is a  $\Delta - \nu \times 1$  matrix and  $\mathbf{V}^\text{b}$  is  $\nu \times 1$  matrix.

Similarly,

$$[\mathbf{U}_{i-1}^\Delta]^\text{H} \mathbf{q}_k = \begin{bmatrix} \mathbf{0} & \mathbf{0} \\ \mathbf{0} & \mathbf{W}_k \end{bmatrix}_{(N+M-1) \times N} \mathbf{u}_{i-1} \tag{3.30}$$

where  $\mathbf{W}_k$  is a lower diagonal  $(N - \nu - \Delta + M - 1) \times (N - \nu - \Delta + M - 1)$  matrix defined as



$$\mathbf{W}_k = \begin{bmatrix} 0 & 0 & \cdots & 0 & q_k^0 \\ 0 & 0 & \cdots & q_k^0 & q_k^1 \\ \vdots & & & \vdots & \vdots \\ q_k^0 & q_k^1 & \cdots & \cdots & q_k^{N-\nu-\Delta+M-2} \end{bmatrix} \quad (3.31)$$

Then

$$\left[ \mathbf{U}_{i,L}^\Delta \right]^H \mathbf{q}_k = \begin{bmatrix} \mathbf{V}_k & \mathbf{0} \\ \mathbf{0} & \mathbf{0} \end{bmatrix}_{(N+M-1) \times N} \mathbf{u}_i \quad (3.32)$$

and

$$\left[ \mathbf{U}_{i,U}^\Delta \right]^H \mathbf{q}_k = \begin{bmatrix} \mathbf{0} & \mathbf{0} & \mathbf{0} \\ \mathbf{0} & \mathbf{W}_k & \mathbf{0} \end{bmatrix}_{(N+M-1) \times N} \mathbf{u}_i \quad (3.33)$$

Now we can go forward with the derivation in

$$\begin{aligned} E[\mathbf{S2}] &= \mathbf{H}^T \begin{bmatrix} \mathbf{V}_k^b & \mathbf{0} & \mathbf{V}_k^u \\ \mathbf{0} & \mathbf{0} & \mathbf{0} \end{bmatrix} E[\mathbf{u}_{i+1} \mathbf{u}_{i+1}^T] \begin{bmatrix} \left[ \mathbf{V}_k^b \right]^H & \mathbf{0} \\ \mathbf{0} & \mathbf{0} \\ \left[ \mathbf{V}_k^u \right]^H & \mathbf{0} \end{bmatrix} \mathbf{H} \\ &= \sigma_s^2 \mathbf{H}^T \begin{bmatrix} \mathbf{V}_k^b \left[ \mathbf{V}_k^b \right]^H + \mathbf{V}_k^u \left[ \mathbf{V}_k^u \right]^H & \mathbf{0} \\ \mathbf{0} & \mathbf{0} \end{bmatrix} \mathbf{H} \\ &= \sigma_s^2 \mathbf{H}_u^T \mathbf{V}_k \mathbf{V}_k^H \mathbf{H}_u \end{aligned} \quad (3.34)$$

where

$$\mathbf{H} = \begin{bmatrix} (\mathbf{H}_u)_{\Delta \times M} \\ (\mathbf{H}_c)_{\nu \times M} \\ (\mathbf{H}_b)_{(N-\nu-\Delta+M-1) \times M} \end{bmatrix} \quad (3.35)$$

Similarly,

$$E[\mathbf{S1}] = \mathbf{H}^T \begin{bmatrix} \mathbf{0} & \mathbf{0} \\ \mathbf{0} & \mathbf{W}_k \end{bmatrix} E[\mathbf{u}_{i-1} \mathbf{u}_{i-1}^T] \begin{bmatrix} \mathbf{0} & \mathbf{0} \\ \mathbf{0} & \mathbf{W}_k^H \end{bmatrix} \mathbf{H}$$

$$\begin{aligned}
&= \sigma_s^2 \mathbf{H}^T \begin{bmatrix} \mathbf{0} & \mathbf{0} \\ \mathbf{0} & \mathbf{W}_k \end{bmatrix} \begin{bmatrix} \mathbf{0} & \mathbf{0} \\ \mathbf{0} & \mathbf{W}_k^H \end{bmatrix} \mathbf{H} \\
&= \sigma_s^2 \mathbf{H}_b^T \mathbf{W}_k \mathbf{W}_k^H \mathbf{H}_b
\end{aligned} \tag{3.36}$$

where  $\mathbf{H}_b$  is defined in (3.35).

Following a similar procedure, we arrive at the contribution of  $\mathbf{w}^T E[\mathbf{S}\mathbf{3}]\mathbf{w}$ , which is exactly the sum of (3.34) and (3.36). The contribution of AWGN, NEXT and ADC noise are respectively given by

$$\begin{aligned}
E[\mathbf{Pz1}] &= \mathbf{Q}_k^{\text{noise}} E[\mathbf{n}^{\text{AWGN}} (\mathbf{n}^{\text{AWGN}})^T] [\mathbf{Q}_k^{\text{noise}}]^H \\
&= \sigma_{\text{AWGN}}^2 \mathbf{Q}_k^{\text{noise}} [\mathbf{Q}_k^{\text{noise}}]^H
\end{aligned} \tag{3.37}$$

where  $M \times (N + M - 1)$  matrix  $\mathbf{Q}_k^{\text{noise}}$  is defined as

$$\mathbf{Q}_k^{\text{noise}} = \begin{bmatrix} 0 & 0 & \cdots & 0 & q_k^0 & \cdots & q_k^{N-1} \\ 0 & 0 & \cdots & q_k^0 & \cdots & q_k^{N-1} & 0 \\ \vdots & & & & & & \vdots \\ q_k^0 & \cdots & q_k^{N-1} & 0 & \cdots & 0 & 0 \end{bmatrix} \tag{3.38}$$

$$\begin{aligned}
E[\mathbf{Pz2}] &= \mathbf{Q}_k^{\text{noise}} E[\mathbf{n}^{\text{NEXT}} (\mathbf{n}^{\text{NEXT}})^T] [\mathbf{Q}_k^{\text{noise}}]^H \\
&= \mathbf{Q}_k^{\text{noise}} \Sigma_{\text{NEXT}} [\mathbf{Q}_k^{\text{noise}}]^H
\end{aligned} \tag{3.39}$$

$$\begin{aligned}
E[\mathbf{Pz3}] &= \mathbf{Q}_k^{\text{noise}} E[\mathbf{n}^{\text{ADC}} (\mathbf{n}^{\text{ADC}})^T] [\mathbf{Q}_k^{\text{noise}}]^H \\
&= \sigma_{\text{ADC}}^2 \mathbf{Q}_k^{\text{noise}} [\mathbf{Q}_k^{\text{noise}}]^H
\end{aligned} \tag{3.40}$$

Then

$$\begin{aligned}
E[Z_k^H Z_k] &= \mathbf{w}^T 2\sigma_s^2 \left( \mathbf{H}_u^T \mathbf{V}_k \mathbf{V}_k^H \mathbf{H}_u + \mathbf{H}_b^T \mathbf{W}_k \mathbf{W}_k^H \mathbf{H}_b \right) \mathbf{w} \\
&+ \sigma_{\text{AWGN}}^2 \mathbf{w}^T \mathbf{Q}_k^{\text{noise}} [\mathbf{Q}_k^{\text{noise}}]^H \mathbf{w} \\
&+ \mathbf{w}^T \mathbf{Q}_k^{\text{noise}} \Sigma_{\text{NEXT}} [\mathbf{Q}_k^{\text{noise}}]^H \mathbf{w}
\end{aligned}$$

$$\begin{aligned}
& + \sigma_{\text{ADC}}^2 \mathbf{w}^T \mathbf{Q}_k^{\text{noise}} \left[ \mathbf{Q}_k^{\text{noise}} \right]^H \mathbf{w} \\
& + \mathbf{w}^T \frac{\sigma_{\text{DNF}}^2}{\mathbf{w}^T \mathbf{w}} \mathbf{I} \mathbf{w} \\
& = \mathbf{w}^T \tilde{\mathbf{B}}_k \mathbf{w}
\end{aligned} \tag{3.41}$$

where  $\mathbf{I}$  is the  $M \times M$  identity matrix. Thus,

$$\begin{aligned}
\tilde{\mathbf{B}}_k & = 2\sigma_s^2 \left( \mathbf{H}_u^T \mathbf{V}_k \mathbf{V}_k^H \mathbf{H}_u + \mathbf{H}_b^T \mathbf{W}_k \mathbf{W}_k^H \mathbf{H}_b \right) \\
& + \mathbf{Q}_k^{\text{noise}} \left[ \left( \sigma_{\text{AWGN}}^2 + \sigma_{\text{ADC}}^2 \right) \mathbf{I} + \boldsymbol{\Sigma}_{\text{NEXT}} \right] \left[ \mathbf{Q}_k^{\text{noise}} \right]^H + \frac{\sigma_{\text{DNF}}^2}{\mathbf{w}^T \mathbf{w}} \mathbf{I}
\end{aligned} \tag{3.42}$$

Observe that over the constraint set  $\mathcal{S}$ ,  $\mathbf{w}^T \mathbf{w} = 1$ , so that  $\tilde{\mathbf{B}}_k$  becomes independent of the TEQ FIR taps  $\mathbf{w}$ .

### 3.6 Conclusion

In this chapter I derive a new model for the subchannel SNR. The subchannel SNR model is a ratio of the desired signal power over the power of the noise, where both the numerator and the denominator are quadratic functions of the TEQ taps and the Hessian matrices are positive definite. The desired signal was defined by noting that the DMT frame that is circularly convolved with the channel does not present any ISI after the FFT. The noise is defined as the difference of the actually received signal and the defined desired signal. The TEQ taps affect primarily the ISI and ICI noise contributions and in the case of optimal TEQ taps the noise contribution comes from non-signal dependent sources such as AWGN, NEXT, ADC noise and DNF as both ISI and ICI have been eliminated. An SNR model maximization necessarily leads to channel shortening as that is the only way to reduce the difference between the desired channel and the received channel. The SNR model proposed here is the foundation of the TEQ design procedure of Chapter 5 that is aimed at designing the TEQ that will maximize the bit rate of a DMT system. The efficient calculation of

matrices present in the subchannel SNR model numerator and denominator is the topic of Chapter 4.

## Chapter 4

# Efficient Computation of Subchannel SNR Model

Chapter 3 introduced the subchannel signal-to-noise ratio model which is a ratio of quadratic functions of the time domain equalizer taps. For the  $k^{\text{th}}$  subchannel, the quadratic functions in the numerator and denominator contain  $M \times M$  matrices ( $\tilde{\mathbf{A}}_k$  and  $\tilde{\mathbf{B}}_k$ , respectively) that have to be computed before a time domain equalizer can be designed. The purpose of this chapter is to introduce computationally and memory efficient algorithms for the computation of the matrices  $\tilde{\mathbf{A}}_k$  and  $\tilde{\mathbf{B}}_k$ . The efficient subchannel SNR algorithms presented in this chapter were developed jointly with Mr. Ketan J. Mandke and Ms. Esther I. Resendiz where my role was to point out the ways in which the necessary computations can be minimized, ensure that the efficient algorithms agreed with the development of Chapter 3, and provide the testing vectors. Ketan J. Mandke and Esther I. Resendiz implemented some of the material in this chapter to satisfy the requirements for their senior design project at The University of Texas at Austin.

## 4.1 Introduction

Computing the elements of the SNR model numerator and denominator matrices,  $\tilde{\mathbf{A}}_k$  and  $\tilde{\mathbf{B}}_k$  respectively, is a computationally intensive task. Computing the matrices using straight matrix multiplications of the constituent matrices in (3.20) and (3.42) would require a large number of computations and memory storage of intermediate results.

This chapter presents methods that take advantage of the symmetry of the matrices in order to reduce the number of computations needed. Each of the algorithms presented uses the fact that the matrices are Hermitian symmetric; thus, it is only necessary to compute either the lower or the upper triangle of the matrices (the remaining elements are complex conjugates of the computed values). However, even within the chosen matrix triangle there exists certain structure which allows us to reduce the computations and temporary memory requirements even further.

Fixed memory storage requirements that cannot be avoided regardless of the computation algorithms is the cost of storing the elements of  $\mathbf{q}_k$ ,  $\mathbf{h}$ , or  $\tilde{\mathbf{A}}_k$  and  $\tilde{\mathbf{B}}_k$  for all  $k \in I$ . Matrices  $\tilde{\mathbf{A}}_k$  and  $\tilde{\mathbf{B}}_k$  and vector  $\mathbf{q}_k$  for all  $k \in I$  are complex-valued.

Section 4.2 defines a computationally efficient algorithm for the calculation of the Hessian matrix of the SNR model numerator. Section 4.3 presents computationally efficient algorithms for the calculation of the Hessian matrix of the SNR model denominator. The calculation of the Hessian matrix of the SNR model denominator is partitioned in the efficient calculations of various noise contribution components. Subsections 4.3.1 and 4.3.2 consider contribution of the ISI, subsection 4.3.3 looks at AWGN and ADC noise, and subsection 4.3.4 discusses efficient computation of NEXT contribution to the Hessian matrix of the SNR model denominator. Section 4.4 details the computational complexity and memory requirements of the described algorithms and compares their performance to the “straight” calculation of the SNR model Hessian matrices. Section 4.5 concludes this chapter.

## 4.2 Subchannel SNR Model Numerator

Matrix  $\tilde{\mathbf{A}}_k = \sigma_s^2 \mathbf{H}^T \mathbf{Q}_k^{\text{circ}} [\mathbf{Q}_k^{\text{circ}}]^H \mathbf{H}$  is defined in (3.20) for all  $k \in \mathcal{I}$ . An element  $(i, j)$  of the  $M \times M$  matrix  $\tilde{\mathbf{A}}_k^{i,j}$  can be written as

$$\tilde{\mathbf{A}}_k^{i,j} = N \mathbf{q}_k^{i-j} \left( \sum_{m=0}^{N+M-2-i} \mathbf{h}^m \mathbf{q}_k^m \right) \left( \sum_{l=0}^{N+M-2-j} \mathbf{h}^l \mathbf{q}_k^{-l} \right) \quad (4.1)$$

Notice that (4.1) can be decomposed as in

$$\tilde{\mathbf{A}}_k^{i,j} = N \mathbf{q}_k^{i-j} [\mathbf{t}_k^i]^* \mathbf{t}_k^j \quad (4.2)$$

where

$$\mathbf{t}_k^i = \sum_{m=0}^{N+M-2-i} \mathbf{h}^m \mathbf{q}_k^m \quad (4.3)$$

and  $[\cdot]^*$  denotes conjugation. To compute elements of the matrix  $\tilde{\mathbf{A}}_k$  I need to compute values of  $\mathbf{t}_k^i$  for  $0 \leq i \leq M-1$ .

A recursive formula for the computation of elements  $\mathbf{t}_k^i$  can be discerned from (4.3). The element  $i$  can be computed using the following recursive relationship

$$\mathbf{t}_k^i = \mathbf{t}_k^{i+1} + \mathbf{h}^{N+M-2-i} \mathbf{q}_k^{N+M-2-i} \quad \text{for } 0 \leq i \leq M-2 \quad (4.4)$$

The first element to be computed is the element  $M-1$ . From (4.3) I obtain

$$\mathbf{t}_k^{M-1} = \sum_{m=0}^{N-1} \mathbf{h}^m \mathbf{q}_k^m \quad (4.5)$$

by substituting  $i = M-1$ .

Since the matrix  $\tilde{\mathbf{A}}_k$  is Hermitian symmetric, I need to calculate only the lower triangle elements of the matrix according to the relationship in (4.2) once the values  $\mathbf{t}_k^i$  are known for all  $i$ . The upper triangle elements are the complex conjugate of the values of corresponding lower triangle values. The algorithm is shown in Figure 4.1. This algorithm for efficient computation of  $\tilde{\mathbf{A}}_k$  requires  $2M$  words of temporary memory space to store the elements of  $\mathbf{t}_k$  beyond any requirements of

```

begin
  compute  $\mathbf{t}_k^{M-1} = \sum_{m=0}^{N-1} \mathbf{h}^m \mathbf{q}_k^m$  using (4.5);
  for  $i = M - 2; i \geq 0; i - -$ ;
    compute  $\mathbf{t}_k^i = \mathbf{t}_k^{i+1} + \mathbf{h}^{N+M-2-i} \mathbf{q}_k^{N+M-2-i}$  using (4.4);
  end
  for  $i = 0; i < M - 1; i + +$ ;
    for  $j = 0; j \leq i; j + +$ ;
       $\tilde{\mathbf{A}}_k^{i,j} = N \mathbf{q}_k^{i-j} [\mathbf{t}_k^i]^* \mathbf{t}_k^j$  using (4.2);
    end
  end
  form upper triangle of  $\tilde{\mathbf{A}}_k$  using Hermitian symmetry;
end

```

Figure 4.1: Algorithm for Efficient Computation of Subchannel SNR Numerator Hessian Matrix

storing the elements of  $\mathbf{q}_k$ ,  $\mathbf{h}$ , or  $\tilde{\mathbf{A}}_k$ . Computation of the lower triangle elements of  $\tilde{\mathbf{A}}_k$  requires order  $O(\max(M^2, N))$  (exactly  $2N + 7M + 5M^2 - 2$ ) real multiply-accumulate (MAC) operations <sup>1</sup>.

### 4.3 Subchannel SNR Model Denominator

Matrix  $\tilde{\mathbf{B}}_k$  is defined in (3.42) for all of the subchannels of interest in  $\mathcal{I}$ . I repeat that definition here and group parts for which I present algorithms requiring fewer calculations than the matrix multiplication of constituent matrices:

$$\begin{aligned}
\tilde{\mathbf{B}}_k &= 2\sigma_s^2 \underbrace{\mathbf{H}_u^T \mathbf{V}_k \mathbf{V}_k^H \mathbf{H}_u}_{\mathbf{B}_k^V} + \underbrace{\mathbf{H}_b^T \mathbf{W}_k \mathbf{W}_k^H \mathbf{H}_b}_{\mathbf{B}_k^W} + \underbrace{\mathbf{Q}_k^{\text{noise}} (\sigma_{\text{AWGN}}^2 + \sigma_{\text{ADC}}^2) \mathbf{I} [\mathbf{Q}_k^{\text{noise}}]^H}_{\mathbf{G}_k^{\text{AWGN}} + \mathbf{G}_k^{\text{ADC}}} \\
&+ \underbrace{\mathbf{Q}_k^{\text{noise}} \Sigma_{\text{NEXT}} [\mathbf{Q}_k^{\text{noise}}]^H}_{\mathbf{G}_k^{\text{NEXT}}} \\
&+ \frac{\sigma_{\text{DNF}}^2}{\mathbf{w}^T \mathbf{w}} \mathbf{I}
\end{aligned} \tag{4.6}$$

<sup>1</sup>In standardized ADSL the largest value of  $N$  used is 512 and  $M$  ranges from 2 to 32 for customer premises equipment.



I will present methods to compute matrices  $\mathbf{B}_k^V$ ,  $\mathbf{B}_k^W$ ,  $\mathbf{G}_k^{\text{NEXT}}$ ,  $\mathbf{G}_k^{\text{ADC}}$  and  $\mathbf{G}_k^{\text{AWGN}}$  efficiently. As the matrix  $\tilde{\mathbf{B}}_k$  is Hermitian symmetric, we propose the efficient calculation of the lower triangle realizing the upper triangle is then known.

### 4.3.1 Transmission channel tail component

The matrix  $\mathbf{B}_k^V$  is defined by  $\mathbf{B}_k^V = \mathbf{H}_u^T \mathbf{V}_k \mathbf{V}_k^H \mathbf{H}_u$  where each constituent matrix is defined in subsection 3.5.2. Hence, an element  $[\mathbf{B}_k^V]^{i,j}$  is a dot product of the  $i^{\text{th}}$  row of the matrix  $\mathbf{H}_u^T \mathbf{V}_k$  and the  $j^{\text{th}}$  column of the matrix  $\mathbf{V}_k^H \mathbf{H}_u$  for all  $0 \leq i, j \leq M-1$ .

Define a temporary  $M \times \Delta$  matrix

$$\mathbf{X}_k = \mathbf{H}_u^T \mathbf{V}_k \quad (4.7)$$

The  $(i, j)$  element of  $\mathbf{X}_k$  is

$$\mathbf{X}_k^{i,j} = \sum_{l=0}^{\Delta-1-(i+j)} \mathbf{h}^l \mathbf{q}_k^{N-\Delta+(i+j)+l} \quad (4.8)$$

The matrix  $\mathbf{X}_k$  is defined for analysis purposes only and will not be constructed in its entirety, as only one row of it is needed to obtain elements of  $\mathbf{B}_k^V$ . A recursive relationship can be established within the elements of the  $i^{\text{th}}$  row of  $\mathbf{X}_k$ .

$$\begin{aligned} \mathbf{X}_k^{i,j} &= \sum_{l=0}^{\Delta-1-i-j} \mathbf{h}^l \mathbf{q}_k^{N-\Delta+i+j+l} \\ &= \mathbf{q}_k^{-1} \left[ \sum_{l=0}^{\Delta-1-i-(j+1)} \mathbf{h}^l \mathbf{q}_k^{N-\Delta+i+(j+1)+l} + \mathbf{h}^{\Delta-1-i-j} \right] \\ &= \mathbf{q}_k^{-1} \left( \mathbf{X}_k^{i,j+1} + \mathbf{h}^{\Delta-1-i-j} \right) \end{aligned} \quad (4.9)$$

Notice that  $\mathbf{q}_k^{N-1} = \mathbf{q}_k^{-1}$ . From (4.8), notice that element  $\mathbf{X}_k^{i,j}$  remains constant for the elements for which the sum  $i + j$  remains constant, e.g. element  $\mathbf{X}_k^{1,2} = \mathbf{X}_k^{2,1}$  along the diagonals of  $\mathbf{X}_k$ . This allows a definition of a useful relationship among the successive rows of  $\mathbf{X}_k$

$$\mathbf{X}_k^{i+1,0:\Delta-1-(i+1)} = \mathbf{X}_k^{i,1:\Delta-1-i} \quad (4.10)$$

where  $(*)^{i,a:b}$  denotes a vector portion of the  $i^{\text{th}}$  row of  $(*)$  between (and including) indices  $a$  and  $b$ . The first element of the first row of  $\mathbf{X}_k$  to be calculated is given by

$$\mathbf{X}_k^{0,\Delta-1} = \mathbf{q}_k^{-1} \mathbf{h}^0 \quad (4.11)$$

The entire first row of  $\mathbf{X}_k$  is then calculated recursively using (4.9).

The knowledge of the first row of  $\mathbf{X}_k$  is enough to calculate  $\mathbf{B}_k^V$ . The element  $(i, j)$  of the matrix  $\mathbf{B}_k^V$  is now recursively defined using the first row of  $\mathbf{X}_k$ :

$$\left[\mathbf{B}_k^V\right]^{i,j} = \left[\mathbf{B}_k^V\right]^{i+1,j+1} + \mathbf{X}_k^{0,i} \left[\mathbf{X}_k^{0,j}\right]^H \quad (4.12)$$

I can proceed with the computation of the lower triangle of  $\mathbf{B}_k^V$ . Compute the last row of  $\mathbf{B}_k^V$  first using

$$\left[\mathbf{B}_k^V\right]^{i,j} = \sum_{g=i}^{\Delta-1} \sum_{s=j}^{\Delta-1-i+j} \mathbf{X}_k^{0,g} \left[\mathbf{X}_k^{0,s}\right]^H \quad \text{for } i = M-1 \text{ and } j \leq i \quad (4.13)$$

where auxiliary variables  $g$  and  $s$  index the appropriate first row elements of  $\mathbf{X}_k$ . Then, one can use (4.12) for the remaining lower triangle elements. The algorithm for efficient computation of  $\mathbf{B}_k^V$  is shown in Figure 4.2.

This algorithm requires the storage of  $2\Delta$  words of the first row complex elements of  $\mathbf{X}_k$ . Computation of the lower triangle elements of  $\mathbf{B}_k^V$  requires exactly  $7M^2 + 4M\Delta + 5\Delta - 3M$  real MAC operations. Usually  $\Delta > M$  so the described algorithm requires order  $O(M\Delta)$  real MACs.

### 4.3.2 Transmission channel head component

The matrix  $\mathbf{B}_k^W$  is given by  $\mathbf{B}_k^W = \mathbf{H}_b^T \mathbf{V}_k \mathbf{W}_k^H \mathbf{H}_b$  where each constituent matrix is defined in the subsection 3.5.2. Hence, an element  $\left[\mathbf{B}_k^W\right]^{i,j}$  is a dot product of the  $i^{\text{th}}$  row of the matrix  $\mathbf{H}_b^T \mathbf{W}_k$  and the  $j^{\text{th}}$  column of the matrix  $\mathbf{W}_k^H \mathbf{H}_b$ .

Define a temporary  $M \times (N - \nu - \Delta + M - 1)$  matrix

$$\mathbf{Z}_k = \mathbf{H}_b^T \mathbf{W}_k \quad (4.14)$$

```

begin
   $\mathbf{X}_k^{0,\Delta-1} = \mathbf{q}_k^{-1} \mathbf{h}^0$  using (4.11);
  for  $j = \Delta - 2; j \geq 0; j --$ ;
     $\mathbf{X}_k^{0,j} = \mathbf{q}_k^{-1} (\mathbf{X}_k^{0,j+1} + \mathbf{h}^{\Delta-1-j})$  using (4.9);
  end
  for  $j = 0; j \leq M - 1; j ++$ ;
     $[\mathbf{B}_k^V]^{M-1,j} = \sum_{g=M-1}^{\Delta-1} \sum_{s=0}^{\Delta-M} \mathbf{X}_k^{0,g} [\mathbf{X}_k^{0,s+j}]^H$  using (4.13);
  end
  for  $i = M - 2; i \geq 0; i --$ ;
    for  $j = i; j \geq 0; j --$ ;
       $[\mathbf{B}_k^V]^{i,j} = [\mathbf{B}_k^V]^{i+1,j+1} + \mathbf{X}_k^{0,i} [\mathbf{X}_k^{0,j}]^*$  using (4.12);
    end
  end
  form upper triangle of  $\mathbf{B}_k^V$  using Hermitian symmetry;
end

```

Figure 4.2: Algorithm for Efficient Computation of Subchannel SNR Denominator Hessian Matrix Contribution of Channel Tail Component.

where

$$\mathbf{z}_k^{i,j} = \sum_{l=N+M-2-(i+j)}^{N+M-2-i} \mathbf{h}^l \mathbf{q}_k^{l-(N+M-2)+(i+j)} \quad (4.15)$$

A recursive relationship can be defined within the elements of a row of  $\mathbf{Z}_k$ .

$$\begin{aligned} \mathbf{z}_k^{i,j+1} &= \sum_{l=p-(i+j+1)}^{p-i} \mathbf{h}^l \mathbf{q}_k^{l-p+(i+j+1)} \\ &= \mathbf{q}_k^1 \sum_{l=p-(i+j+1)}^{p-i} \mathbf{h}^l \mathbf{q}_k^{l-p+(i+j)} \\ &= \mathbf{q}_k^1 \left[ \sum_{l=p-(i+j)}^{p-i} \mathbf{h}^l \mathbf{q}_k^{l-p+(i+j)} + \mathbf{h}^{p-(i+j)-1} \mathbf{q}_k^{-1} \right] \\ &= \mathbf{q}_k^1 \mathbf{z}_k^{i,j} + \mathbf{h}^{p-i-(j+1)} \end{aligned} \quad (4.16)$$

where  $p = N + M - 2$  is defined for notational convenience. Thus, I notice from (4.16) that the column  $j + 1$  of  $\mathbf{Z}_k$ , can be calculated using the  $j^{\text{th}}$  column of  $\mathbf{Z}_k$

```

begin
   $\mathbf{B}_k^{\text{W}} = \mathbf{0}$ ;
   $\mathbf{Z}_k^{0,0} = \mathbf{h}^{N+M-2} \mathbf{q}_k^0$ ;
  for  $i = 0; i < M; i ++$ ;
     $\mathbf{Z}_k^{i,0} = \mathbf{h}^{N+M-2-i} \mathbf{q}_k^0$  using (4.15);
  end
  for  $j = 1; j \leq N - \nu - \Delta + M - 1; j ++$ ;
    for  $i = 0; i < M; i ++$ ;
       $\mathbf{Z}_k^{i,j} = \mathbf{q}_k^1 \mathbf{Z}_k^{i,j-1} + \mathbf{h}^{N+M-2-(i+j)}$  using (4.16);
    end
    for  $m = 0; m \leq M - 1; m ++$ ;
      for  $n = 0; n \leq m; n ++$ ;
         $\{ [\mathbf{B}_k^{\text{W}}]^{m,n} \}_j = \mathbf{Z}_k^{m,j} [\mathbf{Z}_k^{n,j}]^* + \{ [\mathbf{B}_k^{\text{W}}]^{m,n} \}_{j-1}$ ;
        where  $\{*\}_j$  denotes the  $j^{\text{th}}$  iteration
      end
    end
  end
  form upper triangle of  $\mathbf{B}_k^{\text{W}}$  using Hermitian symmetry;
end

```

Figure 4.3: Algorithm for Efficient Computation of Subchannel SNR Denominator Hessian Matrix Contribution of Channel Tail Component.

and the knowledge of  $\mathbf{h}$ .

The algorithm for efficient calculation of  $\mathbf{B}_k^{\text{W}}$  will update the value of the matrix elements with the contribution of each of the columns of  $\mathbf{Z}_k$ . Thus, the updating will be finished in  $N - \nu - \Delta + M - 1$  iterations. The algorithm is shown in Figure 4.3.

The algorithm in Figure 4.3 requires order  $O(NM^2)$  (exactly  $1 + 2M + (N - \nu - \Delta + M - 2)(5M + 8M^2)$ ) real MAC operations and memory storage for the intermediate results of  $4M$  words.

### 4.3.3 Additive white Gaussian and analog-to-digital conversion noise component

The contribution of the additive white Gaussian noise to the overall noise matrix in (4.6) is defined as  $\mathbf{G}_k^{\text{AWGN}} = \mathbf{Q}_k^{\text{noise}} \sigma_{\text{AWGN}}^2 \mathbf{I} [\mathbf{Q}_k^{\text{noise}}]^{\text{H}}$ . The contribution of the ADC noise to the overall noise matrix in (4.6) is defined as  $\mathbf{G}_k^{\text{ADC}} = \mathbf{Q}_k^{\text{noise}} \sigma_{\text{ADC}}^2 \mathbf{I} [\mathbf{Q}_k^{\text{noise}}]^{\text{H}}$ . Thus, an overall AWGN and ADC contribution can be computed simultaneously by adding the powers of the noise  $\sigma_{\text{ADC}}^2 + \sigma_{\text{AWGN}}^2$ .

$$\mathbf{G}_k^{\text{AWGN/ADC}} = \mathbf{Q}_k^{\text{noise}} \left( \sigma_{\text{ADC}}^2 + \sigma_{\text{AWGN}}^2 \right) \mathbf{I} [\mathbf{Q}_k^{\text{noise}}]^{\text{H}} \quad (4.17)$$

Matrix  $\mathbf{G}_k^{\text{AWGN/ADC}}$  is Hermitian symmetric and Toeplitz and it is only necessary to compute elements of its first column. The remaining elements are then defined by the Hermitian symmetry and Toeplitz structure. An element of  $\mathbf{G}_k^{\text{AWGN/ADC}}$  can be efficiently computed as

$$\left[ \mathbf{G}_k^{\text{AWGN/ADC}} \right]^{i,j} = \left( \sigma_{\text{AWGN}}^2 + \sigma_{\text{AWGN}}^2 \right) (N - |i - j|) \mathbf{q}_k^{i-j} \quad (4.18)$$

where  $|*|$  denotes the absolute value of the argument. The algorithm is shown in Figure 4.4. The proposed method requires 2 words of memory to store the intermediate results and  $4M$  real MACs.

### 4.3.4 Near-end crosstalk component

The matrix  $\mathbf{G}_k^{\text{NEXT}}$  models the contribution of the near-end crosstalk to the overall noise matrix. Let

$$\mathbf{G}_k^{\text{NEXT}} = \mathbf{Q}_k^{\text{noise}} \boldsymbol{\Sigma}_{\text{NEXT}} [\mathbf{Q}_k^{\text{noise}}]^{\text{H}} \quad (4.19)$$

Matrix  $\boldsymbol{\Sigma}_{\text{NEXT}}$  is symmetric and possess Toeplitz structure. Only need the first column of  $\boldsymbol{\Sigma}_{\text{NEXT}}$  is needed to calculate  $\mathbf{G}_k^{\text{NEXT}}$ . The  $(i, j)$  element of  $\mathbf{G}_k^{\text{NEXT}}$  from (4.19) can be rewritten as

$$\left[ \mathbf{G}_k^{\text{NEXT}} \right]^{i,j} = \sum_{n=i}^{N-1+i} \sum_{m=j}^{N-1+j} \boldsymbol{\Sigma}_{\text{NEXT}}^{|m-n|,0} \mathbf{q}_k^{m-n+i-j}$$

```

begin
   $j = 0;$ 
   $\sigma^2 = (\sigma_{\text{AWGN}}^2 + \sigma_{\text{AWGN}}^2);$ 
  for  $j = 0; j \leq M - 1; j ++;$ 
     $[\mathbf{G}_k^{\text{AWGN/ADC}}]^{0,j} = \sigma^2(N - j)\mathbf{q}_k^{-j}$  using (4.18);
  end
  form the lower triangle of  $\mathbf{G}_k^{\text{AWGN/ADC}}$  according to Toeplitz structure;
  form the upper triangle of  $\mathbf{G}_k^{\text{AWGN/ADC}}$  using Hermitian symmetry;
end

```

Figure 4.4: Algorithm for Efficient Computation of Subchannel SNR Denominator Hessian Matrix Contributions of White Gaussian Noise and Analog-to-Digital Conversion Noise.

$$= \sum_{n=0}^{N-1} \sum_{m=0}^{N-1} \Sigma_{\text{NEXT}}^{|n-m+i-j|,0} \mathbf{q}_k^{m-n} \quad (4.20)$$

The dependance of the element  $\mathbf{G}_k^{\text{NEXT}}(i, j)$  on the index  $i - j$  of the matrix  $\Sigma_{\text{NEXT}}$  means that  $\mathbf{G}_k^{\text{NEXT}}$  also is symmetric and Toeplitz. Only the first column of  $\mathbf{G}_k^{\text{NEXT}}$  is needed to completely define it. The element of  $[\mathbf{G}_k^{\text{NEXT}}]^{i+1,0}$  is

$$\begin{aligned}
[\mathbf{G}_k^{\text{NEXT}}]^{i+1,0} &= \sum_{n=i+1}^{N-i} \sum_{m=0}^{N-1} \Sigma_{\text{NEXT}}^{|m-n|,0} \mathbf{q}_k^{m-n+i+1} \\
&= \mathbf{q}_k^1 \sum_{n=i}^{N-i-1} \sum_{m=0}^{N-1} \Sigma_{\text{NEXT}}^{|m-n|,0} \mathbf{q}_k^{m-n+i} \\
&+ \sum_{m=0}^{N-1} \left( \Sigma_{\text{NEXT}}^{|m-n|,0} \mathbf{q}_k^{m-n+i} \Big|_{n=N-i} - \Sigma_{\text{NEXT}}^{|m-n|,0} \mathbf{q}_k^{m-n+i} \Big|_{n=i} \right) \\
&= \mathbf{q}_k^1 [\mathbf{G}_k^{\text{NEXT}}]^{i,0} \\
&+ \mathbf{q}_k^1 \sum_{m=0}^{N-1} \left( \Sigma_{\text{NEXT}}^{|m-i+M-1|,0} - \Sigma_{\text{NEXT}}^{|m-i|,0} \right) \mathbf{q}_k^m \quad (4.21)
\end{aligned}$$

Further simplification of (4.21) is possible by eliminating the absolute value operation ( $| * |$ ) and by taking advantage of the fact that elements of  $\Sigma_{\text{NEXT}}$  repeat

modulo  $N + M - 1$ . Thus, (4.21) can be re-written as

$$\begin{aligned} [\mathbf{G}_k^{\text{NEXT}}]^{i+1,0} &= \mathbf{q}_k^1 [\mathbf{G}_k^{\text{NEXT}}]^{i,0} + \mathbf{q}_k^1 \sum_{m=0}^i \left( \Sigma_{\text{NEXT}}^{m-i+M-1,0} - \Sigma_{\text{NEXT}}^{i-m,0} \right) \mathbf{q}_k^m \\ &+ \mathbf{q}_k^1 \sum_{m=i+1}^{N-1} \left( \Sigma_{\text{NEXT}}^{m-i+M-1,0} - \Sigma_{\text{NEXT}}^{m-i,0} \right) \mathbf{q}_k^m \end{aligned} \quad (4.22)$$

Let  $n = m - i$  so

$$\begin{aligned} [\mathbf{G}_k^{\text{NEXT}}]^{i+1,0} &= \mathbf{q}_k^1 [\mathbf{G}_k^{\text{NEXT}}]^{i,0} + \mathbf{q}_k^1 \sum_{n=-i}^0 \left( \Sigma_{\text{NEXT}}^{n+M-1,0} - \Sigma_{\text{NEXT}}^{-n,0} \right) \mathbf{q}_k^{n+i} \\ &+ \mathbf{q}_k^1 \sum_{n=1}^{N-1-i} \left( \Sigma_{\text{NEXT}}^{n+M-1,0} - \mathbf{q}_k^1 \Sigma_{\text{NEXT}}^{n,0} \right) \mathbf{q}_k^{n+i} \\ &= \mathbf{q}_k^1 \left[ [\mathbf{G}_k^{\text{NEXT}}]^{i,0} + \mathbf{q}_k^i \mathbf{d}_{\text{NEXT}}^i \right] \end{aligned} \quad (4.23)$$

where

$$\mathbf{d}_{\text{NEXT}}^i = \sum_{n=-i}^{N-1-i} \left( \Sigma_{\text{NEXT}}^{n+M-1,0} - \Sigma_{\text{NEXT}}^{|n|,0} \right) \mathbf{q}_k^n \quad (4.24)$$

The vector  $\mathbf{d}_{\text{NEXT}}$  can be computed using a recursive relationship:

$$\begin{aligned} \mathbf{d}_{\text{NEXT}}^{i+1} &= \mathbf{d}_{\text{NEXT}}^i + \left( \Sigma_{\text{NEXT}}^{M-2-i,0} - \Sigma_{\text{NEXT}}^{i+1,0} \right) \mathbf{q}_k^{-i-1} \\ &- \left( \Sigma_{\text{NEXT}}^{N+M-2-i,0} - \Sigma_{\text{NEXT}}^{N-i-1,0} \right) \mathbf{q}_k^{-i-1} \end{aligned} \quad (4.25)$$

The described recursive relationships give an efficient way to compute elements of  $\mathbf{G}_k^{\text{NEXT}}$ ; however, I still need to calculate the first element  $[\mathbf{G}_k^{\text{NEXT}}]^{0,0}$ . This can be accomplished efficiently in the following manner. From (4.20) for  $i = j = 0$

$$[\mathbf{G}_k^{\text{NEXT}}]^{0,0} = \sum_{n=0}^{N-1} \sum_{m=0}^{N-1} \Sigma_{\text{NEXT}}^{|n-m|,0} \mathbf{q}_k^{m-n} \quad (4.26)$$

Let  $z = m - n$  so that

$$\begin{aligned} [\mathbf{G}_k^{\text{NEXT}}]^{0,0} &= \sum_{n=0}^{N-1} \sum_{z=-n}^{N-1-n} \Sigma_{\text{NEXT}}^{|z|,0} \mathbf{q}_k^z \\ &= \sum_{n=0}^{N-1} \sum_{z=0}^{N-1-n} \Sigma_{\text{NEXT}}^{z,0} \mathbf{q}_k^z + \sum_{n=0}^{N-1} \sum_{z=0}^n \Sigma_{\text{NEXT}}^{z,0} \mathbf{q}_k^{-z} \\ &- \sum_{n=0}^{N-1} \Sigma_{\text{NEXT}}^{0,0} \end{aligned} \quad (4.27)$$

```

begin
   $[\mathbf{G}_k^{\text{NEXT}}]^{0,0} = \sum_{n=0}^{N-1} 2\text{Re}\{\mathbf{q}_k^n\} \boldsymbol{\Sigma}_{\text{NEXT}}^{n,0} (N-n) - N\boldsymbol{\Sigma}_{\text{NEXT}}^{0,0}$  using (4.28);
   $\mathbf{d}_{\text{NEXT}}^0 = \sum_{n=0}^{N-1} (\boldsymbol{\Sigma}_{\text{NEXT}}^{n+M-1,0} - \boldsymbol{\Sigma}_{\text{NEXT}}^{|n|,0}) \mathbf{q}_k^n$  using (4.24);
  for  $i = 0; i < M - 1; i++$ ;
     $[\mathbf{G}_k^{\text{NEXT}}]^{i+1,0} = \mathbf{q}_k^1 \left[ [\mathbf{G}_k^{\text{NEXT}}]^{i,0} + \mathbf{q}_k^i \mathbf{d}_{\text{NEXT}}^i \right]$  using (4.23);
     $\mathbf{d}_{\text{NEXT}}^{i+1} = \mathbf{d}_{\text{NEXT}}^i + \left( \boldsymbol{\Sigma}_{\text{NEXT}}^{M-2-i,0} - \boldsymbol{\Sigma}_{\text{NEXT}}^{i+1,0} \right) \mathbf{q}_k^{-i-1}$ 
       $- \left( \boldsymbol{\Sigma}_{\text{NEXT}}^{N+M-2-i,0} - \boldsymbol{\Sigma}_{\text{NEXT}}^{N-i-1,0} \right) \mathbf{q}_k^{-i-1}$  using (4.25);
  end
  form the lower triangle of  $\mathbf{G}_k^{\text{NEXT}}$  according to Toeplitz structure;
  form the upper triangle of  $\mathbf{G}_k^{\text{NEXT}}$  using Hermitian symmetry;
end

```

Figure 4.5: Algorithm for Efficient Computation of Subchannel SNR Denominator Hessian Matrix Contributions of Near-end Crosstalk.

The first two summation terms in (4.27) are complex conjugates of each other. Each member of the summations is present in both terms hence I can group them together.

Thus,

$$\begin{aligned}
[\mathbf{G}_k^{\text{NEXT}}]^{0,0} &= \sum_{n=0}^{N-1} \sum_{z=0}^{N-1-n} \boldsymbol{\Sigma}_{\text{NEXT}}^{z,0} (\mathbf{q}_k^z + \mathbf{q}_k^{-z}) - \sum_{n=0}^{N-1} \boldsymbol{\Sigma}_{\text{NEXT}}^{0,0} \\
&= \sum_{n=0}^{N-1} \sum_{z=0}^{N-1-n} 2\text{Re}\{\mathbf{q}_k^z\} \boldsymbol{\Sigma}_{\text{NEXT}}^{z,0} - N\boldsymbol{\Sigma}_{\text{NEXT}}^{0,0} \\
&= \sum_{n=0}^{N-1} 2\text{Re}\{\mathbf{q}_k^n\} \boldsymbol{\Sigma}_{\text{NEXT}}^{n,0} (N-n) - N\boldsymbol{\Sigma}_{\text{NEXT}}^{0,0} \tag{4.28}
\end{aligned}$$

where  $\text{Re}\{*\}$  denotes the real part of the data. The algorithm shown in Figure 4.5 requires  $2M$  words of memory to store the vector  $\mathbf{d}_{\text{NEXT}}$  beyond the requirement to store the final result, matrix  $\mathbf{G}_k^{\text{NEXT}}$  and  $4N + 15M + 1$  real MACs.



```

begin
  for  $i = 0; i < m; i ++;$ 
    for  $j = 0; j < n; j ++;$ 
      for  $k = 0; k < p; k ++;$ 
         $\mathbf{C}^{i,j} = \mathbf{A}^{i,k} \mathbf{B}^{k,j} + \mathbf{C}^{i,j};$ 
      end
    end
  end
end

```

Figure 4.6: General Matrix Multiply-update Algorithm

## 4.4 Implementation Complexity

This section shows the computational savings afforded by the algorithms developed in this chapter for the computation of the signal  $\tilde{\mathbf{A}}_k$  and noise matrix  $\tilde{\mathbf{B}}_k$  for sub-channel  $k$ . The results compare the calculations of SNR components using a matrix multiply-update algorithm that takes into account the Hermitian symmetry of the SNR matrices to compute only the lower triangle elements (shown in Section 4.4.1), against the methods presented in the chapter, which I will refer to as iterative methods (shown in Section 4.4.2).

### 4.4.1 Matrix multiply-update

The following content can be found in [56, p. 18] and [70, p. 68] and is summarized here for the reader's convenience. Let  $\mathbf{A} \in \mathcal{C}^{m \times p}$  and  $\mathbf{B} \in \mathcal{C}^{p \times n}$ . Figure 4.6 shows an algorithm that can be employed to calculate the matrix multiply-update  $\mathbf{C} = \mathbf{AB} + \mathbf{C}$ . The elements of all the matrices are assumed complex-valued. We need 4 multiply-accumulate operations to obtain the new value of  $\mathbf{C}^{i,j}$ . The total number of MACs needed to compute the entire matrix  $\mathbf{C}$  is then equal to  $4mnp$ . Notice that if the matrix elements were real the number of real MACs would be only  $mnp$ .

```

begin
  for  $i = 0; i < m; i ++;$ 
    for  $j = 0; j < i; j ++;$ 
      for  $k = 0; k < p; k ++;$ 
         $\mathbf{C}^{i,j} = \mathbf{A}^{i,k} [\mathbf{A}^H]^{k,j} + \mathbf{C}^{i,j};$ 
      end
    end
  end
end

```

Figure 4.7: Hermitian Symmetric Matrix Multiply-update Algorithm

Table 4.1: SNR Component Initialization Requirements Matrix Multiply-update Algorithm

SNR Component	Real MACs
$\mathbf{A}_k$	$4M(N + M - 1)(N + \frac{3M-1}{2})$
$\mathbf{B}_k^V$	$4M\Delta(\Delta + \frac{M+1}{2})$
$\mathbf{B}_k^W$	$4M(N - \nu - \Delta + M - 1)(N - \nu - \Delta + \frac{3M-1}{2})$
$\mathbf{G}_k^{\text{AWGN/ADC}}$	$4M(N + M - 1)\frac{M+1}{2}$
$\mathbf{G}_k^{\text{NEXT}}$	$4M(N + M - 1)(N + 2M - 1)$

If  $\mathbf{B} = \mathbf{A}^H$  and the resulting matrix  $\mathbf{C}$  is Hermitian symmetric, then I only need to calculate the elements of  $\mathbf{C}$  below and including the main diagonal as the rest can be obtained by Hermitian symmetry. In this case the matrix multiply-update algorithm is shown in Figure 4.7. The total number of MACs needed to calculate the entire matrix  $\mathbf{C}$  is now  $4pm\frac{m+1}{2}$  as  $(\sum_{i=1}^m 4pi) = (4p \sum_{i=1}^m i) = (4pm\frac{m+1}{2})$ .

#### 4.4.2 Iterative time domain equalizer initialization methods

Table 4.2 shows the memory requirements and computational complexity of the algorithms described in this chapter. The memory requirements in Table 4.2 do not capture the cost of storing the SNR component matrices. The overall memory

Table 4.2: SNR Component Initialization Requirements

SNR Component	Real MACs	Words
$\mathbf{A}_k$	$2N + 7M + 5M^2 - 2$	$2M$
$\mathbf{B}_k^V$	$7M^2 + 4M\Delta + 5\Delta - 3M$	$2\Delta$
$\mathbf{B}_k^W$	$1 + 2M + (N - \nu - \Delta + M - 2)(5M + 8M^2)$	$4M$
$\mathbf{G}_k^{\text{AWGN/ADC}}$	$4M$	$2$
$\mathbf{G}_k^{\text{NEXT}}$	$4N + 15M + 1$	$2M$

Table 4.3: Memory Requirements: Transmission Channel, Noise and FFT Parameters

Parameter	Words
$\mathbf{Q}$	$2N^2$
$\mathbf{h}$	$N$
$\mathbf{H}_u$	$M\Delta$
$\mathbf{H}_b$	$M(N - \nu - \Delta + M - 1)$
$[\boldsymbol{\Sigma}_{\text{NEXT}}]^{0,0:N-1}$	$N$

requirements are  $8M + 2\Delta + 2$  words while the overall computational load expressed in the number of real MACs is  $(N - \nu - \Delta)(5 + 8M)M + 6N + 8M^3 + 9M^2 + 15M + 4M\Delta + 5\Delta$  which is of  $\mathcal{O}(M^2N)$  complexity. The number of MACs needed to solve for signal and noise matrices in the data-carrying set of subchannels  $\mathcal{I}$  would be a linear multiple of the complexity described in here, and so would be the memory requirement. The algorithms described in this chapter require the knowledge of several noise and channel parameters as well as the knowledge of the FFT twiddle factors. The memory requirements of storing these parameters are shown in Table 4.3. The computational load of the proposed efficient algorithms is compared to the computational load of matrix multiply-update as a function of the number of TEQ taps  $M$  in Figure 4.8. Table 4.4 shows the number MACs obtained for  $N = 512, \nu = 32$  and  $\Delta = 26$  for the values of  $M = 3, 17$  and  $32$  for both the proposed

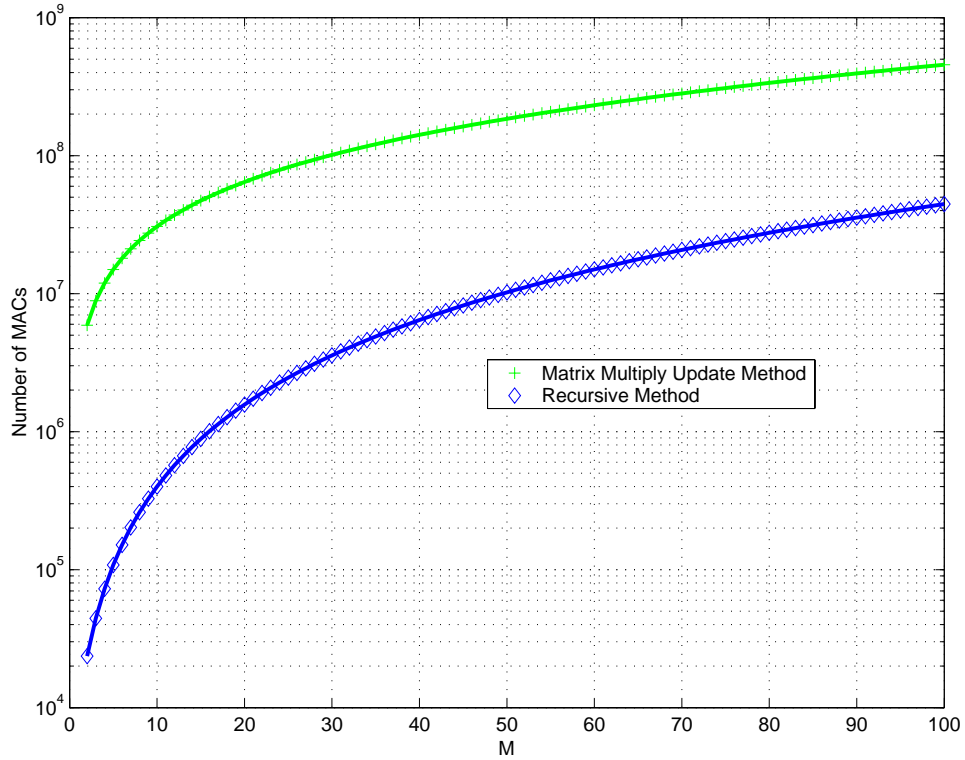


Figure 4.8: Computational Complexity of Proposed Iterative Initialization of Sub-channel SNR Numerator and Denominator Hessian Matrices vs. Complexity of Straight Matrix Multiply-update

iterative algorithms and the matrix multiply-update approach. The comparison does not take into account the memory requirements of the proposed methods and only compares the computational load. The proposed algorithms reduce the number of computations significantly, e.g. for  $M = 3$  the reduction is more than 164 times. The cost of creating matrices  $\mathbf{A}_k$  and  $\mathbf{B}_k$  for all  $k \in \mathcal{I}$  taking into account that the matrices are symmetric, positive definite with a special structure (see Chapter 3) is of the order  $|\mathcal{I}|\mathcal{O}(M^2N)$  operations where  $M$  is the size of the TEQ FIR ranging from 2 to 32 in our simulations and  $N = 512$  in G.DMT downstream.

Table 4.4: Number of Multiply-accumulate Operations for Proposed Iterative Algorithms/Discrete Multitone Subchannel vs. Matrix Multiply-update/Discrete Multitone Subchannel for  $N = 512, \nu = 32$  and  $\Delta = 26$  as Function of Length of Time Domain Equalizer  $M$

M	Proposed iterative algorithms	Matrix multiply-update
3	72,529	11,908,240
17	1,272,721	57,408,408
32	4,332,571	112,984,608

## 4.5 Conclusion

Chapter 3 presented a new model for the subchannel SNR. This chapter introduces algorithms for the efficient initialization of matrices  $\tilde{\mathbf{A}}_k$  and noise matrix  $\tilde{\mathbf{B}}_k$  present in the proposed subchannel SNR model (3.17). The algorithms exploit the structure of the matrices to reduce the number of computations by up to 164 times compared to a straight multiply update approach that could be taken if no such structure existed. The chapter also shows the low temporary memory requirements of the proposed algorithms. The proposed initialization algorithms would have to be run for every subchannel of interest to obtain all of the necessary matrices for the following stage that will produce time domain equalizer coefficients. Chapter 5 will propose a new time domain equalizer design that uses the model of the subchannel SNR to show the dependency of the bit rate on time domain equalizer coefficients.

## Chapter 5

# Optimal Time Domain Equalizer Design

Chapter 3 introduced a model of the subchannel signal-to-noise ratio that establishes the functional dependency of the bit rate on time domain equalizer coefficients and enables the formulation of bit rate maximization time domain equalizer designs. The design of the time domain equalizer should be linked with the improvement in the bit rate of the system. The bit rate equation is maximized in time domain equalizer coefficients to produce the optimal time domain equalizer filter bank (TEQFB) where a finite-impulse response time domain equalizer is designed for every subchannel of interest. Next, a single finite impulse response time domain equalizer design is designed for all subchannels. The single time domain equalize design matches the performance of the time domain equalizer filter bank if possible, with a significantly reduced numerical complexity during data transmission.

## 5.1 Introduction

Time domain equalizer is one of the few tools available to a DMT receiver to maximize the bit rate thus capturing most of the capacity of the transmission channel. Higher bit rate means that the higher bandwidth content or more services can be offered through a single ADSL or VDSL line. A DMT receiver can maximize the bit rate or can choose to trade some of that bit rate for the improved reliability of the link (increased margin). A DMT receiver can for a set data rate also choose to establish a link at a greater distance thereby allowing greater coverage of the consumer base. All of these objectives can be achieved if the receiver can rely on the time domain equalizer to provide most of the capacity available.

In this chapter, I express the bit rate as a function of the time domain equalizer coefficients through the subchannel SNR model (3.17) defined in Chapter 3. The bit rate is a highly non-linear integer-valued function of time domain equalizer coefficients with multiple maxima (for time domain equalizer size  $M > 2$ ) and sharp peaks. The bit rate is maximized using an optimal time domain equalizer filter bank where each subchannel of interest is assigned time domain equalizer that maximizes the number of bits that subchannel can support. Another time domain equalizer design procedure is presented where a single time domain equalizer is designed to match the performance of the time domain equalizer filter bank at a much lower numerical complexity during data transmission.

In this chapter, Section 5.2 shows the dependency of the bit rate on the time domain equalizer coefficients through the subchannel SNR model. Section 5.3 analyzes the impact of the channel transmission delay on the time domain equalizer design. Section 5.4 discusses the optimal time domain equalizer filter bank. Section 5.5 presents the single time domain equalizer design procedure. Section 5.6 shows the numerical complexity of both design methods in the initialization stage and during data transmission. Section 5.7 concludes this chapter.

## 5.2 Bit Rate as Function of Time Domain Equalizer

I substitute the proposed subchannel SNR model into the bit rate equation in order to show the dependence of the bit rate on TEQ taps. By substituting the subchannel SNR model,  $\text{SNR}^{\text{Model}}_k(\mathbf{w})$  (3.17) into (1.9), I obtain

$$\begin{aligned} b_{\text{DMT}}^{\text{int}}(\mathbf{w}, \mathcal{I}) &= \sum_{k \in \mathcal{I}} \left[ \log_2 \left( \frac{\mathbf{w}^T (\Gamma_k \tilde{\mathbf{B}}_k + \tilde{\mathbf{A}}_k) \mathbf{w}}{\mathbf{w}^T \Gamma_k \tilde{\mathbf{B}}_k \mathbf{w}} \right) \right] \\ &= \sum_{k \in \mathcal{I}} b_k^{\text{int}}(\mathbf{w}) \\ &= \sum_{k \in \mathcal{I}} [b_k(\mathbf{w})] \end{aligned} \quad (5.1)$$

and include the dependence of  $b_{\text{DMT}}^{\text{int}}$  on  $\mathbf{w}$ . For further notational convenience, let  $\mathbf{A}_k = \Gamma_k \tilde{\mathbf{B}}_k + \tilde{\mathbf{A}}_k$  and  $\mathbf{B}_k = \Gamma_k \tilde{\mathbf{B}}_k$ . Thus,

$$b_{\text{DMT}}^{\text{int}}(\mathbf{w}, \mathcal{I}) = \sum_{k \in \mathcal{I}} \left[ \log_2 \left( \frac{\mathbf{w}^T \mathbf{A}_k \mathbf{w}}{\mathbf{w}^T \mathbf{B}_k \mathbf{w}} \right) \right] \quad (5.2)$$

Matrices  $\mathbf{A}_k$  and  $\mathbf{B}_k$  are positive definite, since both the numerator and denominator are always positive numbers for  $\mathbf{w} \neq \mathbf{0}$ , which is what is expected given that both represent power.

The bit rate maximization problem as a function of TEQ taps,  $\mathbf{w}$  is

$$\mathbf{w}_{\text{opt}} = \arg \max_{\mathbf{w}} \left\{ b_{\text{DMT}}^{\text{int}}(\mathbf{w}, \mathcal{I}) \mid \mathbf{w} \in \mathcal{S} \right\} \quad (5.3)$$

where  $\mathcal{S}$  is a set of constraints imposed on  $\mathbf{w}$  and  $\mathcal{I} \subseteq \{0, \dots, N/2 - 1\}$ . Given that (5.2) is scale invariant (i.e.,  $b_{\text{DMT}}^{\text{int}}(\mathbf{w}, \mathcal{I}) = b_{\text{DMT}}^{\text{int}}(\alpha \mathbf{w}, \mathcal{I}), \forall \alpha \neq 0$ )<sup>1</sup> and noticing from (3.11) that choosing  $\mathbf{w}^T \mathbf{w} = \|\mathbf{w}\|^2 = 1$  does not enhance the ADC noise  $\mathbf{n}_y$ , I adopt the unit norm constraint set  $\mathcal{S} = \{\mathbf{w} : \mathbf{w}^T \mathbf{w} = \|\mathbf{w}\|^2 = 1\}$ . Notice that,  $\tilde{\mathbf{B}}_k$  becomes independent of  $\mathbf{w}$  over this constraint set since the last term in (3.42) becomes  $\sigma_{\text{DNF}}^2 \mathbf{I}$ .

---

<sup>1</sup>This is not the case for the DNF noise if  $\sigma_{\text{DNF}}^2$  is not small or  $\mathbf{w}$  imposes a null, but I assume that these cases are not generated by the TEQ design method proposed in this dissertation.



### 5.3 Impact of Transmission Delay on Time Domain Equalizer Design

Dependence of the SNR (or correspondingly the bit rate) on the transmission delay is not clearly visible from (5.2); however, transmission delay is an important design parameter. The transmission delay marks the amount of time that it takes the signal to reach the receiver from the time it has been transmitted. An additional filter such as a TEQ may add some delay to the shortened channel impulse response by shifting the energy to later coefficients. Jointly, the delays of channel impulse response and TEQ make up the transmission delay  $\Delta$  referred to first in (3.3) and then used throughout in the definition of the proposed SNR measure. Delay  $\Delta$  as the parameter which selects the beginning of a frame from a stream of samples coming into the receiver. Notice that once  $\Delta$  is defined, all of the matrices that compose the SNR are defined, as well as (3.16). Thus, defining  $\Delta$  prior to TEQ design also defines (5.2) and its optimal solution. A different  $\Delta$  may result in a higher value for (5.2).

As of yet there is no known way to search for the optimal  $\Delta$  without searching exhaustively through all possible values of  $\Delta$  where  $\Delta \in [0, N - 1]$  and solving the optimization problem for each  $\Delta$ . This dissertation does not propose a better or less costly method. A general statement can, however, be formulated saying that the sensitivity of the final bit rate on the value of the transmission delay should decrease with the increased length of the TEQ. This is a heuristic that was observed from a number of simulation runs performed as a part of this dissertation. It can be justified by noting that an increased number of TEQ coefficients lends more parameters that can be used to accommodate various choices of the transmission delay parameter. Developing a method of choosing the optimal transmission delay  $\Delta$  as an input parameter of the time domain equalizer design remains an open research problem.

## 5.4 Time Domain Equalizer Filter Bank

There are  $N/2$  possible data carrying subchannels in DMT. I propose a method of finding the optimal  $\mathbf{w}$  for every one of them, i.e.  $\mathbf{w}_k$  where  $k$  is the subchannel of interest. I maximize data rate given by (5.1), which is the sum of the rates on individual subchannels by maximizing each element of the sum with potentially different TEQ FIR filter. Maximizing the fractional number of bits in each subchannel  $b_k(\mathbf{w})$  is equal to maximizing the integer number of bits in the subchannel  $b_k^{\text{int}}(\mathbf{w})$ . Maximizing the fractional number of bits allocated in a single subchannel,  $b_k(\mathbf{w})$  means maximizing the argument of the log function. Since the log is a monotonically increasing function for a non-negative argument, maximizing its non-negative argument will also maximize the function. Mathematical notation for this statement is

$$\begin{aligned} b_k^{\text{opt}} &= \max_{\mathbf{w}_k: \|\mathbf{w}_k\|^2=1} \left( \log_2 \left( \frac{\mathbf{w}_k^{\text{T}} \mathbf{A}_k \mathbf{w}_k}{\mathbf{w}_k^{\text{T}} \mathbf{B}_k \mathbf{w}_k} \right) \right) \\ &= \log_2 \left( \max_{\mathbf{w}_k: \|\mathbf{w}_k\|^2=1} \left( \frac{\mathbf{w}_k^{\text{T}} \mathbf{A}_k \mathbf{w}_k}{\mathbf{w}_k^{\text{T}} \mathbf{B}_k \mathbf{w}_k} \right) \right) \end{aligned} \quad (5.4)$$

From [105], the maximization of a single ratio can be transformed into

$$p_k(\mathbf{w}_k, \lambda_k) = \max_{\mathbf{w}_k: \|\mathbf{w}_k\|^2=1} \left\{ \mathbf{w}_k^{\text{T}} \mathbf{A}_k \mathbf{w}_k - \lambda_k \mathbf{w}_k^{\text{T}} \mathbf{B}_k \mathbf{w}_k \right\} \quad (5.5)$$

where  $\lambda_k$  is a scalar. To solve (5.5), I compute the derivative of the argument of the maximum operator with respect to  $\mathbf{w}_k$  and set the derivative to zero, which yields

$$\mathbf{A}_k^r \mathbf{w}_k = \lambda_k \mathbf{B}_k^r \mathbf{w}_k \quad (5.6)$$

Here  $(\cdot)^r$  denotes the real part. This is the well-known generalized eigenvalue problem [70] and the solution is the generalized eigenvector  $\mathbf{w}_k^{\text{opt}}$  corresponding to the largest generalized eigenvalue  $\lambda_k^{\text{opt}}$  of  $(\mathbf{A}_k^r, \mathbf{B}_k^r)$ :

$$\lambda_k^{\text{opt}} = \frac{\left( \mathbf{w}_k^{\text{opt}} \right)^{\text{T}} \mathbf{A}_k^r \mathbf{w}_k^{\text{opt}}}{\left( \mathbf{w}_k^{\text{opt}} \right)^{\text{T}} \mathbf{B}_k^r \mathbf{w}_k^{\text{opt}}} = \frac{\left( \mathbf{w}_k^{\text{opt}} \right)^{\text{T}} \mathbf{A}_k \mathbf{w}_k^{\text{opt}}}{\left( \mathbf{w}_k^{\text{opt}} \right)^{\text{T}} \mathbf{B}_k \mathbf{w}_k^{\text{opt}}} \quad (5.7)$$

Hence,  $b_k^{\text{opt}} = \log_2(\lambda_k^{\text{opt}})$ . If an optimal TEQ were found for every subchannel, then the bit allocation for every one of those subchannels would be maximized which leads to

$$\left[ b_{\text{DMT}}^{\text{int}} \right]^{\text{opt}} = \sum_{k \in \mathcal{I}} \left[ \log_2 \left( \frac{(\mathbf{w}_k^{\text{opt}})^T \mathbf{A}_k \mathbf{w}_k^{\text{opt}}}{(\mathbf{w}_k^{\text{opt}})^T \mathbf{B}_k \mathbf{w}_k^{\text{opt}}} \right) \right] \quad (5.8)$$

The implementation of (5.8) is achieved with the optimal time domain equalizer filter bank architecture where each subchannel time domain equalizer satisfies (5.7).

Figure 5.1 shows the architecture of a DMT receiver with the time-domain equalizer filter bank structure. The received  $N + \nu \times 1$  sample vector  $\mathbf{x}$  is split into  $|I|$  identical sample vectors where again  $|I|$  is the cardinality of the set containing the subchannels of interest. Each vector is then filtered using a subchannel time domain equalizer. Thus, there are as many TEQ FIR as there are subchannels of interest. After the TEQFB, the cyclic prefix samples are removed to obtain the  $N \times 1$  vector  $\mathbf{y}_k$ . The transfer to the frequency domain is performed using a bank of Goertzel [106] filters, each one tuned to the frequency of the desired subchannel and computing a single point DFT coefficient. Since  $\mathbf{y}_k$  is the signal after every subchannel time domain equalizer, then the corresponding frequency response  $Y_k$  for the  $k^{\text{th}}$  subchannel is

$$\mathbf{G}_k^n = \mathbf{y}_k^n + 2 \cos \left( \frac{2\pi k}{N} \right) \mathbf{G}_k^{n-1} - \mathbf{G}_k^{n-2} \quad (5.9)$$

$$\begin{aligned} Y_k &= \left[ \mathbf{G}_k^N - \mathbf{G}_k^{N-1} \cos \left( \frac{2\pi k}{N} \right) \right] \\ &+ j \left[ \mathbf{G}_k^{N-1} \sin \left( \frac{2\pi k}{N} \right) \right] \end{aligned} \quad (5.10)$$

where  $\mathbf{G}_k^{-1} = \mathbf{G}_k^{-2} = 0$  and  $n = 0, 1, \dots, N$ . After the Goertzel filter bank there are  $N/2$  complex values  $Y_k$ , which are equalized using the standard one-tap FEQ per subchannel and subsequently decoded. In Figure 5.1 shows the block architecture of a DMT receiver with the new TEQFB where the shaded blocks represent the new TEQFB architecture addition to the standard DMT receiver.

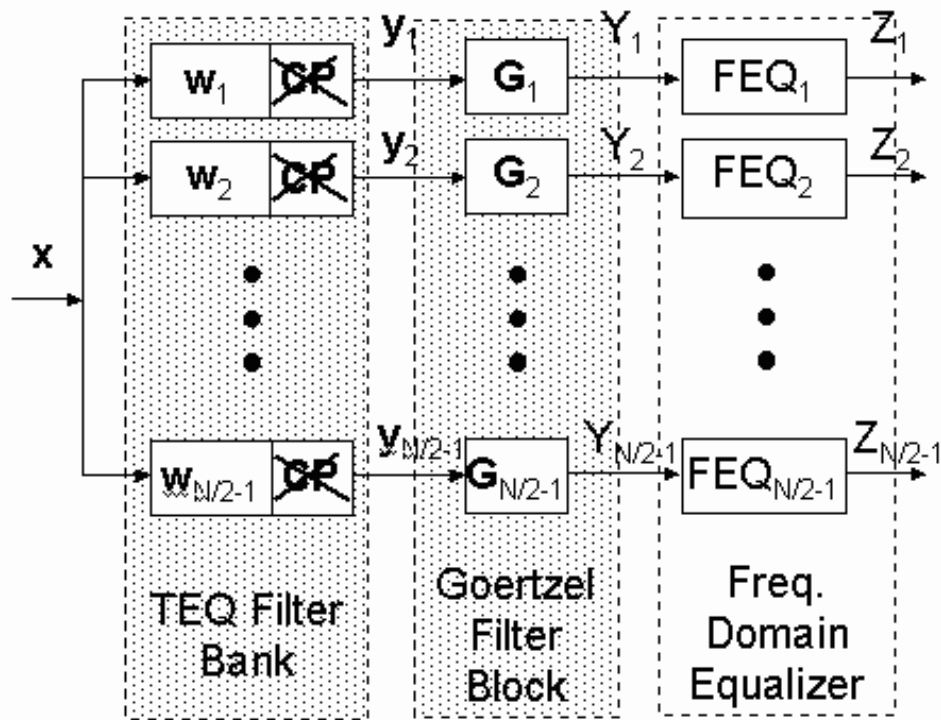


Figure 5.1: Block Diagram of Discrete Multitone Receiver with Time Domain Equalizer Filter Bank Architecture.

TEQFB architecture maximizes (5.1) and is thus an optimal architecture for the DMT receiver with the optimal subchannel TEQ FIR provided by the solution of (5.6). This architecture and the corresponding TEQ FIR solutions is what I collectively call the time-domain equalizer filter bank or TEQFB. Thus, any other arrangement of TEQ filters, be it a single TEQ or multiple, can only perform at par with the TEQFB or worse for the given set of subchannels of interest.

## 5.5 Single Time Domain Equalizer for Data-carrying Subchannels

This section presents a single time domain equalizer design for all subchannels of interest. The single time domain equalizer performance as measured by the data rate could match the data rate achieved by the time domain equalizer filter bank or it will match than the performance of the best of the subchannel equalizers that are a part of TEQFB solution when evaluated across the subchannels of interest. The standard single time domain equalizer architecture has the advantage of being numerically inexpensive and more easily implementable than time domain equalizer filter bank due to the presence of only one FIR filter and the ability to use the FFT block instead of a bank of Goertzel filters.

### 5.5.1 Solution space

As only integer bit loading is allowed in DMT ADSL and VDSL, it is possible that more than one  $\mathbf{w}$  achieves maximum integer bit loading for the  $k^{\text{th}}$  subchannel. Let the set of single TEQ FIR solutions for a single subchannel  $k$  be

$$\mathcal{J}_k = \{\mathbf{w} : \lfloor b_k(\mathbf{w}) \rfloor = \lfloor b_k(\mathbf{w}_k^{\text{opt}}) \rfloor, \mathbf{w} \in \mathcal{S}\} \quad (5.11)$$

I search for a single TEQ FIR that will maximize (5.1), i.e. perform as well as the TEQFB. The set of these filters is

$$\mathcal{J} = \{\mathbf{w} : \mathbf{w} \in \bigcap_{k \in \mathcal{I}} \mathcal{J}_k\} \quad (5.12)$$

Set  $\mathcal{J}$  may contain many single TEQ FIR due to the integer-valued  $b_{\text{DMT}}^{\text{int}}$ , or may be an empty set. The maximization of (5.1) should result in a member of  $\mathcal{J}$  if one exists, or if  $\mathcal{J}$  is a null set, it should find a single TEQ that performs as close as possible to TEQFB. So far, I am not aware of a method that lets us determine in advance if  $\mathcal{J}$  is empty or not.

### 5.5.2 Fractional bit rate as function of the time domain equalizer taps

The maximization of the integer bit rate equation given by (5.1) with respect to a single TEQ FIR  $\mathbf{w}$  is not mathematically tractable. I make a simplification to (5.1) and propose to maximize a related function. The function is the fractional bit rate and is given by

$$\begin{aligned} b_{\text{DMT}}(\mathbf{w}, \mathcal{I}) &= \sum_{k \in \mathcal{I}} \log_2 \left( \frac{\mathbf{w}^T (\Gamma_k \tilde{\mathbf{B}}_k + \tilde{\mathbf{A}}_k) \mathbf{w}}{\mathbf{w}^T (\Gamma_k \bar{\mathbf{B}}_k) \mathbf{w}} \right) \\ &= \sum_{k \in \mathcal{I}} b_k(\mathbf{w}) \end{aligned} \quad (5.13)$$

The difference with the integer bit rate equation given by (5.1) lies in the absence of the flooring function.

But, is the maximizer of (5.13) also the maximizer of (5.1)? Figures 5.2 and 5.3 plot the values of both (5.2) and (5.13) for all possible values of  $\mathbf{w}$  of length 2 and 3 taps, respectively, for a CIR involving a standard transmission channel carrier serving area (CSA) loop 3 and transmit and receive filters. The maxima of both (5.2) and (5.13) happen for the same  $\mathbf{w}$  in both 2- and 3-dimensional space. This is also true for the other seven CSA loops. Thus, maximizing (5.2) maximizes (5.13) in these two cases; however, I cannot guarantee that this will be the case in general. I make the approximation because (5.13) is mathematically easier to maximize than (5.1) and the simulation results presented lend some hope that their maximizers will be the same because of the parameters of the problem like the transmission channel, FFT structure, etc. Similar simplification was also made in the published work on the topic notably [63, 86].

Thus, the problem to solve is

$$\mathbf{w}_{\text{opt}} = \arg \max_{\mathbf{w}} \{ b_{\text{DMT}}(\mathbf{w}, \mathcal{I}) \} \quad (5.14)$$

One way to solve it is to parameterize the problem by imposing a constraint that

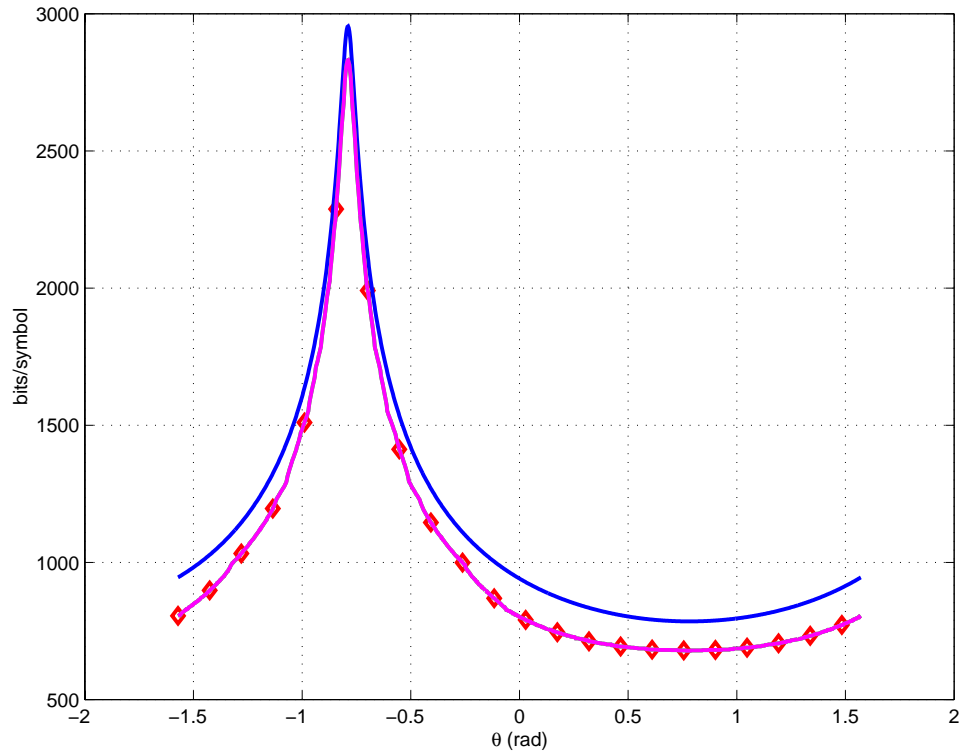


Figure 5.2: Evaluation of Fractional Bit Rate  $b_{\text{DMT}}$  (solid) and Integer Bit Rate  $b_{\text{DMT}}^{\text{int}}$  (Solid with Diamonds) for All Values of Time Domain Equalizer  $\mathbf{w} = [\sin(\theta), \cos(\theta)]^T$ ,  $\theta = [-\frac{\pi}{2}, \frac{\pi}{2}]$  of Length  $M = 2$  for Carrier Service Area Loop 3 with Transmission Delay  $\Delta=15$ , FFT Size  $N = 512$ , Cyclic Prefix Length  $\nu = 32$ , Input Power = 0.2472 W, Additive White Gaussian Noise Power = -140 dBm/Hz, Near-end Crosstalk modelled as 49 ADSL Disturbers and  $\theta$  Sampled with 1081 Points. Notice That  $b_{\text{DMT}}^{\text{int}}$  and  $b_{\text{DMT}}$  Share Global Maximizer.

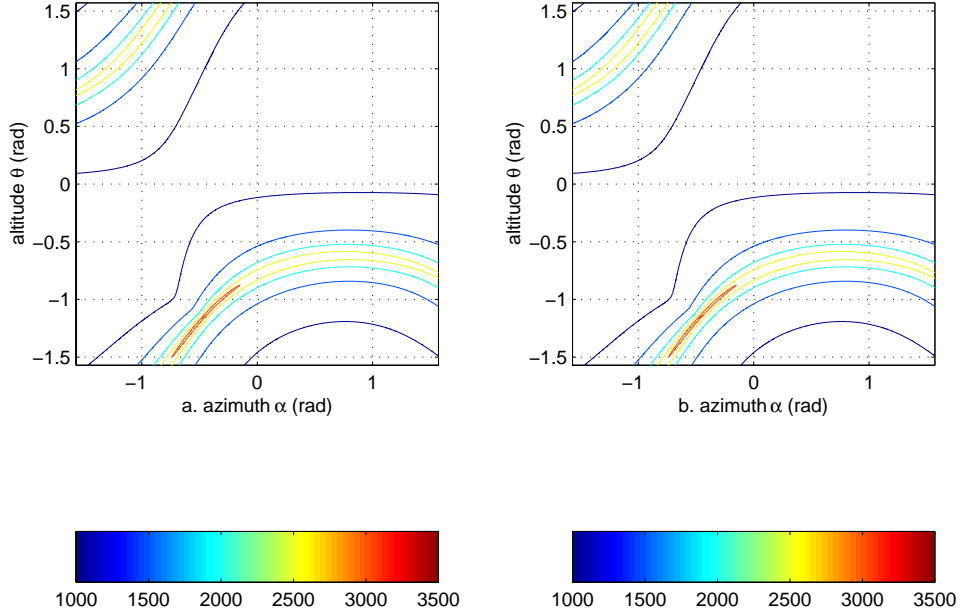


Figure 5.3: The Evaluation of a.  $b_{\text{DMT}}^{\text{int}}$  and b.  $b_{\text{DMT}}$  for All Values of  $\mathbf{w} = [\sin(\alpha) \sin(\theta), \cos(\alpha) \sin(\theta), \cos(\theta)]^T$  for Azimuth Angle  $\alpha = [-\frac{\pi}{2}, \frac{\pi}{2}]$  and Altitude Angle  $\theta = [-\frac{\pi}{2}, \frac{\pi}{2}]$  for Channel Impulse Response Containing Carrier Service Area Loop 3 with Time Domain Equalizer Length  $M = 3$ , with Transmission Delay  $\Delta=15$ , FFT Size  $N = 512$ , Cyclic Prefix Length  $\nu = 32$ , Input Power = 0.2472 W, Additive White Gaussian Noise Power = -140 dBm/Hz, Near-end Crosstalk modelled as 49 ADSL Disturbers and  $\theta$  Sampled with 1081 Points. The Maxima of Both  $b_{\text{DMT}}$  and  $b_{\text{DMT}}^{\text{int}}$  Occur for  $\alpha = -0.4741$  rad and  $\theta = -1.1606$  rad



$M \times 1$  TEQ vector  $\mathbf{w}$  is a point on the  $M$ -dimensional unit hyper-sphere, given by

$$\mathbf{w}^0 = \prod_{l=1}^{M-1} \sin(\theta_l) \quad (5.15)$$

$$\mathbf{w}^m = \cos(\theta_m) \prod_{l=m+1}^{M-1} \sin(\theta_l), \quad m = 1, 2, \dots, M-1 \quad (5.16)$$

The solution is then reached by performing an exhaustive search on the set

$$\mathcal{T} = \{(\theta_1, \theta_2, \dots, \theta_{M-1}) | \theta_m \in [-\pi/2, \pi/2], m = 1, 2, \dots, M-1\} \quad (5.17)$$

The unit hyper-sphere constraint allows us to represent the solution using compact notation and it does not unduly constrain us as to leave possible theoretical solutions out of the scope of the problem. For example, for  $M=2$ , all of the possible  $\mathbf{w}$ 's lie on a unit circle. Changing the size of the circle would change the amplitude of each  $\mathbf{w}$  but does not change their performance relative to each other. When  $M = 2$ , this approach leads to a simple line search on  $\theta_1 \in [-\pi/2, \pi/2]$ . In this case, there is a single mode corresponding to the global maximum of the function and is found for a particular value of  $\theta_1$ . Therefore, the solution can be found using virtually any method that can handle a line search and a single maximum.

However, for  $M > 2$  the structure changes to a multimodal structure with several maxima as demonstrated in Figure 5.3. The exhaustive search for the case  $M > 2$  is unfeasible due to the number of points to probe on the surface of the  $M$ -dimensional unit hyper-sphere. Hence, a better algorithm is needed to solve the problem in finite time.

### 5.5.3 Single time domain equalizer design algorithm

Equation (5.13) is a sum of logarithms whose argument is a ratio of two convex quadratic forms of  $\mathbf{w}$ . A method to maximize a sum-of-ratios is an active research topic in the fractional programming community for which no definitive solution

exists yet (see e.g. [105, 107]). However, (5.13) is a sum of logarithms of ratios, thus maximizing it is an even more involved problem than maximizing a sum of ratios.

The maximization method of (5.13) presented here grew out of an attempt to maximize another function. This function is

$$s(\mathbf{w}, \mathcal{I}) = \sum_{k \in \mathcal{I}} \frac{\mathbf{w}^T (\Gamma_k \tilde{\mathbf{B}}_k + \tilde{\mathbf{A}}_k) \mathbf{w}}{\mathbf{w}^T (\Gamma_k \tilde{\mathbf{B}}_k) \mathbf{w}} \quad (5.18)$$

Equation (5.18) is the sum of the subchannel SNR models and the maximization of it is the sum-of-ratios problem. Almogly and Levin [108] present a method to solve a sum-of-ratios problem

$$b = \max_{x \in R} \sum_{i=1}^n \frac{f_i(x)}{g_i(x)} \quad (5.19)$$

by transforming it into the parametric problem

$$H_n(\mathbf{q}) = \max_{x \in R} \sum_{i=1}^n [f_i(x) - q_i g_i(x)] \quad (5.20)$$

where,  $\mathbf{q} = [q_1, q_2, \dots, q_n]^T$  and where by analogy to the single-ratio maximization Dinkelbach approach (which is the same as Lagrangian multipliers [109]), they defined

$$q_i = \frac{f_i(x_p)}{g_i(x_p)} \quad (5.21)$$

where  $x_p$  is the solution of the maximization in the previous step. The single-ratio maximization parametric equation  $H_1(q_1)$  is a convex, non-increasing function of  $q_1$  with a single root as shown in Figure 5.4. In a single-ratio problem ( $n = 1$ ) the solution is reached when  $H_1(q_1) = 0$ . The value of  $q_1$  where  $H_1(q_1) = 0$  is  $q_1 = q_1^{\text{opt}}$  and the point  $x$  maximizing the current iteration is the same as the value that maximized the previous iteration  $x_p$ . In the maximization algorithm  $q_1$  increases with every iteration, while  $H_1(q_1)$  decreases.

By analogy to Dinkelbach method, Almogly and Levin solve sum-of-ratio parametric equation  $H_n(\mathbf{q}) = 0$  to find the optimal solution of the sum-of-ratios problem. Their approach is erroneous as shown by Falk and Palocsay [110] and

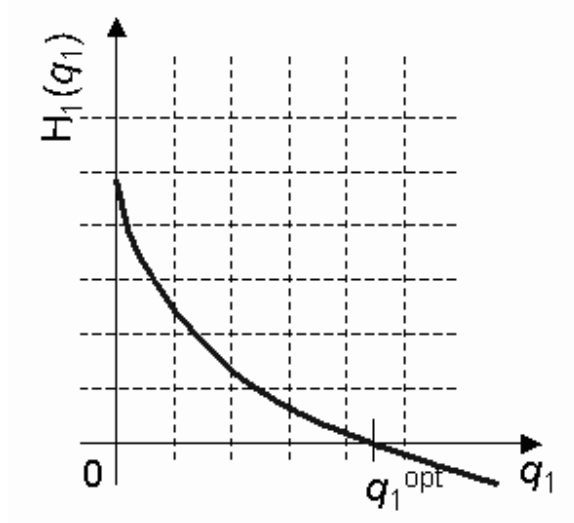


Figure 5.4: Parametric Equation for Single-ratio Maximization

validated in our experiments in using Almgly and Levin’s iteration to maximize a version of (5.18).

The function  $H_n(\mathbf{q})$  is still a convex, non-increasing function of  $\mathbf{q}$  with a single crossing [105]. In the sum-of-ratios problem, finding a zero of  $H_n(\mathbf{q})$  does not produce  $b$ . However, Almgly and Levin’s iteration does find the roots of the nonlinear  $H_n(\mathbf{q})$  efficiently. Hence, I use their idea with modifications specific to the maximization of (5.13), to find a root of the gradient of (5.13) that corresponds to the closest local maximum to the initial point.

The gradient of (5.13) is

$$\frac{db_{\text{DMT}}(\mathbf{w}, \mathcal{I})}{d\mathbf{w}} = \frac{2}{\ln 2} \sum_{k \in \mathcal{I}} r_k(\mathbf{w}) [\mathbf{A}_k^T - \lambda_k(\mathbf{w}) \mathbf{B}_k^T] \mathbf{w} \quad (5.22)$$

where

$$r_k(\mathbf{w}) = \frac{1}{\mathbf{w}^T \mathbf{A}_k \mathbf{w}} \quad \text{and} \quad \lambda_k(\mathbf{w}) = \frac{\mathbf{w}^T \mathbf{A}_k \mathbf{w}}{\mathbf{w}^T \mathbf{B}_k \mathbf{w}} \quad (5.23)$$

Notice that

$$b_{\text{DMT}}(\mathbf{w}, \mathcal{I}) = \sum_{k \in \mathcal{I}} \log_2 [\lambda_k(\mathbf{w})] \quad (5.24)$$

thus, increasing  $\lambda_k(\mathbf{w})$  increases  $b_{\text{DMT}}(\mathbf{w}, \mathcal{I})$ . Now I can write

$$\mathbf{C}_k(\mathbf{w}) = r_k(\mathbf{w}) [\mathbf{A}_k^r - \lambda_k(\mathbf{w})\mathbf{B}_k^r] \quad \text{and} \quad \mathbf{C}(\mathbf{w}, \mathcal{I}) = \sum_{k \in \mathcal{I}} \mathbf{C}_k(\mathbf{w}) \quad (5.25)$$

This leads to an equation similar to (5.20) in which  $r_k(\mathbf{w})$ ,  $\lambda_k(\mathbf{w})$  and  $\mathbf{C}_k(\mathbf{w})$  are projected according to (5.23) and (5.25) during the iterative procedure that finds the optimal root of (5.22). Let

$$\begin{aligned} H(\lambda) &= \max_{\mathbf{w} \in \mathcal{S}} \mathbf{w}^T \mathbf{C}(\mathbf{w}, \mathcal{I}) \mathbf{w} \\ &= \max_{\mathbf{w} \in \mathcal{S}} \sum_{k \in \mathcal{I}} r_k \left[ \mathbf{w}^T \mathbf{A}_k^r \mathbf{w} - \lambda_k \mathbf{w}^T \mathbf{B}_k^r \mathbf{w} \right] \end{aligned} \quad (5.26)$$

where  $\lambda = [\dots, \lambda_k, \dots]^T, k \in \mathcal{I}$ . The proposed method uses Almgly and Levin's method as a basis, not to find a maximum of a sum-of-ratios problem but to find a zero of (5.26) corresponding to the closest maximum of (5.13). As the algorithm progresses,  $\lambda_k(\mathbf{w})$  will always increase due to the properties of the Almgly-Levin parametric equation behavior, thereby increasing (5.13).

However, the algorithm will only find a local maximum that is closest to the initial point. Given a good initial point, the local maximum can be a global maximum. The initial point for the value of  $\mathbf{w}$  will be the TEQFB subchannel equalizer that results in the highest value of (5.13) for all subchannels of interest when compared to the other TEQFB subchannel equalizers. In the context of the maximization of (5.13), the  $\frac{N}{2}$  TEQ filters that comprise TEQFB can be used to evaluate (5.13) at  $\frac{N}{2}$  points. The TEQFB filter that performs the best on all of the subchannels is intuitively a good starting point that is likely to be the closest to the global solution. The simulation results presented in Chapter 7 support that assertion.

The single TEQ design algorithm is shown in Figure 5.5. The key steps in the proposed single TEQ design algorithm (Figure 5.5) are the computations of  $b_{\text{DMT}}(\mathbf{w}_k^{\text{opt}}, \mathcal{I}), k \in \mathcal{I}$  and  $\mathbf{w}_{\text{new}}, i = 1, 2, \dots$ , which are solved by finding the generalized eigenvector corresponding to the largest eigenvalue of a pair of matrices.

The presented algorithm based on the Almgly/Levin's iteration [108] finds the closest local maximum to our starting point with quadratic convergence, without the oscillatory behavior associated with standard steepest ascent algorithms [109].

## 5.6 Computational Complexity

### 5.6.1 Initialization cost

TEQFB algorithm requires up to  $|I|$  (all DMT data-carrying subchannels) solutions of symmetric-definite problems, i.e. largest generalized eigenvalue-eigenvector pair. From [56, p. 465] the largest generalized eigenvalue-eigenvector pair can be found using an extension of the Rayleigh quotient iteration. The cost of this procedure is  $iter_R(M^3/3 + 12M^2 + 4M)$  where  $iter_R$  is the number of iterations used. Thus, the initialization cost of TEQFB, i.e. the cost of finding the optimal TEQ FIR for each subchannel is  $N_u * iter_R(M^3/3 + 12M^2 + 4M)$ . The initialization cost of the proposed single TEQ algorithm is

$iter_S [|I|(9M^2 + 12M) + iter_R(M^3/3 + 12M^2 + 4M)]$  where  $iter_S$  is the number of iterations of the maximization procedure. The initialization cost of the single TEQ FIR does not include the cost of finding the TEQFB and then finding subchannel TEQ which is a member of the TEQFB and which achieves the highest performance over all of the subchannels of interest. The number of iterations in the simulations averaged 100 after which the change in the calculated TEQ taps was negligible.

### 5.6.2 Data transmission complexity

The complexity during data transmission governs the amount of computations that the G. DMT receiver will perform to process data per second of time. The numbers presented thus take into account the computations performed at a symbol rate and at sample rate executed in a single second. The computational complexity and

Table 5.1: Data Transmission Computational Complexity for Sample Rate  $f_s = 2.208$  MHz, Symbol Rate  $f_{\text{sym}} = 4$  kHz, FFT size  $N = 512$ , Cyclic Prefix Length  $\nu = 32$  and Time Domain Equalizer Filters Length  $M = 2$  to 32.

<b>single TEQ</b>	<b>Real MACs</b>	<b>Words/Sym</b>
TEQ	$Mf_s$	$2M$
FFT	$2N \log_2 N f_{\text{sym}}$	$4N$
FEQ	$2N f_{\text{sym}}$	$2N$
<b>TEQFB</b>	<b>Real MACs</b>	<b>Words/Sym</b>
TEQ FB	$\frac{N}{2} M f_s$	$M(1 + \frac{N}{2})$
Goertzel FB	$(N^2 + N) f_{\text{sym}}$	$4N$
FEQ	$2N f_{\text{sym}}$	$2N$
<b>PTE</b>	<b>Real MACs</b>	<b>Words/Sym</b>
FFT	$2N \log_2 N f_{\text{sym}}$	$4N + 2\nu$
Sliding FFT	$2(M - 1)N f_{\text{sym}}$	$N$
Combiner	$2NM f_{\text{sym}}$	$(M + 1)N$

memory requirements during data transmission for the conventional, single TEQ architecture, TEQFB and per-tone (PTE) architectures are shown in Table 5.1. The PTE architecture introduced in Chapter 1, Section 2.6 is used here to show the burden imposed by another alternative solution to the TEQ problem that is realized in a per-tone architecture. The assumption is that the number of data-carrying subchannels is equal to the number of subchannels available in G.DMT being  $\frac{N}{2}$ . This assumption simplifies the notation, however in a system employing G.DMT in the field, that number would be smaller and would vary with the length of the copper twisted pair and of the data rate required by the services that are used by the customer.

Figure 5.6 shows the memory requirements for the compared DMT receiver TEQ block architectures obtain from the second column of Table 5.1 for  $M$  varying from 2 to 32. From Figure 5.6, TEQFB can have lower memory needs than PTE, however it has significantly higher computational requirements during data

transmission that make it too expensive for cost-effective embedded implementation today.

## 5.7 Conclusion

This chapter presents the bit rate equation dependency on the time domain equalizer. The bit rate equation is related to the TEQ taps through the SNR model defined in Chapter 3, Section 5.2. The bit rate equation is an integer-valued function derived as a sum of the logarithms of ratios. The signal to noise ratios have a convex numerator quadratic in the TEQ taps and a convex denominator again quadratic in the TEQ taps. The maximization over the TEQ block of the integer-valued bit rate function is achieved through a novel TEQ block architecture where each subchannel is assigned a TEQ FIR filter designed to maximize the bit rate in that particular subchannel. Each member of the sum constituting the system bit rate is maximized thus maximizing the sum. The optimal subchannel time domain equalizer is found as the solution to the generalized eigenvalue problem being the eigenvector of the pair  $(\mathbf{A}_k, \mathbf{B}_k)$  corresponding to the maximum generalized eigenvalue.

Then the attention turned to a more standard TEQ block architecture where only one time domain equalizer “covers” all of the subchannels. This architecture simpler and numerically less expensive than time domain equalizer filter bank. I proceed to find a single time domain equalizer that potentially maximizes the bit rate equation having seen how TEQFB does it. A simplification removes the integer only constraint from the bit rate equation in order to create a mathematically more amenable cost function. Examples are given where the maxima of the new fractional bit rate is the same as the maxima of the integer-valued bit rate; however, no proof is offered that is so for all cases covered by the parameters of the problem. The design of a single time domain equalizer is performed using Almqvist/Levin [108] iteration to find the zero of the gradient of the fractional bit rate equation. As such,

this method will find the nearest local maximum and does not guarantee an optimal solution. The starting point of the iterative algorithm is provided by the member of the TEQFB which results in the highest fractional data rate when evaluated in the traditional single time domain equalizer architecture.

Finally, this chapter concludes with a look at the initialization and data transmission complexity of the proposed design algorithms. The initialization and data transmission complexity of the TEQFB architecture make it not feasible as a solution in current real-time embedded systems; however, it is the optimal solution and provides an analysis tool for comparison of the performance of other TEQ methods.



```

begin
   $k_o = \arg \max_k \{b_{\text{DMT}}(\mathbf{w}_k^{\text{opt}}, \mathcal{I}), k \in \mathcal{I}\};$ 
   $\mathbf{w}_{\text{opt}} = \mathbf{w}_{k_o}^{\text{opt}};$ 
   $\mathbf{w} = \mathbf{w}_{k_o}^{\text{opt}};$ 
  for  $k = 0; k < |\mathcal{I}|; k ++;$ 
     $r_k = 0;$ 
     $\lambda_k = 0;$ 
  end
   $\alpha = 0;$ 
  for  $i = 0; i < i_{\text{max}}; i ++;$ 
    for  $k = 0; k < |\mathcal{I}|; k ++;$ 
       $r_k = \alpha r_k + (1 - \alpha) \frac{1}{\mathbf{w}^T \mathbf{A}_k \mathbf{w}};$ 
       $\lambda_k = \alpha \lambda_k + (1 - \alpha) \frac{\mathbf{w}^T \mathbf{A}_k \mathbf{w}}{\mathbf{w}^T \mathbf{B}_k \mathbf{w}};$ 
       $\mathbf{C}(\mathbf{w}, \mathcal{I}) = \mathbf{C}(\mathbf{w}, \mathcal{I}) + r_k [\mathbf{A}_k^r - \lambda_k \mathbf{B}_k^r];$ 
    end
     $\mathbf{w}_{\text{new}} = \arg \max \{\mathbf{v}^T \mathbf{C}(\mathbf{w}, \mathcal{I}) \mathbf{v} | \mathbf{v}^T \mathbf{v} = 1\};$ 
    if  $\|\mathbf{w}_{\text{new}} - \mathbf{w}\|_{\infty} < \epsilon$ 
      break;
    end
    if  $b_{\text{DMT}}(\mathbf{w}_{\text{new}}, \mathcal{I}) < b_{\text{DMT}}(\mathbf{w}, \mathcal{I})$ 
       $\alpha = \frac{1+\alpha}{2};$ 
    else
       $\mathbf{w}_{\text{opt}} = \mathbf{w}_{\text{new}};$ 
    end
     $\mathbf{w} = \mathbf{w}_{\text{new}};$ 
     $\mathbf{C}(\mathbf{w}, \mathcal{I}) = \mathbf{0};$ 
  end
end

```

Figure 5.5: Proposed Single Time Domain Equalizer Design Algorithm

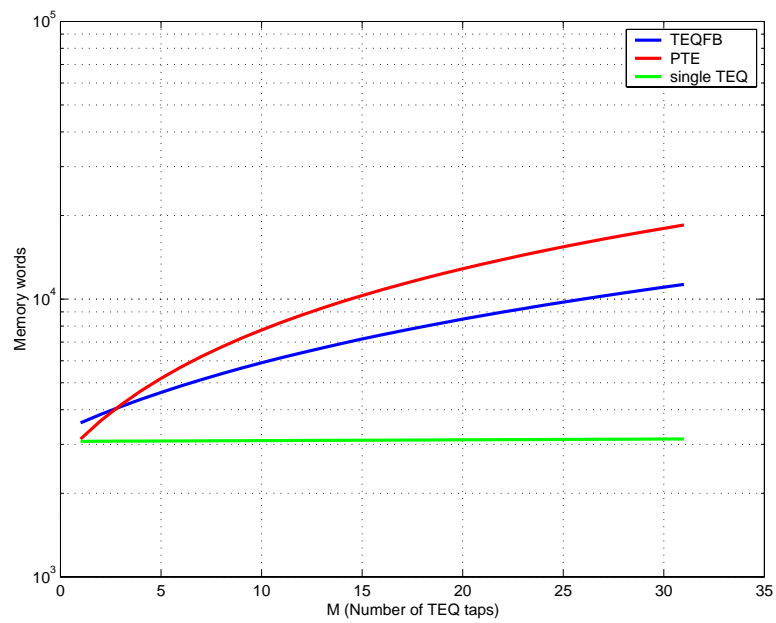


Figure 5.6: Memory Requirements of Proposed Time Domain Equalizer Design Methods During Data Transmission Using the Maximum Number of Subchannels.

## Chapter 6

# Multichannel Time Domain Equalizer Design

Chapter 5 focused on a design of a TEQ block that maximizes the DMT system bit rate for a single known transmission channel. However, there are applications where the time domain equalizer should shorten known multiple channels simultaneously. I propose a method to design a single time domain equalizer to shorten multiple channels by maximizing a weighted sum of channel shortening signal-to-noise ratios where the shortening signal-to-noise ratio was defined in [67, 68, 69]. The proposed method outperforms the joint channel shortening method of Melsa, Younce, and Rohrs [67] because it achieves higher weighted sum of shortening signal-to-noise ratio of the used channels.

### 6.1 Introduction

Melsa, Younce, and Rohrs [67, 68, 69] propose a method for joint shortening of two channels using a single FIR, which I refer to as Joint MSSNR. This method jointly shortens a single channel impulse response and the near-end echo impulse response

using a single TEQ FIR. A TEQ simultaneously minimizes ISI in the received data and shortens the near-end echo impulse response thus, simplifying the removal of the near-end echo.

In some cases, it may be desirable for a central office to use a single FIR TEQ that would shorten a number of DMT channel impulse responses. The situation may arise when a broadband service provider desires to reduce the variability in the performance of its modems from one link to the next, which occurs when a DMT modem re-designs the TEQ every time it is powered and attempts to establish a link. The central office provider may have access to a number of channels in its carrier service area, which it can use to perform the TEQ design off-line. The TEQ design would provide a single TEQ that will perform well for the given set of channels. Similarly, in wireless OFDM applications, it may be desirable to have a TEQ that will simultaneously shorten a number of transmission channels for multiple users.

I propose the Maximum Composite SSNR (MCSSNR) method to design a single FIR TEQ to shorten more than one channel by maximizing a sum of modified channel SSNRs. The modified SSNR measure defined in [72] uses the ratio of the channel energy inside the target window to the overall energy. The modified SSNR measure improves numerical stability in the calculation because it takes values from 0 (maximum ISI) to 1 (minimum ISI), inclusive, and is conveniently represented on fixed-point programmable digital signal processors used in commercial ADSL modems. The proposed method outperforms the joint channel shortening method of Melsa, Younce, and Rohrs (Joint MSSNR) because it achieves higher weighted sum of SSNRs of the used channels.

This chapter is organized as follows. Section 6.2 summarizes the MMSNR and Joint MSSNR method as proposed by Melsa, Younce, and Rohrs. Section 6.3 derives the proposed MCSSNR time domain equalizer design method. Section 6.4 proposes a time domain equalizer that will simultaneously shorten multiple channel

impulse responses. Section 6.5 concludes this chapter.

## 6.2 Background

I consider a discretized transmission channel modelled as an FIR filter with an impulse response of  $N_h$  samples denoted  $\mathbf{h}$ , and a single FIR TEQ with impulse response of  $M$  samples denoted  $\mathbf{w}$ . The cyclic prefix is  $\nu$  samples long; hence, the receiver needs to shorten the channel so that most of the energy of the shortened channel impulse response lies in at most  $\nu + 1$  samples. The linear convolution of the channel impulse response and TEQ results in an effective (and hopefully shortened) channel  $\mathbf{h}_{\text{eff}}$ .

Melsa, Younce, and Rohrs [67] partition  $\mathbf{h}_{\text{eff}}$  into two channels: (1)  $\mathbf{h}_{\text{win}}$ , which consists of samples of  $\mathbf{h}_{\text{eff}}$  lying within the desired  $\nu + 1$  window, and (2)  $\mathbf{h}_{\text{wall}}$ , which consists of the remaining samples of  $\mathbf{h}_{\text{eff}}$ . The effective channel impulse response  $\mathbf{h}_{\text{eff}}$  can be written as  $\mathbf{h}_{\text{eff}} = \mathbf{H}\mathbf{w}$  where  $\mathbf{H}$  is the  $(N_h + M - 1) \times M$  convolution matrix of  $\mathbf{h}$ . So,  $\mathbf{h}_{\text{win}} = \mathbf{H}_{\text{win}}\mathbf{w}$  and  $\mathbf{h}_{\text{wall}} = \mathbf{H}_{\text{wall}}\mathbf{w}$  where  $\mathbf{H}_{\text{win}}$  consists of  $\nu$  rows of  $\mathbf{H}$  starting from position  $\Delta$ , where  $\Delta$  is the transmission delay, and  $\mathbf{H}_{\text{wall}}$  consists of the remaining rows of  $\mathbf{H}$ . Melsa, Younce, and Rohrs define the SSNR as

$$p(\mathbf{w}) = \frac{\mathbf{w}^T \mathbf{H}_{\text{win}}^T \mathbf{H}_{\text{win}} \mathbf{w}}{\mathbf{w}^T \mathbf{H}_{\text{wall}}^T \mathbf{H}_{\text{wall}} \mathbf{w}} = \frac{\mathbf{w}^T \mathbf{A} \mathbf{w}}{\mathbf{w}^T \mathbf{B} \mathbf{w}} \quad (6.1)$$

In order to maximize  $p(\mathbf{w})$ , Melsa, Younce, and Rohrs minimize  $\mathbf{w}^T \mathbf{B} \mathbf{w}$  subject to the constraint that  $\mathbf{w}^T \mathbf{A} \mathbf{w} = 1$ , which yields the MSSNR TEQ design method.

Joint MSSNR uses the previously defined  $\mathbf{H}_{\text{wall}}$  and  $\mathbf{H}_{\text{win}}$  matrices and introduces equivalently defined matrices  $\mathbf{H}_{\text{wall,e}}$  and  $\mathbf{H}_{\text{win,e}}$  derived from the near-end echo impulse response  $\mathbf{h}_e$ . Matrices  $\mathbf{A}$  and  $\mathbf{B}$  are defined in terms of the real-valued parameter  $\alpha$ , where  $0 < \alpha < 1$ , as follows:

$$\mathbf{A}(\alpha) = \alpha \mathbf{H}_{\text{win}}^T \mathbf{H}_{\text{win}} + (1 - \alpha) \mathbf{H}_{\text{win,e}}^T \mathbf{H}_{\text{win,e}} \quad (6.2)$$

$$\mathbf{B}(\alpha) = \alpha \mathbf{H}_{\text{wall}}^T \mathbf{H}_{\text{wall}} + (1 - \alpha) \mathbf{H}_{\text{wall,e}}^T \mathbf{H}_{\text{wall,e}} \quad (6.3)$$

In order to maximize  $p(\mathbf{w}, \alpha)$  jointly, Melsa, Younce, and Rohrs [67] minimize  $\mathbf{w}^T \mathbf{Q}(\alpha) \mathbf{w}$  subject to the constraint that  $\mathbf{w}^T \mathbf{A}(\alpha) \mathbf{w} = 1$ , which yields the Joint MSSNR TEQ design method. However, when the TEQ becomes longer than the cyclic prefix the matrix  $\mathbf{B}$  becomes singular. In order to remedy this, Yin and Yue [72] propose a denominator that uses the energy of the entire channel and not only the energy in outside the window of interest. I use their numerator definition in the following section.

### 6.3 Composite Shortening Signal-to-Noise Ratio

I extend the approach of the Joint MSSNR design method from two channels to multiple channels. For  $K$  channels, I propose a composite shortening signal-to-noise ratio (CSSNR)

$$p(\mathbf{w}) = \sum_{k=1}^K \alpha_k p_k(\mathbf{w}) = \sum_{k=1}^K \alpha_k \frac{\mathbf{w}^T \mathbf{A}_k \mathbf{w}}{\mathbf{w}^T \mathbf{Q}_k \mathbf{w}} \quad (6.4)$$

where  $\mathbf{A} = \mathbf{H}_{k,\text{win}}^T \mathbf{H}_{k,\text{win}}$ ,  $\mathbf{Q}_k = \mathbf{H}_k^T \mathbf{H}_k$ , and  $\alpha_k$  is the weighting of the contribution of the  $k^{\text{th}}$  channel to the overall measure so that  $\sum_{k=1}^K \alpha_k = 1$  and  $\alpha > 0$ . Each weight  $\alpha_k$  can be different, e.g. if the service provider wanted to attach more or less importance to a particular channel or a set of channels. If each weight  $\alpha_k$  had the same value, then a convenient setting would be  $\alpha_k = \frac{100\%}{K}$ . In this case,  $p(\mathbf{w})$  would be composed of equal contributions from all channels.

So, in that case  $p_k(\mathbf{w})$  approaches a value of  $\alpha_k$  as  $\mathbf{w}$  approaches the solution. My goal is to find  $\mathbf{w}_{\text{opt}}$  such that  $p(\mathbf{w})$  is maximized. The proposed solution consists of the following major steps:

1. find the optimal solutions  $\mathbf{w}_k^{\text{opt}}$  for all  $k \in \{1, \dots, K\}$
2. select the solution  $\mathbf{w} = \mathbf{w}_k^{\text{opt}}$  for which  $p(\mathbf{w}_k^{\text{opt}})$  attains the highest value as the initial point, and

3. find the zero of the gradient of  $p(\mathbf{w})$ , by using the Almqvist/Levin iteration [108], to find the maximum of the objective function closest to the initial point, a.k.a. the MCSSNR.

A similar approach for a single channel was taken in [38], in which the objective function was the sum of the bit rates per DMT subchannel.

## 6.4 Multichannel Time Domain Equalizer

From Yin and Yue [72], maximization of the modified SSNR-based ratio in (6.4) for a single channel can be transformed the well-known generalized eigenvalue problem [70], and the solution is the generalized eigenvector  $\mathbf{w}_k^{\text{opt}}$  that corresponds to the largest generalized eigenvalue  $\lambda_k^{\text{opt}}$  of  $(\mathbf{A}_k^r, \mathbf{B}_k^r)$ . Finding a single TEQ that will maximize the proposed sum of modified SSNR leads to a more difficult problem. Maximization of a sum-of-ratios is an active research topic in fractional programming for which a definitive solution has not been discovered [105, 107]. Thus, I propose a solution that achieves good experimental results, although no guarantee of optimality can be given.

I apply Almqvist and Levin's method [108], which is based on the Dinkelbach approach [111], to find the root of the first derivative of (6.4). The algorithm development follows the exposition given in Section 5.5.3 where I described how to find a single TEQ that will maximize the bit rate of multiple subchannels. Now, I have changed the objective to designing a single TEQ for multiple channels, however the mathematical form of the problem is similar to the one laid out in Section 5.5.3. The proposed multichannel TEQ design algorithm is outlined in Figure 6.1.

## 6.5 Conclusion

In this chapter I propose a time domain equalizer design method that will shorten multiple channels simultaneously. I maximize a new objective function that captures the contributions of different channels in a weighted sum of SSNR-based ratios. This approach is an application of the sum-of-ratios maximization approach of Chapter 5. The problem is similar to the problem of designing the single time domain equalizer analyzed in the previous chapter; however, now I design a time domain equalizer for multiple channels. The algorithm does not guarantee a solution that will maximize a sum of ratios however simulation results show that with a good initial point it achieves better results than Joint MSSNR. This approach is still work-in-progress and future work may include some of the developments of the multiple-in multiple-out equalizers.



1. Create matrices  $\mathbf{A}_k$  and  $\mathbf{B}_k$  for all  $k$ .
2. Compute the value of  $p(\mathbf{w})$  for  $\mathbf{w}$  equal to an impulse.
3. Compute the optimal  $\mathbf{w}_k^{\text{opt}}$  for each channel (generalized eigenvalue problem for a pair of matrices  $\mathbf{A}_k$  and  $\mathbf{B}_k$  for each  $k$ ).
4. Compute the value of  $\sum_{k=1}^K \alpha_k p_k(\mathbf{w}_k^{\text{opt}})$  - this is the upper bound I hope to achieve.
5. Compute the value of  $p(\mathbf{w}_k^{\text{opt}})$  for each  $k$  and chose the maximum of all those values and the associated  $\mathbf{w} = \mathbf{w}_{\text{opt}} = \mathbf{w}_k^{\text{opt}}$  as the initial point.
6.  $r_k = \beta r_k + (1 - \beta) \frac{1}{\mathbf{w}^T \mathbf{B}_k \mathbf{w}}, \forall k$ .
7.  $\lambda_k = \beta \lambda_k + (1 - \beta) \frac{\mathbf{w}^T \mathbf{A}_k \mathbf{w}}{\mathbf{w}^T \mathbf{B}_k \mathbf{w}}, \forall k$ .
8. Compute  $\mathbf{C}(\mathbf{w}) = \sum_{k=1}^K r_k [\mathbf{A}_k^r - \lambda_k \mathbf{B}_k^r]$ .
9.  $\mathbf{w}_{\text{new}} = \arg \max \{ \mathbf{v}^T \mathbf{C}(\mathbf{w}) \mathbf{v}, \|\mathbf{v}\|^2 = 1 \}$ .
10. If  $\|\mathbf{w}_{\text{new}} - \mathbf{w}\|_{\infty} < \epsilon$  OR  $i > i_{\text{max}}$  return  $\mathbf{w}_{\text{opt}}$  and jump to 16) .
11. Calculate  $p(\mathbf{w}_{\text{new}})$ .
12. If  $p(\mathbf{w}_{\text{new}}) < p(\mathbf{w})$  set  $\beta = (1 + \beta)/2$ , ELSE  $\mathbf{w}_{\text{opt}} = \mathbf{w}_{\text{new}}$ .
13.  $\mathbf{w} = \mathbf{w}_{\text{new}}$ .
14.  $i = i + 1$ .
15. Go back to step 6 and repeat.
16. Done.

Figure 6.1: Proposed Maximum Composite Shortening Signal-to-Noise Ratio Multichannel Time Domain Equalizer Design Algorithm. The Algorithm is Initialized by Setting the Iteration Counter  $i = 0$ , the Smoothing Factor  $\beta = 0$  and  $r_k$  and  $\lambda_k$  to Zero for All Subchannels.

## Chapter 7

# Performance Evaluation

This chapter presents the results of the simulations that were performed to test the proposed time domain equalizer filter bank and single time domain equalizer architectures and initialization algorithms. The performance of the proposed methods is put into context by comparison with representative previously published time domain equalizer design methods. The transmission channels included standard carrier service area (CSA) loops, transmitter and receiver analog front-end filters and various noise sources included in the subchannel signal-to-noise ratio model of Chapter 3. The simulation results compare the performance of the proposed time domain equalizer design with minimum inter-symbol interference, maximum bit rate, per-tone equalizer initialized using the least-squares method and minimum mean squared error time domain equalizer design. The results of the simulations show that the theoretical optimality of the time domain equalizer filter bank architecture and initialization algorithm is followed by its best-in-class performance against peer methods. The results also show that the proposed single time domain equalizer method achieves on average more than 99% of time domain equalizer filter bank performance with significantly simpler architecture.

## 7.1 Introduction

The presentation of the new TEQ design methods would hardly be complete without a test of their performance versus other previously published methods. The simulation results compare the performance of the proposed TEQ design methods with Min-ISI, MBR, MMSE and LS PTE initialized using the least-squares method. There is a large number of previously published methods and the assessment of their performance and the performance of the TEQ design methods of this dissertation has to be fair and not biased toward a particular method's objective function or training method. The best measure of the performance of a TEQ design method is the bit rate that could be measured in a DMT receiver for a given bit error rate. If a TEQ design method produces a TEQ block that results in a higher data rate with all other things being equal such as the transmission channel used, the amount and shaping of the noise, then that design method has superior performance versus its peers. In a DMT receiver, the bit rate is a function of the measured subchannel SNR on each data-carrying subchannel. Proposed single TEQ and TEQFB and its peer design methods evaluated in this simulation such as Min-ISI, MBR and LS PTE design methods are evaluated using the measured SNR and corresponding achievable bit rate, which establishes a common testing platform. In the past, some TEQ design methods have used objective functions that have been derived from their formulation of the problem (such as MSE or Geometric SNR) to report the validity of their design. There is no assurance that the superior performance as defined using some of those measures indeed translates into superior bit rate as it is measured and applied in an actual ADSL DMT system initialization. That is why this work evaluates the performance of the proposed and previously published methods using SNR measured very closely to the way it is defined in ADSL DMT systems and not using the proposed subchannel SNR model. The intent is to use an objective method of testing a TEQ design that relates the success of the TEQ

design to the data rate measurable on an ADSL DMT system.

Section 7.2 introduces the simulation parameters including the characteristics of the transmission channels used, the properties and levels of the channel-induced noise and the procedure used to generate the random signals used to excite the channel and measure the SNR and corresponding bit rate. Section 7.3 presents the simulation results in a series of graphs and tables that show the performance of the proposed methods against the published methods. Finally, Section 7.4 concludes this chapter.

## 7.2 Simulation Parameters

The simulations use eight standard downstream CSA loops [20] convolved with transmit and receive filters as the test channel impulse response. The standard CSA loops are shown in Figure 7.1 and are specified in the form  $x/y$  where  $x$  is the length of the wire while  $y$  is the wire gauge. The transmit and receive filters are modelled as first-order high-pass infinite impulse response filters, which are designed to separate the ADSL frequency band from the 0-4 kHz voice band (a double zero is located at  $z = 1$ , while conjugate symmetric poles are located at  $z = 0.9799 \pm j0.0317$  in Figure 7.2). All CSA channel impulse responses consist of 512 samples sampled at 2.208 MHz. The standard downstream G.DMT uses a bandwidth of up to 1.104 MHz and the length of a downstream frame during the channel identification initialization is 512 samples without the cyclic prefix of length 32. This DMT frame structure enables identification of 512 samples of the channel impulse response.

The simulations use the FFT size  $N = 512$  standard in downstream ADSL with  $\Gamma = 9.8$  dB, and do not add a coding gain or a margin <sup>1</sup>. All of the power

---

<sup>1</sup>The bit loading tables in ADSL are designed to yield the bit-error rate (BER) of  $10^{-7}$  at 0 dB margin. The measured SNR is used to determine bit loading. In practice, often additional safety is sought in the form of margin to budget for unforeseen increases in noise or insufficiently accurate SNR measurements.

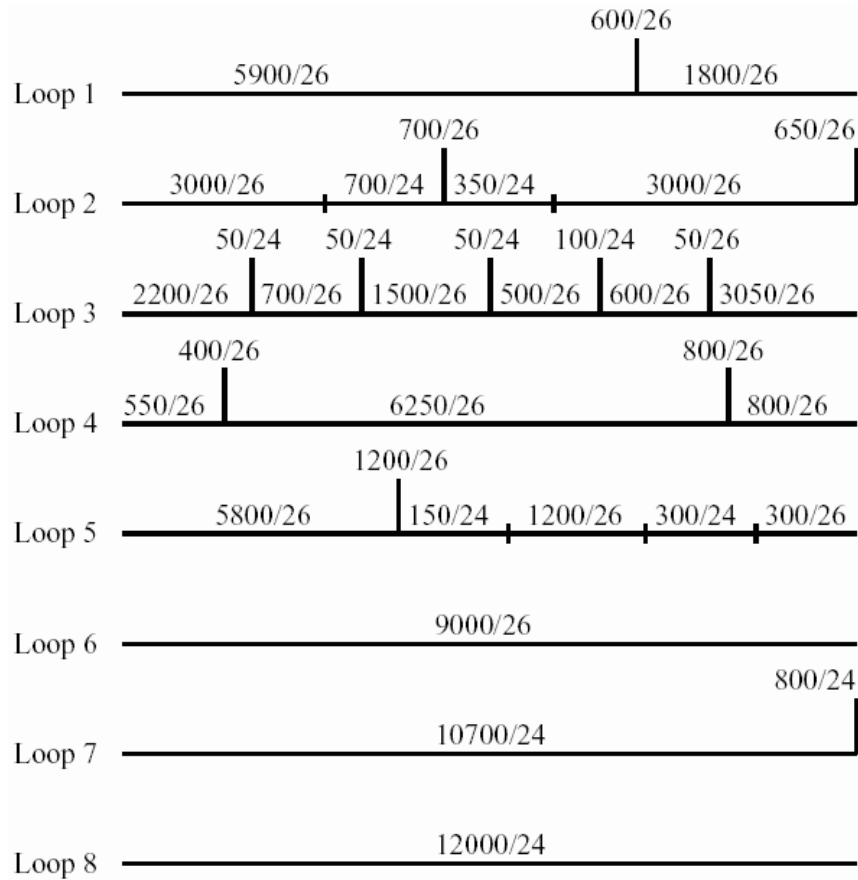


Figure 7.1: Standard Carrier Area Service Loops are Specified as  $x/y$  Where  $x$  is Length of Wire and  $y$  is Wire Gauge. Vertical Lines are Bridge Taps.

used in the simulations is defined with respect to a  $100 \Omega$  resistance. The power of the signal is  $0.2475 \text{ W}$  spread equally over all of the subchannels. Additive white Gaussian noise power is equal to  $-140 \text{ dBm/Hz}$  over the bandwidth of  $1.104 \text{ MHz}$  with the near-end crosstalk source being modelled as 49 ADSL disturbers. The power spectral density of near-end crosstalk is defined in G.DMT [20]. Van de Velde, Pollet and Moeneclaey [112] discuss the effects of the copper twisted-pair and noise on ADSL performance (QAM implementation) and conclude that near-end crosstalk

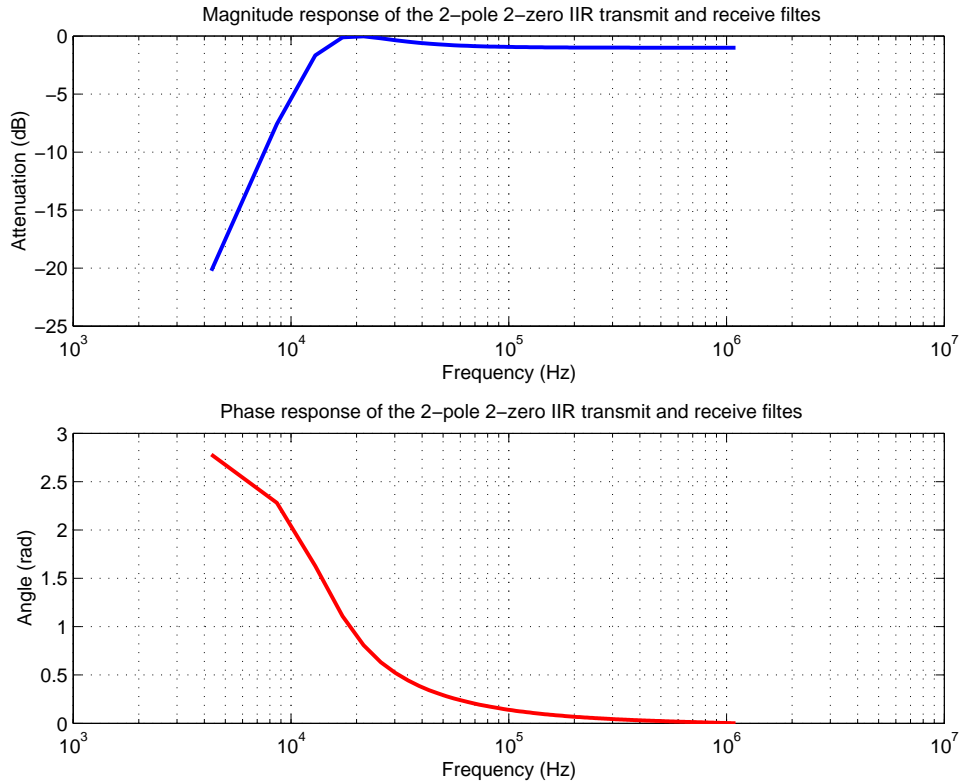


Figure 7.2: Phase and Magnitude Response of the Infinite Impulse Response Filter Modelling Discrete Multitone Transmit and Receive Filters. Double Zero is Located at 1, while Conjugate Symmetric Poles are Located at  $0.9799 \pm j0.0317$ . Transmit and Receive High-pass Filters Separate the Telephone Band from Asymmetric Digital Subscriber Line Band.

from competing services (other ADSL, HDSL, etc.) in the same bundle <sup>2</sup> have the most effect on the ADSL bit rate.

The delay  $\Delta$  is a free parameter in the optimization and is varied over values 0 to 40 with the best achieved data rate taken to be the best result. The upper limit of 40 was heuristically determined for the tested channels. Thus, once  $\Delta_{\text{opt}}$  is chosen, the simulation designs the time domain equalizer according to the method in question (TEQFB, MBR, etc.). TEQ designed by Min-ISI, MBR, and MMSE

<sup>2</sup>Bundle refers to a grouping of unshielded cabling emerging from the central office and emanating toward the carrier service area

methods is obtained using the Matlab DMT TEQ Design Toolbox [113].

Per-tone equalizer structures of [90] were designed using the least-squares method that does not require knowledge of the channel model. The length of the training sequence (measured in DMT frames) used for LS PTE convergence was 300 frames. The number of frames in the LS PTE training sequence was the same for all PTE equalizer lengths. The number of frames used for the LS PTE convergence arose from the simulations in which the training sequence length was varied from 300 to 1024 frames for a limited number of cases involving various CSA loops and various PTE equalizer lengths. The difference in the data rate achieved by tripling the LS PTE training sequence length from 300 to 900 frames was less than the statistical uncertainty inherent in the SNR measurement, i.e. less than 60 kbps.

The system SNR is measured as it would be measured in a G.DMT system during modem initialization. During training, all subchannels are loaded with a randomly chosen two-bit constellation point at the transmitter (Figure 1.7). The frames are convolved with the channel impulse response (including the transmit filter, a CSA loop impulse response and a receive filter), passed through the TEQ block designed by one of the methods being evaluated (i.e. proposed TEQ, proposed TEQFB, Min-ISI, MBR, LS PTE, MMSE-UTC and MMSE-UEC). The received frame is demodulated using the FFT block. The frequency domain equalizer removes the phase and magnitude distortion. QAM decoding compares the complex value received in a particular subchannel with the transmitted value resulting in a complex error (magnitude and phase components are present). The measured subchannel SNR in the subchannel  $k$  results from the power of the estimation error in that subchannel averaged over a 1000 frames. The measured subchannel SNR is

$$\text{SNR}_k = 10 \log_{10} \left( \frac{2}{\frac{1}{S} \sum_{i=0}^{S-1} \|X_k^i - Y_k^i\|^2} \right) \quad (7.1)$$

where  $S = 1000$  frames,  $X_k^i$  is the transmitted 2-bit constellation data in the subchannel  $k$  in the  $i^{\text{th}}$  frame,  $Y_k^i$  is the received data in the subchannel  $k$  in the

$i^{\text{th}}$  frame and 2 comes from the power of two-bit constellation point at locations  $(\pm 1, \pm 1)$ . The bit rates reported are calculated using the measured SNR (7.1) on subchannels 7-256, following the G.DMT standard for  $10^{-7}$  bit error rate (BER) and up to 15 bits allowed per subchannel.

The bound on the SNR measurement using 1000 frames is approximately  $\pm 0.5$  dB which means that the measured SNR is within 0.5 dB of the true SNR. This result was obtained using confidence intervals for variance estimation [114, p. 298]. The term “true” SNR refers to the SNR that would be measured at the output of the frequency domain equalizer as  $S \rightarrow \infty$  in (7.1). Given a 1000-frame measurement, the reported bit rates are accurate up to  $\pm 60$  kbps. The measured SNR was calculated using double-precision arithmetic.

### 7.3 Simulation Results

This chapter presents the simulations results. The simulation were designed to test the proposed TEQ design methods in a variety of conditions under different transmission channels against the peer TEQ design methods. My intent was to explore the behavior of the proposed methods and reveal strengths and weaknesses of the design and also check the agreement of the theoretical expectations and practical simulation results.

Figure 7.3 shows the measured SNR and the proposed model SNR for the case of  $M = 32$  and CSA loop 2. The measured SNR was obtained with the TEQFB in the signal path. The TEQFB was obtained by applying the described TEQFB design procedure. The model SNR was obtained by evaluating (3.16) for the calculated TEQFB. The proposed model SNR closely approximates the measured SNR.

Figure 7.4 shows how the achieved bit rate varies with the change in the number of TEQ taps  $M$  ranging from 2 to 32 as an example for the channel impulse



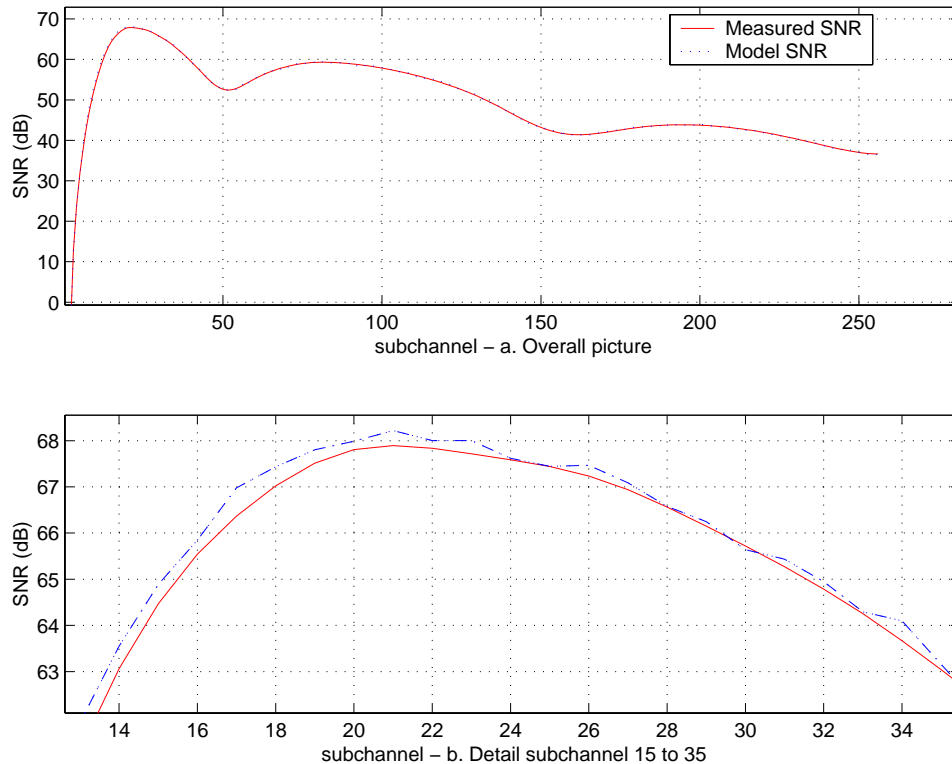


Figure 7.3: Comparison of Measured Subchannel SNR and Subchannel SNR model on Carrier Service Area Loop 2 for Time Domain Equalizer Length  $M = 32$ . Shows Closeness of Measured Subchannel SNR and Subchannel SNR model with Most of ISI Removed.

response containing CSA loop 2. The bit rate grows significantly from 2 to 3 TEQ taps. The upward slope is present with the further increase in the number of TEQ taps  $M$  but it is significantly moderated. LS PTE follows TEQFB closely for  $M = 2$  to 8, outperforming TEQFB for  $M = 6$ ; however, the LS PTE performance drops off for larger sizes of  $M$  for the largest gap of 140 kbps. The proposed single TEQ design performs closely to TEQFB outperforming LS PTE for some sizes of  $M$  and performs better than Min-ISI, or MBR for all sizes of  $M$  in this figure.

Table 7.1 lists the data rate achieved with the proposed optimal TEQFB for the channel impulse response including CSA loops 1-8. These data rates represent

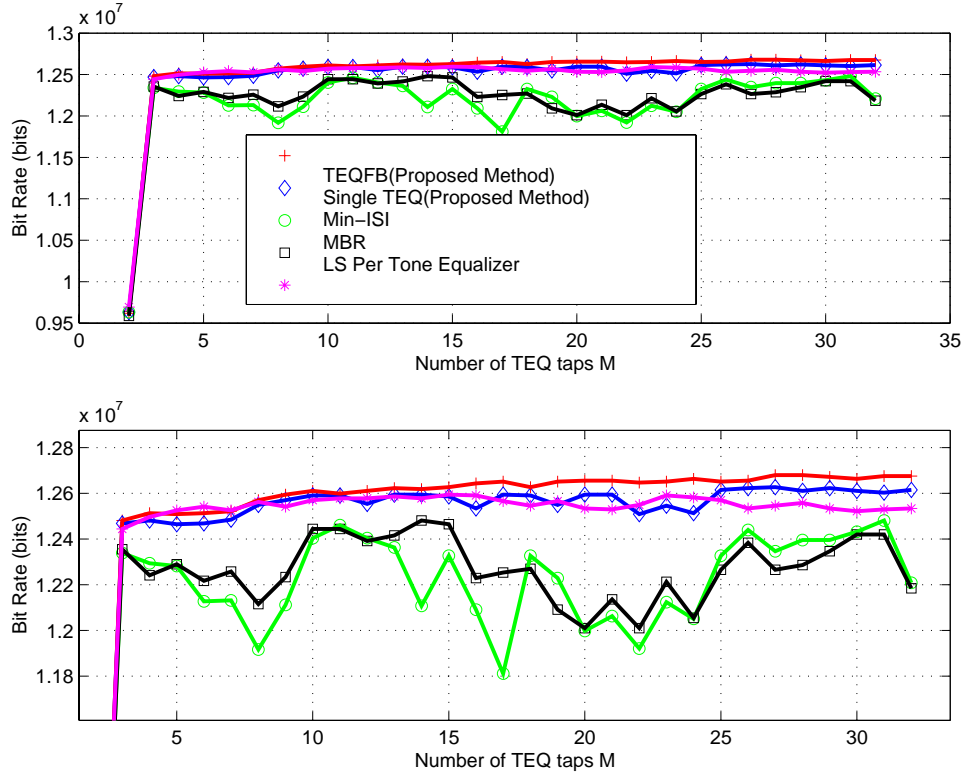


Figure 7.4: Simulation Data Rates Achieved on Carrier Service Area Loop 2 vs. the Length of Time Domain Equalizer for FFT size  $N = 512$ , Cyclic Prefix Length  $\nu = 32$  with Input Power = 0.2472 W, Additive White Gaussian Noise Power = -140 dBm/Hz, Near-end Crosstalk Modelled as 49 ADSL Disturbers and Optimal Transmission Delay  $\Delta$ . a. Entire Graph b. Detail of Higher Data Rates. Reported Rates are up to  $\pm 60$  Kbps Away from True Values

the maximum data rate that can be achieved as a function of TEQFB for the given signal and noise power levels.

Table 7.2 shows the achieved data rates of the proposed single TEQ design method, MBR, Min-ISI, MMSE-UEC, MMSE-UTC, and LS PTE for the channel impulse response including CSA loops 1-8 as percentage (%) of the data rate of the proposed TEQFB. The row entry under  $LA(CSA, A)$ , where  $LA$  stands for “loop

Table 7.1: Highest Achieved Bit Rates for Time Domain Equalizer Filter Bank on Standard Carrier Service Area Loops 1-8 with Transmit and Receive High-pass Filters for FFT size  $N = 512$ , Cyclic Prefix Length  $\nu = 32$  with Input Power = 0.2472 W, Additive White Gaussian Noise Power = -140 dBm/Hz, Near-end Crosstalk Modelled as 49 ADSL Disturbers and Optimal Transmission Delay  $\Delta$ . Each Time Domain Equalizer Filter Bank Subchannel Time Domain Equalizer is of Length  $M$ . There are  $N/2$  data-carrying subchannels and no limitations on the bit allocation.

CSA loop	Prop. TEQFB (Mbps)	$\Delta_{\text{opt}}$	$M$
1	11.417	15	8
2	12.680	22	12
3	10.995	26	8
4	11.288	35	6
5	11.470	32	16
6	10.861	20	8
7	10.752	34	13
8	9.615	35	11

average” and  $A$  for “TEQ design algorithm” is calculated as

$$LA(CSA, A) = \frac{1}{31} \sum_{M=2}^{32} \frac{b_A(\Delta_{\text{opt}}, CSA, M)}{b_{\text{DMT}}^{\text{opt}}(CSA, M)} * 100\% \quad (7.2)$$

where  $b_A(*)$  is the highest bit rate achieved by the evaluated algorithm for the given TEQ size  $M$ ;  $\Delta_{\text{opt}}$  is found using line search, and  $b_{\text{DMT}}^{\text{opt}}$  is the bit rate of TEQFB defined in (5.8) for the given TEQ size  $M$ . Simulations are performed for each CSA loop with  $M$  ranging from 2 to 32 for standard  $N = 512$  and  $\nu = 32$ . The last row entry is the average for the evaluated algorithm.

$$Avg(A) = \frac{1}{8} \sum_{CSA=1}^8 LA(CSA, A) \quad (7.3)$$

I intended to show how the evaluated algorithm may perform on “average” across loops and TEQ filter sizes because in a deployed ADSL DMT system the algorithm will need to work across varying loop topologies and may use different TEQ sizes.

TEQFB is always higher than the compared methods. The proposed single TEQ design method achieves higher percentage for each channel impulse response

Table 7.2: Performance of Simulated Time Domain Equalizer Methods vs. Time Domain Equalizer Filter Bank Averaged over Time Domain Equalizer Length  $M \in \{2, \dots, 32\}$  for Standard Carrier Area Service Loops 1-8 with Transmit and Receive High-pass Filters for FFT size  $N = 512$ , Cyclic Prefix Length  $\nu = 32$  with Input Power = 0.2472 W, Additive White Gaussian Noise Power = -140 dBm/Hz, Near-end Crosstalk Modelled as 49 ADSL Disturbers and Optimal Transmission Delay  $\Delta$ . The Design methods are 1-Proposed Single Time Domain Equalizer, 2-MBR, 3-Min-ISI, 4-LS PTE, 5-MMSE-UEC, 6-MMSE-UTC.

CSA	A					
	1	2	3	4	5	6
$LA(1, A)$	99.6%	97.3%	97.5%	99.5%	86.3%	84.4%
$LA(2, A)$	99.6%	97.0%	97.3%	99.5%	87.2%	85.8%
$LA(3, A)$	99.6%	97.8%	97.3%	99.6%	83.9%	83.0%
$LA(4, A)$	99.3%	98.1%	98.2%	99.1%	81.9%	81.5%
$LA(5, A)$	99.6%	97.7%	97.2%	99.5%	88.6%	88.9%
$LA(6, A)$	99.5%	97.7%	98.3%	99.4%	82.7%	79.8%
$LA(7, A)$	98.8%	96.3%	96.3%	99.6%	75.8%	78.4%
$LA(8, A)$	98.7%	97.4%	97.5%	99.2%	82.6%	83.6%
$Avg(A)$	<b>99.3%</b>	<b>97.4%</b>	<b>97.5%</b>	<b>99.4%</b>	<b>83.6%</b>	<b>83.2%</b>

than Min-ISI, MBR or MMSE-based methods. The proposed single TEQ's final average is almost 2% higher than either MBR or the Min-ISI and more than 15% higher than MMSE-UTC or MMSE-UEC. For a data rate of 11 Mbps, a 2% improvement amounts to 220 kbps. The proposed single TEQ matches LS PTE performance on the majority of CSA loops. The proposed single TEQ does not perform as well as the LS PTE; however, the differences are small.

In Figure 7.5, I compare the change in the achieved bit rate with the change in the CP length  $\nu$  from 1 to 32 for a fixed number of TEQ taps,  $M = 3$ . TEQ length  $M = 3$  is used because results in Figure 7.4 show that is the smallest  $M$  to achieve very high data rates. The bit rate steadily increases with the increase in  $\nu$ . The proposed design of TEQFB outperforms other methods. The proposed TEQ design performs closely to TEQFB and outperforms both Min-ISI, and MBR TEQ.

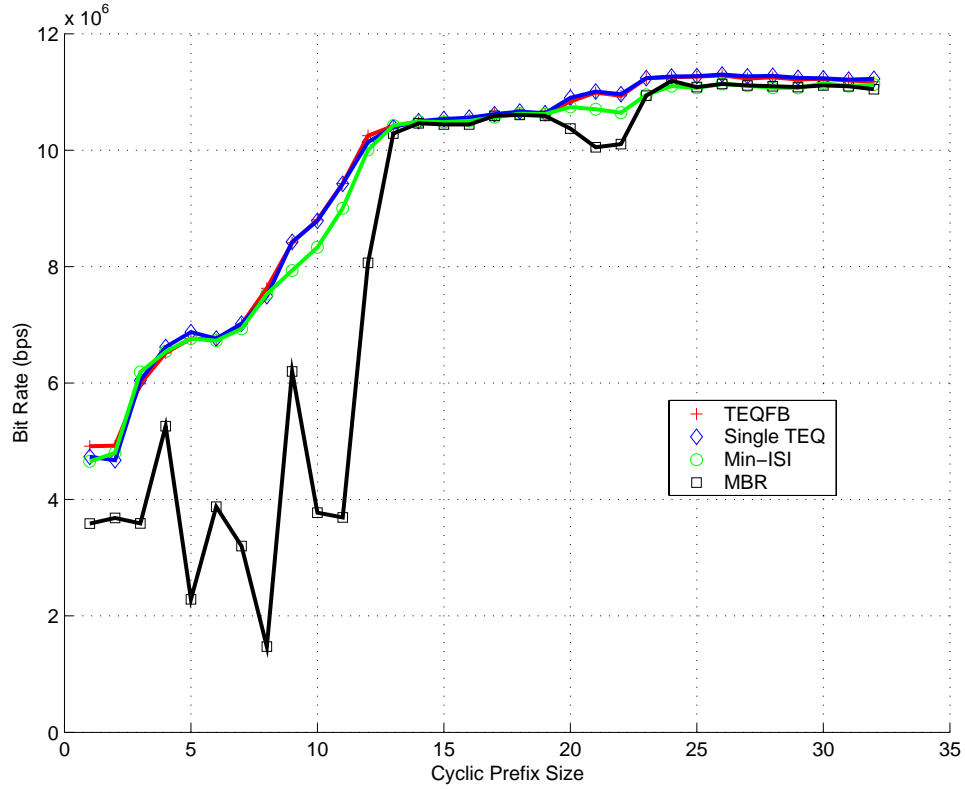


Figure 7.5: Simulation Data Rates Achieved on Carrier Service Area Loop 5 vs. Length of Channel Prefix for Time Domain Equalizer Length  $M = 3$ , FFT size  $N = 512$ , Cyclic Prefix Length  $\nu = 32$  with Input Power = 0.2472 W, Additive White Gaussian Noise Power = -140 dBm/Hz, Near-end Crosstalk Modelled as 49 ADSL Disturbers and Optimal Transmission Delay  $\Delta$

Figure 7.6 shows how the bit rate changes as a function of transmission delay  $\Delta$  for the proposed single TEQ design method. The CIRs tested include CSA loop 1 for TEQ length  $M = \{3, 10, 30\}$ ,  $N = 512$ ,  $\nu = 32$ . Generally, the bit rate rises over a small range of  $\Delta$ , plateaus for a range of  $\Delta$  and declines for the rest of the measured delays. Increasing the number of TEQ taps brings about an increase in the data rate but most prominently increases the range of  $\Delta$  over which the bit rate function plateaus. This reduces the sensitivity of the design to the choice of  $\Delta$  as

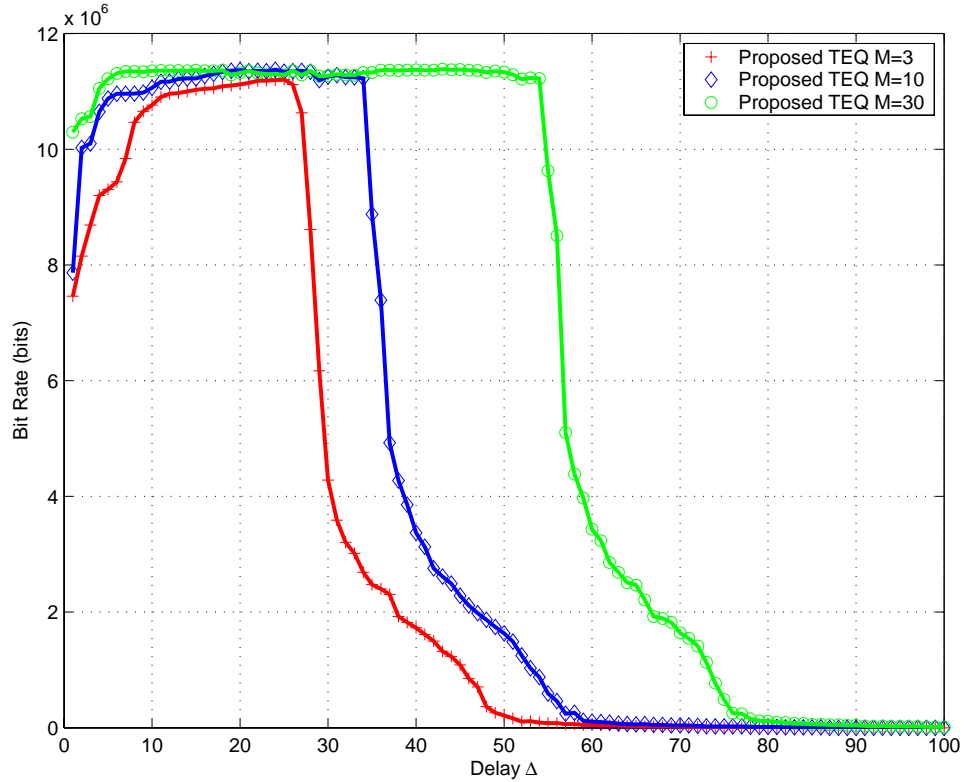


Figure 7.6: Simulation Data Rates of the Proposed Single Time Domain Equalizer Design Achieved on Carrier Service Area Loop 1 vs. Transmission Delay Design Parameter for FFT size  $N = 512$ , Cyclic Prefix Length  $\nu = 32$  with Input Power = 0.2472 W, Additive White Gaussian Noise Power = -140 dBm/Hz, Near-end Crosstalk Modelled as 49 ADSL Disturbances.

the near maximum can be achieved for a larger number of  $\Delta$ . The fact that the bit rate as a function of  $\Delta$  has a high degree of “regularity” can aid TEQ design methods when it comes to the choice of  $\Delta$ .

Figure 7.7 compares the measured SNR achieved with the proposed single TEQ design, MBR and Min-ISI for CSA loop 4. The figure gives insight into why the performance of the proposed TEQ design outperforms the compared methods. Both MBR and Min-ISI in this particular example tend to put nulls in the SNR thus reducing the data rate. The simulation observations suggest that a successful

TEQ has a flat magnitude response over most of the spectrum and a null at the position of the highest ISI whereas a less successful design will put a number of nulls elsewhere in the spectrum.

The simulation results show the performance of the proposed multichannel shortening MCSSNR method vs. the method of joint MSSNR channel shortening method by Melsa, Younce, and Rohrs, for different steps of the proposed algorithm. The comparison with the Joint MSSNR was achieved by designing the best multichannel TEQ using the Joint MSSNR algorithm and the proposed MCSSNR and evaluating the modified SSNR ratio for each of the transmission channels in the set. The final value reported for both methods is then the sum of all the evaluated modified SSNR. The closer the final value is to 100%, the more successful is the designed TEQ FIR in reducing the energy outside of the desired window for each of the transmission channels in the set. I also compare the bit rate/channel of both mentioned methods to the bit rate/channel achieved using single FIR TEQ method in [38], in which each channel under consideration has its own TEQ FIR. The transmission delay  $\Delta$  is chosen by using a line search with respect to the values of  $p(\mathbf{w})$ . The bit rates/channel reported are averages of the bit rates for each of the channels CSA loops 1–8.

The values of interest are the values of the function  $p(\mathbf{w})$  and the bit rate/channel at different steps of the proposed MCSSNR algorithm. These steps are (2), (4), (5), and (16) of Figure 6.1. Each of the  $K$  channels contributed equally to the objective function, so  $\alpha_k = \frac{100\%}{K}$  for all  $k$ .

Table 7.3 lists the values of the objective function and the corresponding bit rate/channel averaged over TEQ FIR sizes  $M$  from 2 to 32. By the end of the proposed maximization (shown under MCSSNR step (16) in Figure 6.1), the objective function increases 1.94% and the corresponding bit rate/channel close to 500 kbps over the initial point TEQ FIR provided by the MCSSNR step (5). The

Table 7.3: Composite Shortening Signal-to-noise Ratio vs. Joint Maximum Signal-to-noise Ratio at Selected Algorithm Steps for Time Domain Equalizer Lengths 2–32, FFT size  $N = 512$ , Cyclic Prefix Length  $\nu = 32$  with Input Power = 0.2472 W, Additive White Gaussian Noise Power = -140 dBm/Hz, Near-end Crosstalk Modelled as 49 ADSL Disturbers. Bit Rate/Channel and Composite Signal-to-noise Ratio are Averaged Over Time Domain Equalizer Lengths: a - MCSSNR Algorithm Step, b - Value of  $p(\mathbf{w})$ , c - Avg. Bit rate/channel (Mbps).

<b>a</b>	<b>b</b>	<b>c</b>
(2)	57.50%	0.79
(4)	99.95%	9.11
(5)	97.77%	8.77
<b>(16)</b>	99.71%	9.26
<b>Joint MSSNR</b>	99.18%	9.07

performance of algorithm step (16) is still worse than the performance afforded by the algorithm step (4) where each subchannel has its own optimal TEQ FIR. The difference in the average value of the objective function is close to 0.24% between MCSSNR steps (4) and (16), although on average the latter achieves higher bit rate/channel. This would be inconsistent if it were not for the fact that maximizing an SSNR-based objective function does not necessarily maximize data rate [63]. The value of the objective function in MCSSNR step (16) is larger than the value obtained using the solution from Joint MSSNR, and so is the achieved bit rate/channel (see the last row of Table 7.3).

Figure 7.8 illustrates the increase in the objective function  $p(\mathbf{w})$  vs. iteration of the proposed algorithm for FIR TEQs of length  $M = 23$  and  $M = 11$  for CIRs including CSA loops 1–8. The initial point value (obtained from MCSSNR step (5)) is shown as the solid line. The objective function rises to nearly 100% although it never quite reaches the value of the objective function given by MCSSNR step (4) (which is the dashed dotted line).

Figure 7.9 shows bit rate/channel achieved by varying the number of samples



of the TEQ FIR from 2–32 for MCSSNR steps (2), (4), (5), and (16) for the CIRs including CSA loops 1–8. It also shows the bit rate/channel achieved by Joint MSSNR and the bit rate/channel achieved using single FIR TEQ design in [38], in which each channel under consideration has its own FIR TEQ. Figure 7.9 illustrates that the maximization of the objective function  $p(\mathbf{w})$  given here, which is based on the SSNR ratio (both the Joint MSSNR and the proposed MCSSNR), does not necessarily maximize bit rate/channel. For example, at no time during the simulation did the maximized value of  $p(\mathbf{w})$  at MCSSNR step (16) go beyond the value achieved in the step (4); however, the bit rate achieved at MCSSNR step (16) is sometimes larger than that one achieved at step (4), e.g. for  $M = 13$ . Also, note that the maximum data rate/channel is achieved for  $M = 3$  and drops for higher values, which is not intuitive as a larger number of TEQ taps should result in a higher data rate/channel. The performance of FIR TEQ design in [38] is always better than any result achieved by either the proposed algorithm or the Joint MSSNR, and it increases with an increase in the number of FIR TEQ taps.

Figure 7.10 shows the shortening of CSA loops 1 and 5 by using a single FIR TEQ designed using the proposed method on a set of CSA loops 1–8. The TEQ FIR had  $M = 3$  taps with ADSL standard downstream parameters of  $N = 512$  and  $\nu = 32$ .

## 7.4 Conclusion

This chapter presents the performance of the proposed TEQ architectures and algorithms and compare it to its peers. Both TEQFB and single TEQ FIR algorithms were evaluated over a range of different conditions from the change in the transmission channel characteristics to the change in the DMT frames structure and thus change in the level of ISI introduced. The simulations use the eight standard downstream CSA loops [20] convolved with transmit and receive filters as the test channel

impulse response. Proposed single TEQ and TEQFB and its peer design methods evaluated in this simulation such as Min-ISI, MBR, LS PTE, MMSE-UEC and MMSE-UTC design methods are evaluated using the measured SNR and the corresponding achievable bit rate, which establishes a common testing platform. TEQFB achieved data rate is always higher than the compared methods. The proposed single TEQ design method achieves higher percentage of TEQFB optimal performance for each channel impulse response than Min-ISI, MBR or MMSE-based methods. Proposed single TEQ's final average over tested CSA loops and is almost 2% higher than either MBR or the Min-ISI and more than 15% higher than MMSE-UTC or MMSE-UEC. For a data rate of 11 Mbps, a 2% improvement amounts to 220 kbps. The proposed single TEQ matches LS PTE performance on the majority of CSA loops. Overall single TEQ does not perform as well as the LS PTE, however the differences are small. The sensitivity of the achieved data rate on the transmission delay in the case of the proposed TEQFB and single TEQ FIR methods decreases with the length of the FIR filters used. Even with small length of FIR filters, the change in the data rate as a function of the transmission delay  $\Delta$  shows high regularity: data rate increases for small values of  $\Delta$ , plateaus for mid-range values and drops of rather quickly for "large" values of  $\Delta$ . This level of regularity helps to choose the optimal  $\Delta$ . The simulation observations suggest that a successful TEQ has a flat magnitude response over most of the spectrum and a null at the position of the highest ISI whereas a less successful design will put a number of nulls elsewhere in the spectrum. Thus, the TEQFB reaches the optimal performance in the simulations as predicted by the theoretical model. Single TEQ reaches more than 99% percent of the performance of TEQFB with significantly lower complexity. Currently, the TEQFB has been implemented in the Matlab DMT TEQ Toolbox [113] and a plan for the future work is to implement the single TEQ FIR method.

In simulation using standard ADSL parameters, the proposed MCSSNR

modestly outperforms the Joint MSSNR method [67] by achieving higher joint SSNR-based measure. A higher joint SSNR-based measure indicates better removal on average of the channel energy outside of the desired window. However, the proposed MCSSNR is considerably more computationally intensive than Joint MSSNR, as it requires a larger number of generalized eigenvalue solutions.

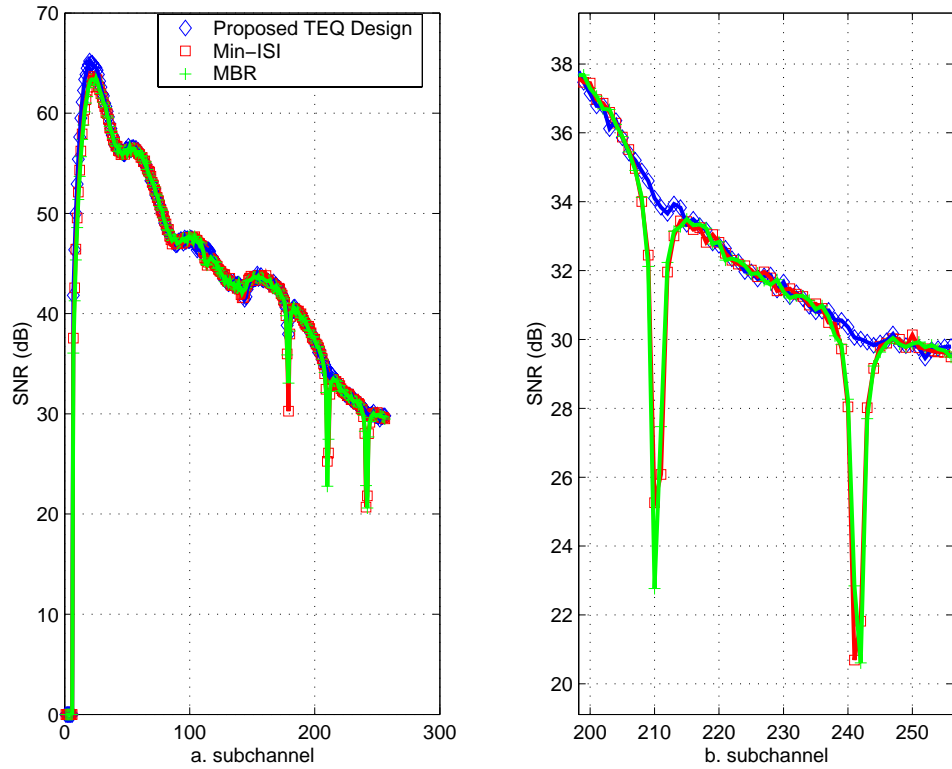


Figure 7.7: Signal-to-noise Ratio of Proposed Single Time Domain Equalizer Design vs. the Maximum Bit Rate Method and Minimum-ISI Method for Carrier Area Service Loop 4 for Time Domain Equalizer Length  $M = 18$ , FFT size  $N = 512$ , Cyclic Prefix Length  $\nu = 32$  with Input Power = 0.2472 W, Additive White Gaussian Noise Power = -140 dBm/Hz, Near-end Crosstalk Modelled as 49 ADSL Disturbers and Optimal Transmission Delay  $\Delta$ ; Maximum Bit Rate Method and Minimum-ISI Methods Place Nulls in the Passband Signal-to-noise Ratio while Proposed Single Time Domain Equalizer Design Does Not. Nulls Limit Data Rate. a. Signal-to-noise Ratio, b. Detail of Nulls

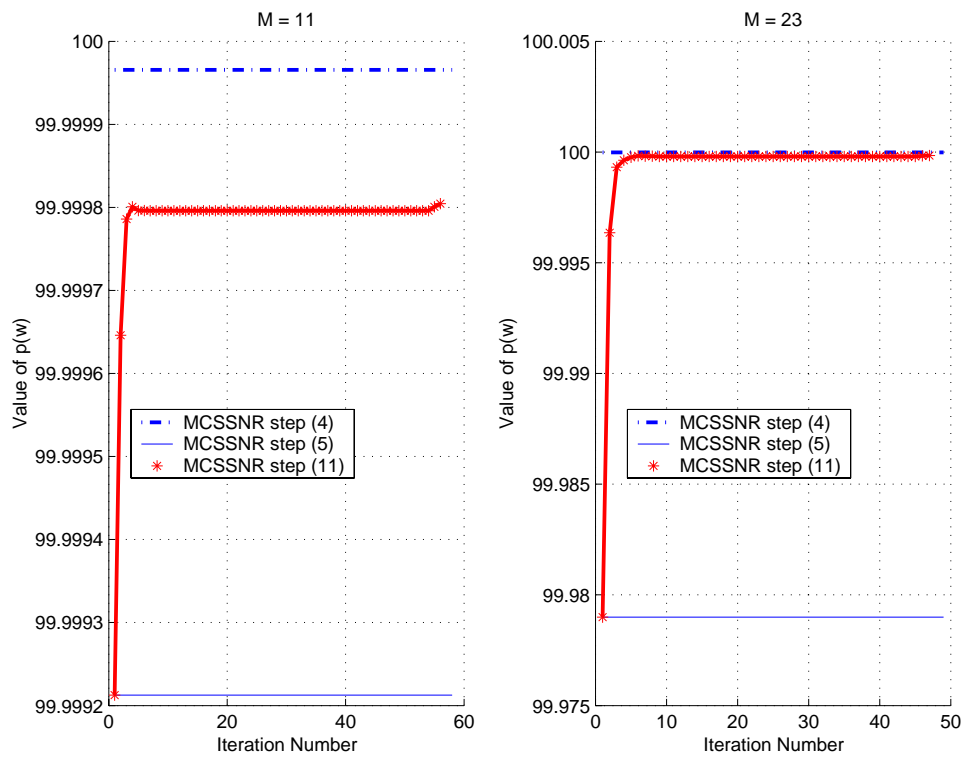


Figure 7.8: Maximization of Composite Shortening Signal-to-Noise Ratio vs. Iteration for FFT Size  $N = 512$ , Cyclic Prefix Length  $\nu = 32$ , and Time Domain Equalizer Lengths  $M = 23$  and  $M = 11$ . The Maximum Achievable Value is Nearly 100% Shown as Dash-dot Line.

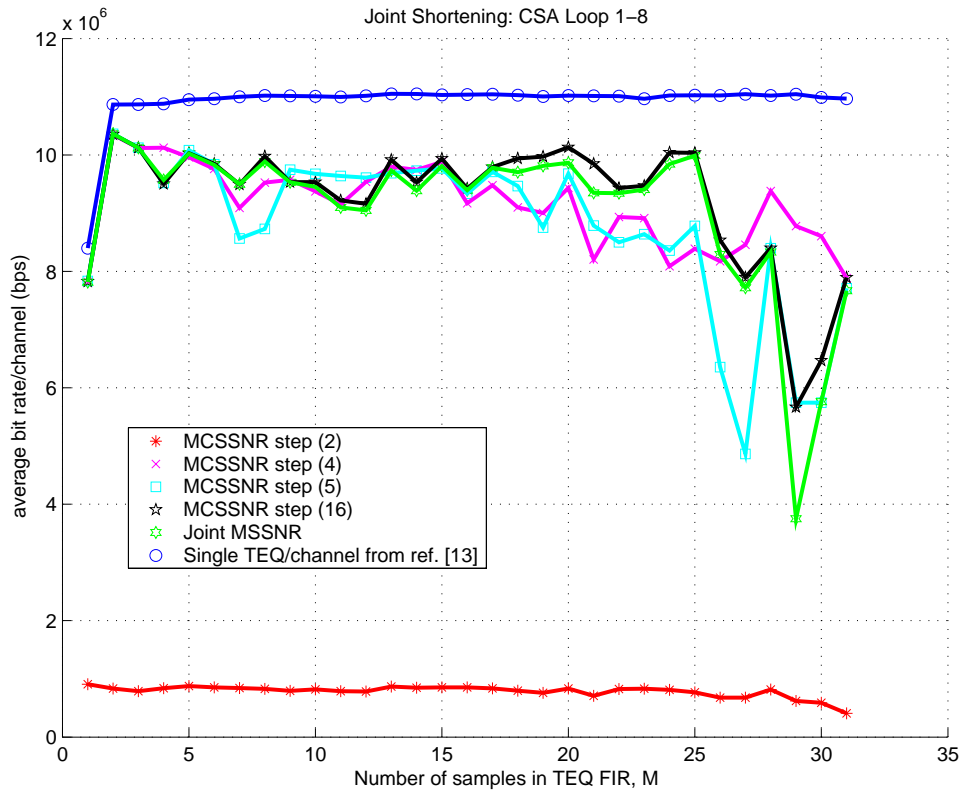


Figure 7.9: Simulation Data Rates per Channel for Multichannel Time Domain Equalizer for Standard Carrier Area Service Loops Averaged over Time Domain Equalizer Lengths 2–32 , FFT size  $N = 512$ , Cyclic Prefix Length  $\nu = 32$  with Input Power = 0.2472 W, Additive White Gaussian Noise Power = -140 dBm/Hz, Near-end Crosstalk Modelled as 49 ADSL Disturbers.

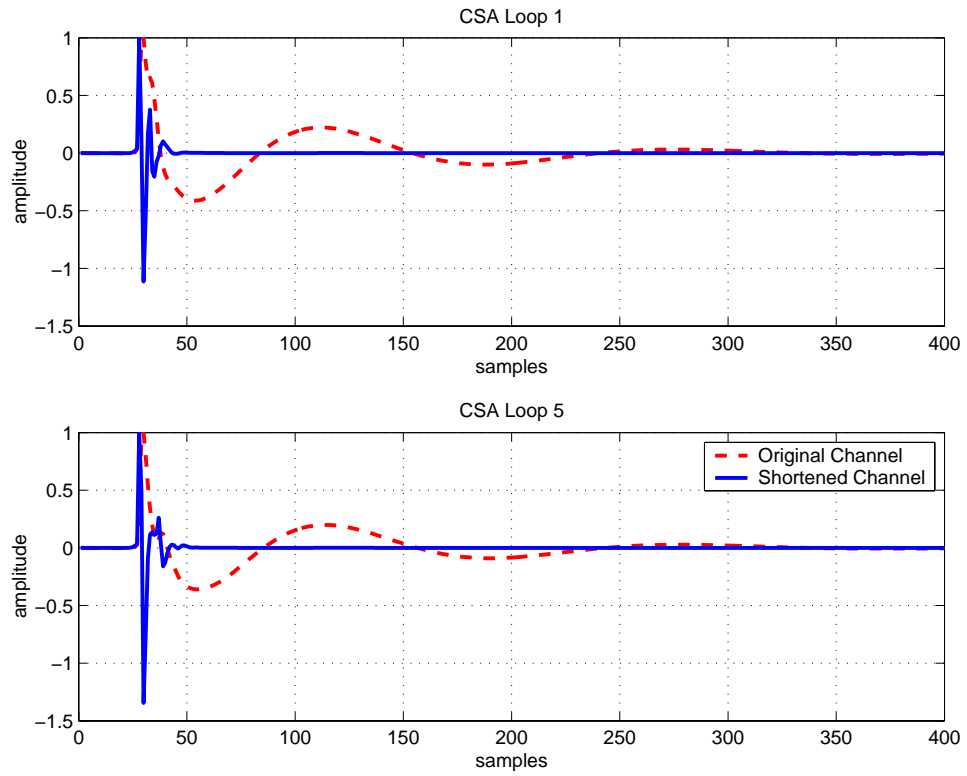


Figure 7.10: Maximum Composite Signal-to-noise Ratio Method Channel Shortening of Carrier Area Service Loops 1–8 with Results for Carrier Area Service Loops 1 and 5 Shown where FFT size = 512, Cyclic Prefix Length is  $\nu = 32$  and Time Domain Equalizer Length is  $M = 3$ . Transmission Delay  $\Delta$  is Found Using Line Search. Time Domain Equalizer Coefficients are  $\mathbf{w} = [0.4135, -0.8161, 0.4037]^T$ .

## Chapter 8

# Conclusions

### 8.1 Summary

The time domain equalizer block in a DMT receiver should be used to maximize the DMT system bit rate, and thus its design should be directly tied to the maximization of the bit rate equation. The published methods that optimize objective functions not directly related to the bit rate do not in general design time domain equalizer filters that also maximize the bit rate. Other time domain equalizer design methods that attempt to maximize the bit rate are forced to make approximations due to the difficult mathematical nature of the bit rate equation. These approximations result in time domain equalizer filters that do not truly maximize the bit rate. The goal of maximizing the bit rate using the time domain equalizer design means that the DMT system noise sources should be included in the SNR measure such as near-end crosstalk, white Gaussian noise, the effects of finite-precision arithmetic, signal quantization noise, in addition to inter-carrier interference and inter-symbol interference. The inclusion of these noise sources in the SNR measure allows the time domain equalizer design to balance their effect so that the system bit rate is maximized. This approach was not fully followed in the previous work.



In Chapter 3, I derive a new model for the subchannel SNR. The subchannel SNR model is a ratio of the desired signal power over the power of the noise, where both the numerator and the denominator are quadratic functions of the time domain equalizer taps and the Hessian matrices are positive definite. The desired signal was defined by noting that the DMT symbol that is circularly convolved with the channel does not present any ISI after the FFT. The noise is defined as the difference of the actually received signal and the defined desired signal. The time domain equalizer taps affect primarily the ISI and ICI noise contributions and in the case of optimal time domain equalizer taps the noise contribution comes from non-signal dependent sources like AWGN, NEXT, ADC noise and DNF as both ISI and ICI have been eliminated. An SNR model maximization procedure will necessarily lead to channel shortening as that is the only way to reduce the difference between the desired channel and the received channel. The SNR model proposed here is the foundation of the time domain equalizer design procedure of Chapter 5 that is aimed at designing the time domain equalizer that will maximize the bit rate of a DMT system. The efficient calculation of the matrices in the subchannel SNR model numerator and denominator is the topic of Chapter 4.

Chapter 4 introduced algorithms for the efficient initialization of matrices  $\tilde{\mathbf{A}}_k$  and noise matrix  $\tilde{\mathbf{B}}_k$  present in the proposed subchannel SNR model being

$$\text{SNR}_k = \frac{\mathbf{w}^T \tilde{\mathbf{A}}_k \mathbf{w}}{\mathbf{w}^T \tilde{\mathbf{B}}_k \mathbf{w}} \quad (8.1)$$

derived in Chapter 3. The algorithms exploit the structure of the matrices to reduce the number of computations by up to 164 times compared to a straight multiply update approach that could be taken if no such structure existed. Chapter 4 also shows the low temporary memory requirements of the proposed algorithms. The proposed initialization algorithms would have to be run for every subchannel of interest to obtain all of the necessary matrices for the following stage that will produce time domain equalizer coefficients.

Chapter 5 begins by presenting the bit rate equation dependency on the time domain equalizer taps. The bit rate equation is related to the time domain equalizer taps through the SNR model defined in Chapter 3. The bit rate equation is an integer-valued function derived as a sum of the logarithms of ratios. The ratios had a convex numerator quadratic in the time domain equalizer taps and a convex denominator again quadratic in the time domain equalizer taps. The maximization over the time domain equalizer block of the integer-valued bit rate function is achieved through a novel time domain equalizer block architecture where each subchannel is assigned a time domain equalizer FIR filter designed to maximize the bit rate in that particular subchannel. Each member of the sum constituting the system bit rate is maximized which, in turn, maximizes the sum. The optimal time domain equalizer FIR subchannel filter is found as the solution to the generalized eigenvalue problem where the time domain equalizer FIR is the eigenvector of the pair  $(\mathbf{A}_k, \mathbf{B}_k)$  corresponding to the maximum generalized eigenvalue. During data transmission this time domain equalizer filter bank employs Goertzel filters to arrive at the frequency domain point corresponding to the particular subchannel. This approach reduces the number of computations needed. Then the attention turned to a more standard time domain equalizer block architecture where only one time domain equalizer FIR “covers” all of the subchannels. This architecture simpler and numerically less expensive than time domain equalizer filter bank. The problem is how to find a single time domain equalizer FIR that performs as close as possible to time domain equalizer filter bank. A simplification removes the integer only constraint from the bit rate equation in order to create a mathematically more tractable cost function. Examples are given where the maxima of the new fractional bit rate is the same as the maxima of the integer-valued bit rate; however, no proof is offered that is so for all cases covered by the parameters of the problem. The design of a single time domain equalizer FIR is done using Almgly/Levin [108] iteration

to find the zero of the gradient of the fractional bit rate equation. As such, this method will find the nearest local maximum and does not guarantee an optimal solution. However, the starting point of the iterative algorithm is provided by the member of the time domain equalizer filter bank which performs the best when the fractional bit rate is evaluated with that member being the single time domain equalizer FIR block. Finally, Chapter 5 concludes with a look at the initialization and data transmission complexity of the proposed time domain equalizer design algorithms. The initialization and data transmission complexity of the time domain equalizer filter bank architecture make it not feasible as a solution in current real-time embedded systems however it is the optimal solution and provides an analysis tool for comparison of the performance of other time domain equalizer methods.

Chapter 6 discusses a new single FIR time domain equalizer design method that will shorten multiple channels simultaneously. I arrive at the single time domain equalizer by maximizing a new objective function that captures the contributions of different channels in a weighted sum of SSNR-based ratios. This approach is an application of the sum-of-ratios maximization approach of Chapter 5; however, instead of finding a time domain equalizer that would maximize the data rate over numerous subchannels of a single channel, I design a single time domain equalizer for multiple channels. The algorithm does not guarantee a solution that will maximize a sum of ratios; however, the simulation results show that with a good initial point it achieves modestly better results than Joint MSSNR. This approach is still work-in-progress and future work may include some of the developments of the multiple-in multiple-out equalizers.

Chapter 7 presents the performance of the proposed time domain equalizer architectures and algorithms and compare it to its peers. Both time domain equalizer filter bank and single time domain equalizer FIR algorithms were evaluated over a range of different conditions from the change in the transmission channel charac-

teristics to the change in the DMT symbols structure and thus change in the level of ISI introduced. The simulations use the eight standard downstream CSA loops [20] convolved with transmit and receive filters as the test CIR. Proposed single time domain equalizer and time domain equalizer filter bank and its peer design methods Min-ISI, MBR, LS PTE, MMSE-UEC and MMSE-UTC design methods are evaluated using the measured SNR and the corresponding achievable bit rate, which establishes a common testing platform. Time domain equalizer filter bank achieved data rate is always higher than the compared methods. The proposed single time domain equalizer design method achieves higher percentage of time domain equalizer filter bank optimal performance for each channel impulse response than Min-ISI, MBR or MMSE-based methods. Proposed single time domain equalizer's final average over tested CSA loops and is almost 2% higher than either MBR or the Min-ISI and more than 15% higher than MMSE-UTC or MMSE-UEC. For a data rate of 11 Mbps, a 2% improvement amounts to 220 kbps. The proposed single time domain equalizer matches LS PTE performance on the majority of CSA loops. Overall single time domain equalizer does not perform as well as the LS PTE, however the differences are small. The sensitivity of the achieved data rate on the transmission delay in the case of the proposed time domain equalizer filter bank and single time domain equalizer FIR methods decreases with the length of the FIR filters used. Even with small length of FIR filters, the change in the data rate as a function of the transmission delay  $\Delta$  shows high regularity: data rate increases for small values of  $\Delta$ , plateaus for mid-range values and drops of rather quickly for "large" values of  $\Delta$ . This level of regularity helps to choose the optimal  $\Delta$ . The simulation observations suggest that a successful time domain equalizer has a flat magnitude response over most of the spectrum and a null at the position of the highest ISI whereas a less successful design will put a number of nulls elsewhere in the spectrum. Thus, the time domain equalizer filter bank reaches the optimal

performance in the simulations as predicted by the theoretical model. Single time domain equalizer reaches more than 99% percent of the performance of time domain equalizer filter bank with significantly lower complexity. Currently, the time domain equalizer filter bank has been implemented in the MATLAB DMT time domain equalizer Toolbox [113] and a plan for the future work is to implement the single TEQ FIR method.

In simulation using standard ADSL parameters, the proposed MCSSNR outperforms the Joint MSSNR method [67] by achieving higher joint SSNR-based measure. A higher joint SSNR-based measure indicates better removal on average of the channel energy outside of the desired window. However, the proposed MCSSNR is considerably more computationally intensive than Joint MSSNR, as it requires a larger number of generalized eigenvalue solutions.

## 8.2 Future Work

Although a large number of publications has appeared on the topic of time domain equalizer design there is still room for innovation. This dissertation presents the optimal time domain equalizer block architecture in the form of a time domain equalizer filter bank where each subchannel is assigned the optimal time domain equalizer. It also presented a single time domain equalizer method that achieves most of the performance of time domain equalizer filter bank on the tested channels.

It is likely that the transmission channels encountered in practice are more challenging to equalize than the standard carrier service area test loops. Hence, it is possible that the traditional time domain equalizer architecture cannot fully utilize the channel capacity, but the practical concerns find the complexity of the time domain equalizer filter bank prohibitive. Thus, it is of interest to find out if there is a possibility of a reduced time domain equalizer filter bank where groups of subchannels are assigned an optimal time domain equalizer. Dual-path equalizer

structure in [93] already presents a structure where two time domain equalizers are employed. Dual-path design approach optimizes one time domain equalizer across the multiple subchannels and the other over a subset of subchannels e.g. using the minimum inter-symbol interference method thus allowing improved equalization for subchannels in that subset. A study into the variations between the subchannel equalizers that are a part of the time domain equalizer filter bank tested over various channels may reveal the natural separation and grouping of subchannels. A possible outcome may be that some of the subchannels are identified as providing subchannel equalizers that perform well for a certain number of neighboring subchannels. Such “bellwether” subchannels can then be used to design the group time domain equalizer without the need to incorporate the information provided by other subchannels in the same group. Then, the algorithm for the design of a single subchannel equalizer presented in this dissertation can be used. A possible improvement would also be to use the single time domain equalizer design method and the subchannel SNR model proposed in this dissertation to arrive at the equalizer coefficients over sets of subchannels (using the information from all subchannels in the set). This dissertation assumes that all of subchannel equalizers that are a part of time domain equalizer filter bank are of the same length. This assumption does not have to hold as time domain equalizer filters can have different length depending on their position in the filter bank, i.e. the frequency band they equalize. Potentially, longer filters can be assigned to subchannels with higher noise content.

The discrete Fourier transform (DFT) is used for modulation/demodulation in DMT and OFDM systems. DFT has relatively high sidelobes. A spectrally-shaped noise source will most likely not align with the frequencies of the subchannels. Thus, the energy from the interferer will influence not only the subchannels within which the noise lies, but also neighboring subchannels. It is possible then that the signal-to-noise ratio within a subchannel band is not maximized at the frequency of

the transmitted subchannel carrier. The spectral shape of the noise in a subchannel band may require a slight change in the demodulating frequency in order to maximize the subchannel signal-to-noise ratio. Time domain equalizer filter bank presents convenient architecture for dynamic adjustment of frequencies of Goertzel filters performing single-point DFT so that the sampling in the frequency domain can be adjusted to maximize the subchannel SNR. The adjustment of DFT frequencies would be performed at the receiver without the need for the transmitter to change the formatting of transmitted symbols. The development of this technique would require a functional relationship between the time domain equalizer design, SNR in a subchannel and frequency of a respective Goertzel filter. Due to the need to know the SNR functional within a subchannel it is most likely that an FFT of larger size than the number of subchannels is needed. This also leads to a possibility of time domain equalizer design on a fractional sub-sample level in connection with previous point in order to be able to control the filtering within a subchannel.

This dissertation did not include noise sources such as far-end crosstalk (FEXT) or near-end echo to the model of the subchannel SNR. Near-end echo from the local transmitter is a powerful source of noise at it would be worthwhile to include it in future SNR models

Time domain equalizer design methods presented in this dissertation rely on the knowledge of the channel. A modification of the methods in this dissertation to enable adaptive progression to the time domain equalizer without the knowledge of the channel would reduce the computational burden on the processor by “spreading” the computations over the time domain equalizer training sequence. Both single time domain equalizer design and the time domain equalizer filter bank require numerous calculations of the maximum eigenvalue and corresponding eigenvector. The implementation of the power method would reduce computational burden on the processor.

The Min-ISI time domain equalizer design method produces good results with lower numerical complexity when compared to methods presented in this dissertation or to MBR. Min-ISI has a restriction that the length of the time domain equalizer cannot be larger than the length of the cyclic prefix. Min-ISI also requires the knowledge of the channel and the calculation of the minimum eigenvalue and the corresponding eigenvector. An adaptive implementation of the Min-ISI that does not require advance knowledge of the channel impulse response coupled with the implementation of an inverse power iteration and the removal of the constraint on the length of the time domain equalizer would make the Min-ISI method attractive for implementation in current ADSL systems. Also, such improvements would enhance the properties of the dual-path design which utilizes Min-ISI procedure for the design of one of the equalizers.

OFDM employs a multiple-input multiple-output system in which the signal from multiple paths is equalized simultaneously. From the surveyed literature, it follows that the methods applicable to a single-input single-output TEQ design methods can be adapted to a multiple-input multiple-output system approach. Single-input single-output MMSE method has an equivalent in the multiple-input multiple-output approach and it is possible that other methods such as MSSNR can be adapted, as well.

The subchannel SNR model given in this dissertation is derived at the output of the FFT demodulator block. Another equalization step follows which is frequency domain equalization performed by the FEQ block. Modelling SNR at the output of the FEQ block as a function of the time domain equalizer coefficients would include in it the dependency of the FEQ block on time domain equalizer and include it in the objective criterion.

The simulation results presented in this dissertation treat the performance of the time domain equalization methods in the downstream direction. Upstream was



not simulated; however, it may be of interest to find if the performance of the time domain equalization changes as the frame is only 64 samples long with the cyclic prefix of 4 samples.

Finally, Chapter 6 proposes a method whereby multiple channel impulse responses are shortened using a single time domain equalizer. Continued investigation of this area may prove beneficial in OFDM wireless broadband communication where the channel impulse response has a significant delay spread due to the multipath characteristics of the physical medium. It is possible that the resulting channel impulse response can be separated into a set of delayed and overlapping impulse responses and the task of equalizing them can be defined as in Chapter 6.

# Bibliography

- [1] W. Henkel, S. Olcer, K. S. Jacobsen, B. R. Saltzberg, and A. M. Bush, “Guest editorial twisted pair transmission—ever increasing performances on ancient telephone wires,” *IEEE J. on Selected Areas in Comm.*, vol. 20, pp. 877–880, June 2002.
- [2] H. Sari, G. Karam, and I. Jeanclaude, “Transmission techniques for digital terrestrial TV broadcasting,” *IEEE Comm. Mag.*, vol. 33, pp. 100–109, Feb. 1995.
- [3] B. L. Evans, “Equalizer design to maximize bit rate in ADSL transceivers,” Tech. Rep. available at <http://www.ece.utexas.edu/~bevans/projects/adsl/TEQdesign.ppt>, The University of Texas at Austin, Feb. 2003.
- [4] D. Drajić and D. Bajić, “Modems for data transmission over telephone network,” in *Proc. Int. Conf. on Telecomm. in Modern Satellite, Cable and Broadcasting Services*, vol. 1, (Nis, Serbia and Montenegro), pp. 80–87, Oct. 1999.
- [5] M. N. O. Sadiku and C. Aduba, “Cable modem technology: A new quick fix remedy that has been around for decades,” *IEEE Potentials*, pp. 26–27, Oct. 2000.

- [6] A. Dutta-Roy, "An overview of cable modem technology and market perspectives," *IEEE Comm. Mag.*, vol. 39, pp. 81–88, June 2001.
- [7] W. H. Powell, "Developments and prospects for cable modems," in *IEE Colloquium on Optical and Hybrid Access Networks*, vol. 16, pp. 1–5, Mar. 1996.
- [8] S. Temple and R. Hendry, "Cable modems and their place in fast access technology," in *IEE Seminar on Fast SoHo SME/Connectivity*, vol. 3, pp. 1–5, 1999.
- [9] D. Lankford, E. Gameel, A. Boras, and S. Cheema, "Why DOCSIS over IEEE 802.14?," Tech. Rep. available in .pdf format at <http://198.11.21.25/capstoneTest/Students/Papers/docs/Docsis39203.pdf>, 2001.
- [10] W. Goralski, "xDSL loop qualification and testing," *IEEE Comm. Mag.*, pp. 79–83, May 1999.
- [11] Editorial, "Crossed wires," *The Economist*, p. 60, Feb. 2003.
- [12] K. Fitchard, "Broadband deployment: cable is still king," *Telephony*, Nov. 2003.
- [13] J. M. Cioffi, "Meeting minutes," Nov. 2002.
- [14] W. Y. Chen, "The development and standardization of assymmetric digital subscriber line," *IEEE Comm. Mag.*, pp. 68–72, May 1999.
- [15] ANSI, "Integrated service digital network (ISDN)-basic access interface for use on metallic loops for application on the network side of the NT (layer 1 specification)," Tech. Rep. T1601-1992, American National Standards Institute, 1992.

- [16] J. A. C. Bingham, "Multicarrier modulation for data transmission: An idea whose time has come," *IEEE Comm. Mag.*, vol. 28, pp. 5–14, May 1990.
- [17] S. D. Sandberg and M. A. Tzannes, "Overlapped discrete multitone modulation for high speed copper wire communications," *IEEE J. on Selected Areas in Comm.*, vol. 13, pp. 1571–1585, Dec. 1995.
- [18] G. W. Wornell, "Emerging applications of multirate signal processing and wavelets in digital communications," *Proc. of the IEEE*, vol. 84, pp. 586–603, Apr. 1996.
- [19] T. S. Rappaport, A. Annamalai, R. M. Buehrer, and W. H. Tranter, "Wireless communications: Past events and future perspective," *IEEE Comm. Mag.*, vol. 40, pp. 148–161, May 2002.
- [20] ANSI, "Network and customer installation interfaces: Asymmetric digital subscriber line (ADSL) metallic interface," Tech. Rep. T1E1.413, American National Standards Institute, 1998.
- [21] ITU-T, "Asymmetrical digital subscriber line (ADSL) transceivers," Tech. Rep. G.992.1, Int. Telecomm. Union, 1999.
- [22] ITU-T, "Splitterless asymmetric digital subscriber line (ADSL) transceivers," Tech. Rep. G.992.2, Int. Telecomm. Union, 1999.
- [23] VDSLlalliance, "Very-high-speed digital subscriber lines; system requirements; draft technical report," Tech. Rep. T1E1.4/97-131R2, American National Standards Institute, 1997.
- [24] VDSLlalliance, "SDMT VDSL draft standard proposal," Tech. Rep. T1E1.4/97-332, American National Standards Institute, 1997.

- [25] ETSI, “Transmission and multiplexing (TM); access transmission systems on metallic access cables; very high speed digital subscriber line (VDSL); part 2: Transceiver specification,” Tech. Rep. TS 101 270-2, European Telecomm. Standards Institute, 1998.
- [26] J. Cioffi, “A multicarrier primer,” Tech. Rep. T1E1.4/91-157, Amati Comm. Corp. and Stanford University, 1991.
- [27] J. M. Cioffi, V. Oksman, J.-J. Werner, T. Pollet, P. M. P. Spruyt, J. S. Chow, and K. S. Jacobsen, “Very-high-speed digital subscriber lines,” *IEEE Comm. Mag.*, vol. 37, pp. 72–79, Apr. 1999.
- [28] IEEE, “Telecommunications and information exchange between systemslocal and metropolitan area networksspecific requirementspart 11: Wireless LAN medium access control (MAC) and physical layer (PHY) specificationsamendment 1: High-speed physical layer in the 5 GHz band,” Tech. Rep. IEEE 802.11a-1999, The Institute of Electrical and Electronics Engineers, 1999.
- [29] ETSI, “Digital video broadcasting (DVB); interaction channel for digital terrestrial television (DVB-RCT)incorporating multiple access OFDM,” Tech. Rep. EN 301 958 DVB-RCT, European Telecomm. Standards Institute, 2001.
- [30] ETSI, “Broadband radio access networks (BRAN); HIPERLAN-2; physical layer,” Tech. Rep. 2, European Telecomm. Standards Institute, 2000.
- [31] R. van Nee, G. Awater, M. Morikura, H. Takanashi, M. Webster, and K. Halford, “New high-rate wireless LAN standards,” *IEEE Comm. Mag.*, vol. 37, pp. 82–88, Dec. 1999.
- [32] J. Proakis and D. Manolakis, *Digital Signal Processing*, pp. 415–420. Prentice Hall, 3rd ed., 1996.

- [33] T. Starr, J. Cioffi, and P. Silverman, *Understanding Digital Subscriber Line Technology*, pp. 205–206. Prentice-Hall, 1999.
- [34] J. Cioffi, G. Dudevoir, M. Eyuboglu, and G. D. Forney, “Minimum mean-square-error decision feedback equalization and coding - parts I and II,” *IEEE Trans. on Comm.*, vol. 43, pp. 2595–2604, Oct. 1995.
- [35] D. Bengtsson and D. Landstroem, “Coding in a discrete multitone modulation system,” Master’s thesis, Lulea University of Technology, University Campus, Porsn, 97187 Lule, Sweden, Mar. 1996.
- [36] M. Milosevic, L. F. C. Pessoa, B. L. Evans, and R. Baldick, “DMT bit rate maximization with optimal time domain equalizer filter bank architecture,” in *Proc. IEEE Asilomar Conf. on Signals, Systems and Computers*, (Pacific Grove, CA), pp. 377–382, Nov. 2002.
- [37] M. Milosevic, L. F. C. Pessoa, and B. L. Evans, “Simultaneous multichannel time domain equalizer design based on the maximum composite shortening SNR,” in *Proc. IEEE Asilomar Conf. on Signals, Systems and Computers*, (Pacific Grove, CA), pp. 1895–1899, Nov. 2002.
- [38] M. Milosevic, L. F. C. Pessoa, B. L. Evans, and R. Baldick, “Optimal time domain equalization design for maximizing data rate of discrete multi-tone systems,” *IEEE Trans. on Signal Proc.*, Apr. 2003. accepted for publication.
- [39] J. S. Chow, J. C. Tu, and J. M. Cioffi, “A discrete multitone receiver system for HDSL applications,” *IEEE J. on Selected Areas in Comm.*, vol. 9, pp. 895–907, Aug. 1991.
- [40] J. S. Chow and J. M. Cioffi, “A cost-effective maximum likelihood receiver for multicarrier systems,” in *Proc. IEEE Int. Conf. Comm.*, vol. 2, (Chicago, IL), pp. 948–952, June 1992.

- [41] J. S. Chow, J. M. Cioffi, and J. A. C. Bingham, "Equalizer training algorithms for multicarrier modulation systems," in *Proc. IEEE Int. Conf. Comm.*, vol. 2, (Geneva, Switzerland), pp. 761–765, May 1993.
- [42] J. Chow and J. Cioffi, "Method for equalizing a multicarrier signal in a multicarrier communication system," *U.S. Patent Number 5,285,474*, 1994.
- [43] M. V. Bladel and M. Moeneclaey, "Time-domain equalization for multicarrier communication," in *Proc. IEEE Global Telecomm. Conf.*, pp. 167–171, Nov. 1995.
- [44] M. Nafie and A. Gatherer, "Time-domain equalizer training for ADSL," in *Proc. IEEE Int. Conf. Comm.*, vol. 2, (Montreal, Canada), pp. 1085–1089, June 1997.
- [45] I. Lee, J. S. Chow, and J. M. Cioffi, "Performance evaluation of a fast computation algorithm for the DMT in high-speed subscriber loop," *IEEE J. on Selected Areas in Comm.*, vol. 13, pp. 1564–1570, Dec. 1995.
- [46] N. Al-Dhahir and J. Cioffi, "Efficiently computed reduced-parameter input-aided MMSE equalizers for ML detection: A unified approach," *IEEE Trans. on Info. Theory*, vol. 42, pp. 903–915, May 1996.
- [47] J. F. V. Kerchove and P. Spruyt, "Adapted optimization criterion for FDM-based DMT-ADSL equalization," in *Proc. IEEE Int. Conf. Comm.*, vol. 3, (Dallas, TX), pp. 1328–1334, June 1996.
- [48] M. Ho, J. M. Cioffi, and J. A. C. Bingham, "High-speed full-duplex echo cancellation for discrete multitone modulation," in *Proc. IEEE Int. Conf. Comm.*, vol. 2, (Geneva, Switzerland), pp. 772–776, May 1993.
- [49] J. M. Cioffi and J. A. C. Bingham, "A data-driven multitone echo canceller," *IEEE Trans. on Comm.*, vol. 42, pp. 2853–2869, Oct. 1994.

- [50] M. Ho, J. M. Cioffi, and J. A. C. Bingham, "Discrete multitone echo cancellation," *IEEE Trans. on Comm.*, vol. 44, pp. 817–825, July 1994.
- [51] B. Farhang-Boroujeny and M. Ding, "Design methods for time-domain equalizers in DMT transceivers," *IEEE Trans. on Comm.*, vol. 49, pp. 554–562, Mar. 2001.
- [52] N. Al-Dhahir and J. Cioffi, "A band-optimized reduced-complexity equalized multicarrier transceiver," *IEEE Trans. on Comm.*, vol. 45, pp. 948–956, Aug. 1997.
- [53] B. Farhang-Boroujeny and M. Ding, "Channel classification and time-domain equalizer design for ADSL transceivers," in *Proc. IEEE Int. Conf. Comm.*, vol. 2, (Vancouver, Canada), pp. 1059–1063, June 2000.
- [54] B. Wang and T. Adali, "A frequency-domain eigenfilter approach for equalization in discrete multitone systems," in *Proc. IEEE Asilomar Conf. on Signals, Systems and Computers*, vol. 2, (Pacific Grove, CA), pp. 1058–1062, Nov. 1999.
- [55] N. Lashkarian and S. Kiaei, "Fast algorithm for finite-length MMSE equalizers with applications to discrete multitone systems," in *Proc. IEEE Int. Conf. on Acoustics, Speech and Signal Proc.*, vol. 5, (Phoenix, AZ), pp. 2753–2756, Mar. 1999.
- [56] G. H. Golub and C. F. V. Loan, *Matrix Computations*. John Hopkins, 3rd ed., 1996.
- [57] N. Al-Dhahir, "FIR channel-shortening equalizers for MIMO ISI channels," *IEEE Trans. on Comm.*, vol. 49, pp. 213–218, Feb. 2001.
- [58] N. Warke, A. J. Redfern, C. Sestok, and M. Ali, "Performance comparison of TEQ design techniques for FDM ADSL," in *Proc. IEEE Asilomar Conf.*



on *Signals, Systems and Computers*, (Pacific Grove, CA), pp. 367–371, Nov. 2002.

- [59] R. K. Martin, C. R. Johnson, M. Ding, and B. L. Evans, “Infinite length results for channel shortening equalizers,” in *Proc. IEEE Int. Work. on Signal Processing Advances in Wireless Communications*, (Rome, Italy), June 2003. accepted for publication.
- [60] N. Al-Dhahir and J. M. Cioffi, “Optimum finite-length equalization for multicarrier transceivers,” in *Proc. IEEE Global Telecomm. Conf.*, vol. 3, (San Francisco, CA), pp. 1884–1888, Nov. 1994.
- [61] N. Al-Dhahir and J. M. Cioffi, “The combination of finite-length geometric equalization and bandwidth optimization for multicarrier receivers,” in *Proc. IEEE Int. Conf. on Acoustics, Speech and Signal Proc.*, vol. 2, (Detroit, MI), pp. 1201–1204, May 1995.
- [62] N. Al-Dhahir and J. Cioffi, “Optimum finite length equalization for multicarrier transceivers,” *IEEE Trans. on Comm.*, vol. 44, pp. 56–64, Jan. 1996.
- [63] G. Arslan, B. L. Evans, and S. Kiaei, “Equalization for discrete multitone transceivers to maximize bit rate,” *IEEE Trans. on Signal Proc.*, vol. 49, pp. 3123–3135, Dec. 2001.
- [64] N. Lashkarian and S. Kiaei, “Optimum equalization of multicarrier systems via projection onto convex set,” in *Proc. IEEE Int. Conf. Comm.*, vol. 2, (Vancouver, Canada), pp. 968–972, June 1999.
- [65] N. Lashkarian and S. Kiaei, “Optimum equalization of multicarrier systems: A unified geometric approach,” *IEEE Trans. on Comm.*, vol. 49, pp. 1762–1769, Oct. 2001.

- [66] M. Milisavljevic and E. I. Verriest, “Fixed point algorithm for bit rate optimal equalization in multicarrier systems,” in *Proc. IEEE Int. Conf. on Acoustics, Speech and Signal Proc.*, (Phoenix, AZ), pp. 2515–2518, Mar. 1999.
- [67] P. J. W. Melsa, R. C. Younce, and C. E. Rohrs, “Impulse response shortening for discrete multitone transceivers,” *IEEE Trans. on Comm.*, vol. 44, pp. 1662–1672, Dec. 1996.
- [68] P. J. W. Melsa, C. E. Rohrs, and R. C. Younce, “Joint optimal impulse response shortening,” in *Proc. IEEE Int. Conf. on Acoustics, Speech and Signal Proc.*, vol. 3, (Atlanta, GA), pp. 1763–1766, May 1996.
- [69] P. J. W. Melsa and R. C. Younce, “Joint impulse response shortening,” in *Proc. IEEE Global Telecomm. Conf.*, vol. 1, (London, UK), pp. 209–213, Nov. 1996.
- [70] J. Demmel, *Applied Numerical Linear Algebra*, pp. 173–176. SIAM, 1997.
- [71] I. Djokovic, “MMSE equalizers for DMT systems with and without crosstalk,” in *Proc. IEEE Asilomar Conf. on Signals, Systems and Computers*, vol. 1, (Pacific Grove, CA), pp. 545–549, Nov. 1997.
- [72] C. Yin and G. Yue, “Optimal impulse response shortening for discrete multi-tone transceivers,” *Electronics Letters*, vol. 34, pp. 35–36, Jan. 1998.
- [73] R. Schur, J. Speidel, and R. Angerbauer, “Reduction of guard interval by impulse compression for DMT modulation on twisted pair cables,” in *Proc. IEEE Global Telecomm. Conf.*, vol. 3, pp. 1632–1636, 2000.
- [74] W. min Chiu, W. K. Tsai, T. C. Liao, and M. G. Tzoulis, “Time-domain channel equalizer design using the inverse power method,” in *Proc. IEEE Int. Conf. Comm.*, vol. 2, (Vancouver, Canada), pp. 973–977, May 1999.

- [75] B. Lu, L. D. Clark, G. Arslan, and B. L. Evans, “Fast time-domain equalization for discrete multitone modulation systems,” in *Proc. IEEE Digital Signal Processing Workshop*, (Hunt, TX), Oct. 2000.
- [76] B. Lu, *Wireline Channel Estimation and Equalization*. PhD thesis, The University of Texas at Austin, Dec. 2000.
- [77] D. Daly, C. Heneghan, and A. D. Fagan, “A minimum mean-squared error interpretation of residual ISI channel shortening for discrete multitone transceivers,” in *Proc. IEEE Int. Conf. on Acoustics, Speech and Signal Proc.*, vol. 4, pp. 2065–2067, May 2001.
- [78] R. Schur and J. Speidel, “An efficient equalization method to minimize delay spread in OFDM/DMT systems,” in *Proc. IEEE Int. Conf. Comm.*, vol. 5, pp. 1481–1485, June 2001.
- [79] A. Tkacenko and P. P. Vaidyanathan, “Noise optimized eigenfilter design of time-domain equalizers for DMT systems,” in *Proc. IEEE Int. Conf. Comm.*, pp. 54–58, May 2002.
- [80] A. Tkacenko and P. P. Vaidyanathan, “A new eigenfilter based method for optimal design of channel shortening equalizers,” in *Proc. IEEE Int. Conf. Comm.*, pp. 504–507, May 2002.
- [81] A. Tkacenko and P. P. Vaidyanathan, “Eigenfilter design of MIMO equalizers for channel shortening,” in *Proc. IEEE Int. Conf. Comm.*, pp. 2361–2364, May 2002.
- [82] M. G. Troulis and S. Sesia, “A spectrally flat time domain equalizer for rate improvement of multicarrier systems,” in *Proc. IEEE Int. Conf. Comm.*, vol. 3, pp. 1803–1807, May 2002.

- [83] R. K. Martin, J. Balakrishnan, W. A. Sethares, and C. R. Johnson, "A blind adaptive TEQ for multicarrier systems," *IEEE Signal Proc. Letters*, vol. 9, pp. 341–343, Nov. 2002.
- [84] R. K. Martin, C. R. Johnson, M. Ding, and B. L. Evans, "Exploiting symmetry in channel shortening equalizers," in *Proc. IEEE Int. Conf. on Acoustics, Speech and Signal Proc.*, Apr. 2003.
- [85] C. Ribeiro, V. Silva, and P. S. R. Diniz, "Linear phase impulse response shortening for xDSL DMT modems," in *Proc. IEEE Int. Telecomm. Symposium*, (Natal, Brazil), pp. 368–371, Sept. 2002.
- [86] G. Arslan, *Equalization Techniques for MultiCarrier Modulation*. PhD thesis, The University of Texas at Austin, Dec. 2000.
- [87] W. Henkel, G. Taubock, P. Odling, P. O. Borjesson, and N. Petersson, "The cyclic prefix of OFDM/DMT - an analysis," in *Int'l Zurich Seminar Broad-band Commun., Access, Transm., Networking*, vol. 2, pp. 1–3, 2002.
- [88] K. V. Acker, M. Moonen, O. van de Wiel, and T. Pollet, "Per tone equalization for DMT receivers," in *Proc. IEEE Global Telecomm. Conf.*, vol. 5, pp. 2311–2315, 1999.
- [89] K. V. Acker, G. Leus, M. Moonen, and T. Pollet, "Frequency domain equalization with tone grouping in DMT/ADSL receivers," in *Proc. IEEE Asilomar Conf. on Signals, Systems and Computers*, vol. 2, (Pacific Grove, CA), pp. 1067–1070, Nov. 1999.
- [90] K. V. Acker, G. Leus, M. Moonen, O. van de Wiel, and T. Pollet, "Per tone equalization for DMT-based systems," *IEEE Trans. on Comm.*, vol. 49, pp. 109–119, Jan. 2001.

- [91] R. K. Martin and C. R. Johnson, "Blind, adaptive per tone equalization for multicarrier receivers," in *Conf. on Information Sciences and Systems*, Mar. 2002.
- [92] C. R. J. Jr., P. Schniter, T. J. Endres, J. D. Behm, D. R. Brown, and R. A. Casas, "Blind equalization using the constant modulus criterion: A review," in *Proc. of the IEEE*, vol. 86, pp. 1927–1950, Oct. 1998.
- [93] M. Ding, R. Redfern, and B. L. Evans, "A dual-path TEQ structure for DMT-ADSL systems," in *Proc. IEEE Int. Conf. on Acoustics, Speech and Signal Proc.*, vol. 3, pp. 2573–2576, Apr. 2002.
- [94] M. de Courville, P. Duhamel, P. Madec, and J. Palicot, "Blind equalization of OFDM systems based on the minimization of a quadratic criterion," in *Proc. IEEE Int. Conf. Comm.*, pp. 1318–1321, June 1996.
- [95] K.-W. Cheong and J. M. Cioffi, "Precoder for (DMT) with insufficient cyclic prefix," in *Proc. IEEE Int. Conf. Comm.*, vol. 1, pp. 339–343, June 1998.
- [96] I. Djokovic, "Cyclic prefix extension in DMT systems," in *Proc. IEEE Asilomar Conf. on Signals, Systems and Computers*, vol. 1, (Pacific Grove, CA), pp. 65–69, Nov. 1998.
- [97] S. Trautmann, T. Karp, and N. J. Fliege, "Frequency domain equalization of DMT/OFDM systems with insufficient guard interval," in *Proc. IEEE Int. Conf. Comm.*, vol. 3, pp. 1646–1650, 2002.
- [98] S. Trautmann and N. Fliege, "A new equalizer for multitone systems without guard time," *IEEE Comm. Letters*, vol. 6, pp. 34–36, Jan. 2002.
- [99] S. Trautmann and N. Fliege, "Perfect equalization for DMT systems without guard interval," *IEEE J. on Selected Areas in Comm.*, vol. 20, pp. 987–996, June 2002.

- [100] A. J. Redfern, “Multicarrier modulation with data dependent frequency domain redundancy,” in *Proc. IEEE Asilomar Conf. on Signals, Systems and Computers*, (Pacific Grove, CA), pp. 1804–1808, Nov. 2002.
- [101] B. Lu and B. L. Evans, “Channel equalization by feedforward neural networks,” in *Proc. IEEE Int. Sym. on Circuits and Systems*, vol. 5, (Orlando, FL), pp. 587–590, May 1999.
- [102] W. Henkel and T. Kessler, “Maximizing the channel capacity of multicarrier transmission by suitable adaptation of the time-domain equalizer,” *IEEE Trans. on Comm.*, vol. 48, pp. 2000–2004, Dec. 2000.
- [103] H. Stark and J. Woods, *Probability, Random Processes, and Estimation Theory for Engineers*, pp. 213–218. Prentice Hall, 2nd ed., 1994.
- [104] A. Gersho and R. M. Gray, *Vector Quantization and Signal Compression*. Kluwer Academic Publishers, 1992.
- [105] S. Schaible, “Fractional programming - a recent survey,” *Journal of Statistics and Management Systems*, vol. 29, pp. 845–866, Mar. 2001.
- [106] G. Goertzel, *An Algorithm for the Evaluation of Finite Trigonometric Series*, vol. 65, pp. 34–35. American Math. Monthly, 1958.
- [107] R. Freund and F. Jarre, “Solving the sum-of-ratios problem by an interior-point method,” Tech. Rep. 3/99, Bell Labs, 1999.
- [108] Y. Almogly and O. Levin, “A class of fractional programming problems,” in *Operations Research*, vol. 19, pp. 57–67, 1971.
- [109] D. P. Bertsekas, *Nonlinear Programming*, pp. 54–75, 253. Athena Scientific, 1995.

- [110] J. E. Falk and S. W. Palocsay, *Optimizing the Sum of Linear Fractional Functions*, pp. 221–258. Kluwer Academic Publishers, 1992.
- [111] W. Dinkelbach, *On Nonlinear Fractional Programming*, vol. 13, pp. 492–498. Management Science, 1967.
- [112] H. van de Velde, T. Pollet, and M. Moeneclaey, “Effect of cable and system parameters on passband ADSL performance,” *IEEE Trans. on Comm.*, vol. 43, pp. 1248–1251, Feb. 1995.
- [113] G. Arslan, M. Ding, B. Lu, M. Milosevic, Z. Shen, and B. L. Evans, “Matlab DMT TEQ design toolbox,” Tech. Rep. v3.2beta available at <http://www.ece.utexas.edu/~bevans/projects/adsl/dmtteq/>, Embedded Signal Processing Lab, The University of Texas at Austin, Mar. 2003.
- [114] J. L. Devore, *Probability and Statistics for Engineering and the Sciences*, pp. 298–299. Brooks/Cole Publishing Company, 4 ed., 1995.

# Vita

Miloš Milošević was born on February 17, 1974 in Niš, Serbia and Montenegro. He finished his elementary school with a best in class designation and attended high school in his home town. He actively played tennis and had the honor of playing for the national cadet team in addition to winning several junior and cadet championships. The senior year of high school he finished in Atascadero, CA, as a foreign exchange student where his academic achievements earned him a special citation. Miloš Milošević received B.S.E.E. and M.S.E.E. at the Illinois Institute of Technology in Chicago, IL in 1996 and 1998, respectively. He is a recipient of a Tau Beta Pi graduate scholarship. Miloš moved to Austin in 1998 to begin his employment with Motorola's Networking and Communication Systems Division where he worked on the design of an ADSL transceiver based on the Motorola 56300 core. He began his doctoral studies at The University of Texas in the Fall of 1998 alongside his engineering work. His professional experience includes a systems engineering position and digital signal processing algorithm design for the Texas Instruments C6000 DSP core in the Texas Instruments Broadband Division. He is currently a senior engineer in the Acquisition Department, Telemetry Section of Schlumberger in Austin, TX, where he designs the next generation high-speed communication systems for oilfield services. His current research interests are multicarrier communication systems such as ADSL, VDSL or OFDM.



Permanent Address: Sretena Mladenovića 20/23  
18000 Niš  
Serbia and Montenegro

This dissertation was typeset with  $\text{\LaTeX} 2_{\epsilon}$ <sup>1</sup> by the author.

---

<sup>1</sup> $\text{\LaTeX} 2_{\epsilon}$  is an extension of  $\text{\LaTeX}$ .  $\text{\LaTeX}$  is a collection of macros for  $\text{\TeX}$ .  $\text{\TeX}$  is a trademark of the American Mathematical Society. The macros used in formatting this dissertation were written by Dinesh Das, Department of Computer Sciences, The University of Texas at Austin, and extended by Bert Kay and James A. Bednar.